

ELECTROSPINNING AND WET-SPINNING OF ELASTIC FIBERS

by

MUSTAFA M. DEMİR

Submitted to the Graduate School of Engineering and Natural Sciences

In Sabancı University in partial fulfillment of

the requirements for the degree of

Master of Science

Sabancı University

2001

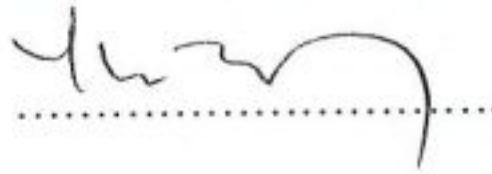
ELECTROSPINNING AND WET-SPINNING OF ELASTIC FIBERS

APPROVED BY:

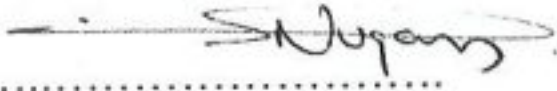
Prof. Dr. Burak Erman
(Thesis Supervisor)



Dr. Yusuf Mencilođlu



Assoc. Prof. Dr. Turgut Nugay



DATE OF APPROVAL:

27/06/2001

ACKNOWLEDGMENTS

Throughout my studies pertaining to the formation of my thesis, an important number of people, academics as well as non-academics, have helped and supported me in various ways. At first, I must acknowledge the contribution of Prof. Dr. Burak Erman, who suggested the topic of my thesis. I would like to present my gratitude to him for having always displayed a concern for my studies. Assoc. Prof. Turgut Nugay also deserves to be cited here, for having encouraged me to pursue an academic career. His careful support has been one of the greatest motivations in my researches. Drs. Yusuf Mencelođlu, Mehmet Ali Glgn, and Canan Baysal have provided a creative and stimulating atmosphere of learning. Beyond the scope of my thesis, they taught me a lot about science and knowledge. Prof. Dr. Miko akmak has given invaluable advice for designing my research tools. Last, but not least, I would like to thank Cemal Karadayı who produced my research apparatuses. As a gifted technician, he has been amiable and supportive throughout my work.

Finally, I find myself in the pleasurable obligation of expressing my thanks to my love and to my family, whose contributions and supports can not be assessed enough. To finish, this kind of work is never done by a single individual, but by someone who needs, and often receives, the contributions of others. I am grateful to everyone whom I can not name here.

TABLE OF CONTENTS

	<u>Page</u>
ACKNOWLEDGMENTS	iii
TABLE OF CONTENTS.....	iv
LIST OF TABLES.....	vi
LIST OF FIGURES	vii
LIST OF ABBREVIATIONS.....	ix
LIST OF SYMBOLS	x
ABSTRACT.....	xi
ÖZET	xiii
1. INTRODUCTION.....	1
2. A BRIEF DESCRIPTION OF ELASTIC FIBERS.....	8
2.1. Conventional Spinning Techniques of Elastic Fibers	10
3. EXPERIMENTS	11
3.1. Materials.....	11
3.1.1. Source of the Polymers	11
3.1.2. Source of the Solvents.....	11
3.1.3. Solution Preparation.....	11
3.2. Molecular Weight Determination	12
3.3. Solution Characterization.....	14
3.3.1. Measurement of Solution Viscosity	15
3.3.2 Measurement of Electrical Conductivity of Solution.....	15
3.3.3 Measurement of Surface Tension.....	15
3.3.4. Rheological Properties of PAN & Ac	16
3.4. Electrospinning Apparatus and Process Characterization	17
3.4.1. Measurement of Current and Voltage	18
3.4.2. Measurement of Flow Rate	18

3.4.3. Measurement of Jet Diameter	19
3.5. Wet Spinning.....	20
3.6. Measurement Techniques	21
3.6.1. Atomic Force Microscopy.....	21
3.6.2. Electron Microscopy	22
4. RESULTS AND DISCUSSION	23
4.1. Electrospinning Process	23
4.1.1. Jet Properties	24
4.1.2. Effect of Solution Characteristics on Fiber Diameter	31
4.1.2.1. Viscosity.....	31
4.1.2.2. Conductivity and surface tension.....	33
4.1.3. Effect of Instrumental Characteristics on Fiber Diameter.....	34
4.1.3.1. Voltage.....	34
4.1.3.2. Spinning distance.....	35
4.1.4. Morphology of Nanofibers.....	35
4.1.4.1. Beads.....	38
4.2. Wet Spinning Process and Morphology of Wet-spun Fibers.....	40
4.2.1. Wet Spinning Process.....	40
4.2.2. Surface Morphology of Wet-spun Fibers.....	41
4.3. Comparison of Nano and Micro Fibers.....	44
4.3.1. Diameter Comparison	44
4.3.2. Surface Elasticity.....	46
4.3.3. Roughness Analysis	50
5. CONCLUSION	54
REFERENCES	57

LIST OF TABLES

<u>Table</u>	<u>Page</u>
Table 3.1. Variation of solution characteristics of PU & urea in DMF	14
Table 3.2. Viscosity of PAN copolymer solution for different Ac content, Pa s.	15
Table 4.1: Number of jets with increasing distance, 9,72 wt% PAN & Ac.....	29
Table 4.2. Multiple jet formation as a function of voltage	30
Table 4.3. Roughness comparison of fiber types and morphologies	53

LIST OF FIGURES

<u>Figure</u>	<u>Page</u>
Figure 2.1. Schematic structure of a polyurethane derivatives.....	8
Figure 2.2. Schematic structure of a polyurethane	9
Figure 3.1. Chemical structure of PU & urea and PAN & Ac.....	12
Figure 3.2. Ubbelohde solution viscosimeter	13
Figure 3.3. Determination of average viscosity MWt of PAN & Ac and PU & urea ..	14
Figure 3.4. Rheological characterization of PAN based solutions	16
Figure 3.5. The inverse lifetime for PAN & Ac with 23% of Ac vs. concentration.....	17
Figure 3.6. Geometrical shape of pasteurre pipette	18
Figure 3.7. Electrospinning appararus	18
Figure 3.8. Measurement of jet diameter by laser diffraction pattern	19
Figure 3.9. Wet spinning apparatus	20
Figure 3.10. Nozzle of the needle used in wet spinning.....	21
Figure 4.1. Electron micrograph web image of PU & urea	24
Figure 4.2. The relationship between jet current and the spinning voltage.....	25
Figure 4.3. Comparison of the current value with flow rate.....	26
Figure 4.4. Effect of spinning distance on jet current.....	26
Figure 4.5. Effect of salt concentration on jet current	27
Figure 4.6. Diameter of jet as a function of voltage	28
Figure 4.7. Jet length as a function of spinning distance and applied voltage.....	28
Figure 4.8. Model of multiple jet formation	29
Figure 4.9. Formation of multiple region on Al foil.....	30
Figure 4.10. AFM images of different concentration PU & urea solutions in DMF.....	31

Figure 4.11. AFD as a function of concentration (a) PAN & Ac (b) PU & urea	32
Figure 4.12. AFM images of electrospaying for 2,5wt% PU & urea solution	32
Figure 4.13. AFD as a function of Ac composition in PAN&Ac (a) 9,1 (b) 11,6 wt%	33
Figure 4.14. Synthesis of triethyl benzyl ammonium chloride salts	34
Figure 4.15. AFD as a function of applied voltage	34
Figure 4.16. AFD as a function of spinning distance	35
Figure 4.17. Fiber diameters of 12,8 wt% concentrated PU & urea solution	36
Figure 4.18. Electron micrographs of size distribution in AFD	36
Figure 4.19. Electron micrographs of fiber morphology with (a) without (b) heating	37
Figure 4.20. Electron micrographs of nanofiber morphology	37
Figure 4.21. AFM images of bead formation of 5,2 wt% PU & urea solution	38
Figure 4.22. Electron micrograph of bead free nanofibers from high viscous solution	39
Figure 4.23. AFM images of electrospun fibers from PAN & Ac solutions	39
Figure 4.24. AFD as a function of rpm in wet-spun PU & urea	41
Figure 4.25. AFD as a function of extrusion rate in wet-spun PU & urea	41
Figure 4.26. AFM images of flat (a), fibrillar (b), disordered (c), structure on wet-spun PU & urea fiber surface at 500 μ l/min extrusion, 39 rpm take-up roll	42
Figure 4.27. AFM images of wet-spun PU & urea fiber surface at 666 μ l/min extrusion, 16-rpm take-up roll.	43
Figure 4.28. AFM image of wet-spun PU & urea fiber surface at 666 μ l/min extrusion, 62-rpm take-up roll.	43
Figure 4.29. Section analyses comparison of fiber diameter (a) on Al foil (b) on fiber cross	45
Figure 4.30. Optical microscope images of PU & urea fibers	46
Figure 4.31. Anatomy of force curve	46
Figure 4.32. Force curve of glass slide and parafilm	48
Figure 4.33. AFM sensitivity of different materials	49
Figure 4.34. Roughness comparison of wet-spun and electrospun fibers	52

LIST OF ABBREVIATIONS

AFD	Average Fiber Diameter
AFM	Atomic Force Microscopy
cP	Centipoise
DC	Direct Current
DMAC	Dimethyl acetamide
DMF	Dimethyl formamide
DNA	Deoxyribonucleic acid
dyn	Dyne
HV	High Voltage Generator
MWt	Molecular Weight
PAN & Ac	Polyacrylonitrile acrylic acid copolymer
Pa s	Pascal second
PE	Polyethylene
PEO	Polyethylene oxide
PP	Polypropylene
PU & urea	Polyurethane urea copolymer
PUR	Polyurethane
rpm	Revolution per Minute
SEM	Scanning Electron Microscope
wt	Weight

LIST OF SYMBOLS

η_{rel}	Relative viscosity
η_{sp}	Specific viscosity
ΔZ	Height difference
C	Concentration
F	Force
k	Spring constant of AFM cantilever
m	Meter
S	Siemens
V	Volt

ABSTRACT

In this thesis, two fiber spinning processes were designed and studied; conventional wet spinning and electrospinning which is relatively novel technique. Several process parameters were identified and characterized for both techniques. Diameter, surface roughness, surface elasticity and surface morphology of fibers were characterized using optical, atomic force, and scanning electron microscopes.

The electrospinning process produces nanoscale fibers by applying electrical force to a fiber forming polymer solution. A charged liquid jet was ejected from polymer solution to the grounded conductive sheet. After the solvent evaporation, a nonwoven mat with a porous structure composed of unusually thin fibers was left on the sheet. The effect of the solution and instrumental characteristics on fiber morphology including viscosity, conductivity and applied electrical field strength were investigated. Polyurethane and polyacrylonitrile based polymers were electrospun successfully within a viscosity controlled interval. The diameter of ultrathin fibers was found to depend mainly on viscosity with a power-law relationship. High viscous polyurethane based polymers exhibited curly, wavy and straight structures whereas fibers obtained from low viscous solutions demonstrated beads on strings morphology. Additionally, the nanofibers were not uniform in diameter.

Macroscale fibers were produced by using the wet spinning technique. The polyurethane based polymer solution was extruded into a water coagulation bath through a nozzle. After coagulation, the single elastic filament was dried with air blow and wound up. The effect of two process variables, the rate of drawing and the rate of extrusion, on the fiber diameter were investigated. The rate of drawing was inversely proportional whereas the rate of extrusion was directly proportional to fiber diameter. AFM characterization has shown that the surface of fibers was heterogeneous in nature including disordered, fibrillar, and flat structures. The morphology exhibited on fiber surface did not depend on the two process variables.

Fiber diameters in the range of 7 nm to 150 μm were successfully spun from polyurethane based polymer with electrospinning and wet spinning, respectively. In the electrospinning process, nanoscale diameter fibers were obtained, and these fibers

provided high surface area to volume ratios. Furthermore, it was found that nanofibers obtained from polyurethane solutions have rougher surface than the wet-spun fibers.

In order to compare surface elasticity of two fibers, AFM sensitivity of reference materials (Glass slide, teflon film and parafilm) were examined. Polyurethane based polymer solution was processed with electrospinning, wet spinning and film casting. Parafilm was found to be the softest material and glass slide was the hardest. Elasticities of the materials processed, were found to be between that of glass and parafilm. Electrospun fibers were harder than the film of the same polymer. The stiffness difference between film and electrospun fibers can be explained by the orientation of electrospun fibers due to the electrical force.

ÖZET

Bu tez kapsamında, iki adet lif çekme yöntemi tasarlanmış ve incelenmiştir. İlki geleneksel ıslak çekme yöntemi ve görece yeni bir yöntem olan elektrik kuvvetiyle çekme yöntemidir. Her iki yöntem için de çeşitli parametreler saptanmış ve tanımlanmıştır. Liflerin çap, yüzey pürüzlülüğü, yüzey esnekliği ve yüzey morfolojisi optik, atom kuvveti tarama ve tarama elektron mikroskoplarıyla tanımlanmıştır.

Elektrik kuvvetiyle çekme yöntemi, polimer çözeltisine elektrik kuvveti uygulanarak nano mertebesinde lifler oluşturmaktır. Yüklü sıvı fiskiyesi polimer çözeltisinden, topraklanmış iletken levhaya çekilmiştir. Çözücünün buharlaşmasının ardından, levha üzerinde beklenmedik incelikte liflerden oluşmuş örgüsüz geçirgen kumaş bir yapı elde edilmiştir. Vizkozite, iletkenlik ve elektrik alan şiddeti gibi çözelti ve alet özelliklerinin lif morfolojisine etkileri araştırılmıştır. Lif çaplarının vizkoziteyle üssel bir bağlantısı olduğu görülmüştür.

Makro mertebede lif oluşturan ıslak çekme yönteminde, sıkışarak çıktığı meme ağzından su banyosuna giren polimer çözeltisi havayla kurutularak sarılmıştır. Lif çapı sıkıştırma hızı ile doğru, sarım hızı ile ters orantılıdır. Heterojen lif yüzeyi; düzensiz, lifli ve düz bir yapı içermektedir. Yüzey morfolojisi ile proses değişkenleri arasında bir bağlantı görülmemiştir.

Elektrik kuvvetiyle çekim sonucunda elde edilen lifler ıslak çekme yöntemiyle elde edilenlere göre daha incedir. Ayrıca yüzey alanı hacim oranları beklenmedik düzeyde daha büyüktür. Yüzey pürüzlülüğü elektron itme kuvveti nedeni ile ıslak çekme yöntemiyle elde edilen liflerden daha fazladır.

ELECTROSPINNING AND WET-SPINNING OF ELASTIC FIBERS

by

MUSTAFA M. DEMİR

Submitted to the Graduate School of Engineering and Natural Sciences

In Sabancı University in partial fulfillment of

the requirements for the degree of

Master of Science

Sabancı University

2001

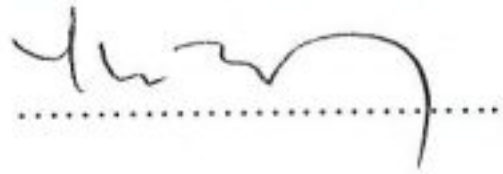
ELECTROSPINNING AND WET-SPINNING OF ELASTIC FIBERS

APPROVED BY:

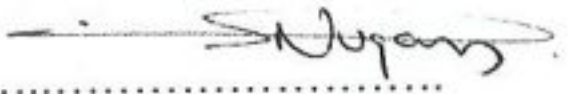
Prof. Dr. Burak Erman
(Thesis Supervisor)



Dr. Yusuf Mencilođlu



Assoc. Prof. Dr. Turgut Nugay



DATE OF APPROVAL:

27/06/2001

ACKNOWLEDGMENTS

Throughout my studies pertaining to the formation of my thesis, an important number of people, academics as well as non-academics, have helped and supported me in various ways. At first, I must acknowledge the contribution of Prof. Dr. Burak Erman, who suggested the topic of my thesis. I would like to present my gratitude to him for having always displayed a concern for my studies. Assoc. Prof. Turgut Nugay also deserves to be cited here, for having encouraged me to pursue an academic career. His careful support has been one of the greatest motivations in my researches. Drs. Yusuf Mencelođlu, Mehmet Ali Gülgün, and Canan Baysal have provided a creative and stimulating atmosphere of learning. Beyond the scope of my thesis, they taught me a lot about science and knowledge. Prof. Dr. Miko akmak has given invaluable advice for designing my research tools. Last, but not least, I would like to thank Cemal Karadayı who produced my research apparatuses. As a gifted technician, he has been amiable and supportive throughout my work.

Finally, I find myself in the pleasurable obligation of expressing my thanks to my love and to my family, whose contributions and supports can not be assessed enough. To finish, this kind of work is never done by a single individual, but by someone who needs, and often receives, the contributions of others. I am grateful to everyone whom I can not name here.

TABLE OF CONTENTS

	<u>Page</u>
ACKNOWLEDGMENTS	iii
TABLE OF CONTENTS.....	iv
LIST OF TABLES.....	vi
LIST OF FIGURES	vii
LIST OF ABBREVIATIONS.....	ix
LIST OF SYMBOLS	x
ABSTRACT.....	xi
ÖZET	xiii
1. INTRODUCTION.....	1
2. A BRIEF DESCRIPTION OF ELASTIC FIBERS.....	8
2.1. Conventional Spinning Techniques of Elastic Fibers	10
3. EXPERIMENTS	11
3.1. Materials.....	11
3.1.1. Source of the Polymers	11
3.1.2. Source of the Solvents.....	11
3.1.3. Solution Preparation.....	11
3.2. Molecular Weight Determination	12
3.3. Solution Characterization.....	14
3.3.1. Measurement of Solution Viscosity	15
3.3.2 Measurement of Electrical Conductivity of Solution.....	15
3.3.3 Measurement of Surface Tension.....	15
3.3.4. Rheological Properties of PAN & Ac	16
3.4. Electrospinning Apparatus and Process Characterization	17
3.4.1. Measurement of Current and Voltage	18
3.4.2. Measurement of Flow Rate	18

3.4.3. Measurement of Jet Diameter	19
3.5. Wet Spinning.....	20
3.6. Measurement Techniques	21
3.6.1. Atomic Force Microscopy.....	21
3.6.2. Electron Microscopy	22
4. RESULTS AND DISCUSSION	23
4.1. Electrospinning Process	23
4.1.1. Jet Properties	24
4.1.2. Effect of Solution Characteristics on Fiber Diameter	31
4.1.2.1. Viscosity.....	31
4.1.2.2. Conductivity and surface tension.....	33
4.1.3. Effect of Instrumental Characteristics on Fiber Diameter.....	34
4.1.3.1. Voltage.....	34
4.1.3.2. Spinning distance.....	35
4.1.4. Morphology of Nanofibers.....	35
4.1.4.1. Beads.....	38
4.2. Wet Spinning Process and Morphology of Wet-spun Fibers.....	40
4.2.1. Wet Spinning Process.....	40
4.2.2. Surface Morphology of Wet-spun Fibers.....	41
4.3. Comparison of Nano and Micro Fibers.....	44
4.3.1. Diameter Comparison	44
4.3.2. Surface Elasticity.....	46
4.3.3. Roughness Analysis	50
5. CONCLUSION	54
REFERENCES	57

LIST OF TABLES

<u>Table</u>	<u>Page</u>
Table 3.1. Variation of solution characteristics of PU & urea in DMF	14
Table 3.2. Viscosity of PAN copolymer solution for different Ac content, Pa s.	15
Table 4.1: Number of jets with increasing distance, 9,72 wt% PAN & Ac.....	29
Table 4.2. Multiple jet formation as a function of voltage	30
Table 4.3. Roughness comparison of fiber types and morhologies	53

LIST OF FIGURES

<u>Figure</u>	<u>Page</u>
Figure 2.1. Schematic structure of a polyurethane derivatives.....	8
Figure 2.2. Schematic structure of a polyurethane	9
Figure 3.1. Chemical structure of PU & urea and PAN & Ac.....	12
Figure 3.2. Ubbelohde solution viscosimeter	13
Figure 3.3. Determination of average viscosity MWt of PAN & Ac and PU & urea ..	14
Figure 3.4. Rheological characterization of PAN based solutions	16
Figure 3.5. The inverse lifetime for PAN & Ac with 23% of Ac vs. concentration.....	17
Figure 3.6. Geometrical shape of pasteurre pipette	18
Figure 3.7. Electrospinning appararus	18
Figure 3.8. Measurement of jet diameter by laser diffraction pattern	19
Figure 3.9. Wet spinning apparatus	20
Figure 3.10. Nozzle of the needle used in wet spinning.....	21
Figure 4.1. Electron micrograph web image of PU & urea	24
Figure 4.2. The relationship between jet current and the spinning voltage.....	25
Figure 4.3. Comparison of the current value with flow rate.....	26
Figure 4.4. Effect of spinning distance on jet current.....	26
Figure 4.5. Effect of salt concentration on jet current	27
Figure 4.6. Diameter of jet as a function of voltage	28
Figure 4.7. Jet length as a function of spinning distance and applied voltage.....	28
Figure 4.8. Model of multiple jet formation	29
Figure 4.9. Formation of multiple region on Al foil.....	30
Figure 4.10. AFM images of different concentration PU & urea solutions in DMF.....	31

Figure 4.11. AFD as a function of concentration (a) PAN & Ac (b) PU & urea	32
Figure 4.12. AFM images of electrospaying for 2,5wt% PU & urea solution	32
Figure 4.13. AFD as a function of Ac composition in PAN&Ac (a) 9,1 (b) 11,6 wt%	33
Figure 4.14. Synthesis of triethyl benzyl ammonium chloride salts	34
Figure 4.15. AFD as a function of applied voltage	34
Figure 4.16. AFD as a function of spinning distance	35
Figure 4.17. Fiber diameters of 12,8 wt% concentrated PU & urea solution	36
Figure 4.18. Electron micrographs of size distribution in AFD	36
Figure 4.19. Electron micrographs of fiber morphology with (a) without (b) heating	37
Figure 4.20. Electron micrographs of nanofiber morphology	37
Figure 4.21. AFM images of bead formation of 5,2 wt% PU & urea solution	38
Figure 4.22. Electron micrograph of bead free nanofibers from high viscous solution	39
Figure 4.23. AFM images of electrospun fibers from PAN & Ac solutions	39
Figure 4.24. AFD as a function of rpm in wet-spun PU & urea	41
Figure 4.25. AFD as a function of extrusion rate in wet-spun PU & urea	41
Figure 4.26. AFM images of flat (a), fibrillar (b), disordered (c), structure on wet-spun PU & urea fiber surface at 500 μ l/min extrusion, 39 rpm take-up roll	42
Figure 4.27. AFM images of wet-spun PU & urea fiber surface at 666 μ l/min extrusion, 16-rpm take-up roll.	43
Figure 4.28. AFM image of wet-spun PU & urea fiber surface at 666 μ l/min extrusion, 62-rpm take-up roll.	43
Figure 4.29. Section analyses comparison of fiber diameter (a) on Al foil (b) on fiber cross	45
Figure 4.30. Optical microscope images of PU & urea fibers	46
Figure 4.31. Anatomy of force curve	46
Figure 4.32. Force curve of glass slide and parafilm	48
Figure 4.33. AFM sensitivity of different materials	49
Figure 4.34. Roughness comparison of wet-spun and electrospun fibers	52

LIST OF ABBREVIATIONS

AFD	Average Fiber Diameter
AFM	Atomic Force Microscopy
cP	Centipoise
DC	Direct Current
DMAC	Dimethyl acetamide
DMF	Dimethyl formamide
DNA	Deoxyribonucleic acid
dyn	Dyne
HV	High Voltage Generator
MWt	Molecular Weight
PAN & Ac	Polyacrylonitrile acrylic acid copolymer
Pa s	Pascal second
PE	Polyethylene
PEO	Polyethylene oxide
PP	Polypropylene
PU & urea	Polyurethane urea copolymer
PUR	Polyurethane
rpm	Revolution per Minute
SEM	Scanning Electron Microscope
wt	Weight

LIST OF SYMBOLS

η_{rel}	Relative viscosity
η_{sp}	Specific viscosity
ΔZ	Height difference
C	Concentration
F	Force
k	Spring constant of AFM cantilever
m	Meter
S	Siemens
V	Volt

ABSTRACT

In this thesis, two fiber spinning processes were designed and studied; conventional wet spinning and electrospinning which is relatively novel technique. Several process parameters were identified and characterized for both techniques. Diameter, surface roughness, surface elasticity and surface morphology of fibers were characterized using optical, atomic force, and scanning electron microscopes.

The electrospinning process produces nanoscale fibers by applying electrical force to a fiber forming polymer solution. A charged liquid jet was ejected from polymer solution to the grounded conductive sheet. After the solvent evaporation, a nonwoven mat with a porous structure composed of unusually thin fibers was left on the sheet. The effect of the solution and instrumental characteristics on fiber morphology including viscosity, conductivity and applied electrical field strength were investigated. Polyurethane and polyacrylonitrile based polymers were electrospun successfully within a viscosity controlled interval. The diameter of ultrathin fibers was found to depend mainly on viscosity with a power-law relationship. High viscous polyurethane based polymers exhibited curly, wavy and straight structures whereas fibers obtained from low viscous solutions demonstrated beads on strings morphology. Additionally, the nanofibers were not uniform in diameter.

Macroscale fibers were produced by using the wet spinning technique. The polyurethane based polymer solution was extruded into a water coagulation bath through a nozzle. After coagulation, the single elastic filament was dried with air blow and wound up. The effect of two process variables, the rate of drawing and the rate of extrusion, on the fiber diameter were investigated. The rate of drawing was inversely proportional whereas the rate of extrusion was directly proportional to fiber diameter. AFM characterization has shown that the surface of fibers was heterogeneous in nature including disordered, fibrillar, and flat structures. The morphology exhibited on fiber surface did not depend on the two process variables.

Fiber diameters in the range of 7 nm to 150 μm were successfully spun from polyurethane based polymer with electrospinning and wet spinning, respectively. In the electrospinning process, nanoscale diameter fibers were obtained, and these fibers

provided high surface area to volume ratios. Furthermore, it was found that nanofibers obtained from polyurethane solutions have rougher surface than the wet-spun fibers.

In order to compare surface elasticity of two fibers, AFM sensitivity of reference materials (Glass slide, teflon film and parafilm) were examined. Polyurethane based polymer solution was processed with electrospinning, wet spinning and film casting. Parafilm was found to be the softest material and glass slide was the hardest. Elasticities of the materials processed, were found to be between that of glass and parafilm. Electrospun fibers were harder than the film of the same polymer. The stiffness difference between film and electrospun fibers can be explained by the orientation of electrospun fibers due to the electrical force.

ÖZET

Bu tez kapsamında, iki adet lif çekme yöntemi tasarlanmış ve incelenmiştir. İlki geleneksel ıslak çekme yöntemi ve görece yeni bir yöntem olan elektrik kuvvetiyle çekme yöntemidir. Her iki yöntem için de çeşitli parametreler saptanmış ve tanımlanmıştır. Liflerin çap, yüzey pürüzlülüğü, yüzey esnekliği ve yüzey morfolojisi optik, atom kuvveti tarama ve tarama elektron mikroskoplarıyla tanımlanmıştır.

Elektrik kuvvetiyle çekme yöntemi, polimer çözeltisine elektrik kuvveti uygulanarak nano mertebesinde lifler oluşturmaktır. Yüklü sıvı fiskiyesi polimer çözeltisinden, topraklanmış iletken levhaya çekilmiştir. Çözücünün buharlaşmasının ardından, levha üzerinde beklenmedik incelikte liflerden oluşmuş örgüsüz geçirgen kumaş bir yapı elde edilmiştir. Vizkozite, iletkenlik ve elektrik alan şiddeti gibi çözelti ve alet özelliklerinin lif morfolojisine etkileri araştırılmıştır. Lif çaplarının vizkoziteyle üssel bir bağlantısı olduğu görülmüştür.

Makro mertebede lif oluşturan ıslak çekme yönteminde, sıkışarak çıktığı meme ağzından su banyosuna giren polimer çözeltisi havayla kurutularak sarılmıştır. Lif çapı sıkıştırma hızı ile doğru, sarım hızı ile ters orantılıdır. Heterojen lif yüzeyi; düzensiz, lifli ve düz bir yapı içermektedir. Yüzey morfolojisi ile proses değişkenleri arasında bir bağlantı görülmemiştir.

Elektrik kuvvetiyle çekim sonucunda elde edilen lifler ıslak çekme yöntemiyle elde edilenlere göre daha incedir. Ayrıca yüzey alanı hacim oranları beklenmedik düzeyde daha büyüktür. Yüzey pürüzlülüğü elektron itme kuvveti nedeni ile ıslak çekme yöntemiyle elde edilen liflerden daha fazladır.

1. INTRODUCTION

Electrospinning is a new technique for fiber formation process, and it provides an alternative to the conventional techniques. The main advantage of electrospinning is the possibility of obtaining fibers with submicron diameter [1]. A high surface area to volume and a higher aspect ratio of fibers generate wide application areas, ranging from textile to composite reinforcement, wound dressing, reaction catalysis, etc.

In melt spinning, one of the conventional techniques, a polymer melt is forced through the spinneret by a pumping mechanism, generally by applying high pressure to the fiber forming polymeric material. Melt spinning processes are broadly applicable to polyolefines, polyesters, and to the whole range of fiber forming polymers. In electrospinning, however, electrical force stemming from the electrical field is the driving force. Electrospinning is applicable to water soluble polymers, biopolymers, and liquid crystalline polymers in the form of both polymer melts [2] and solutions [3].

An electrospinning process takes place by introducing the polymer melt or the solution into an electrical field. A high voltage, DC, power supply, generates the electrical field. The probe charged with voltage is placed into a metallic or glass capillary filled with the fiber forming material. At some distance from the pipette or capillary, a conductive base such as aluminum foil is positioned. Grounding the conductive base completes the electric circuit. The apparatus may be positioned vertically or horizontally. It should be noted that polarity and the type of capillary do not have any effect on the fiber morphology [5].

Upon the application of voltage, the droplet is formed at the end of the tip elongates in the direction of the electrical force. The applied field is around 10^5 Vm^{-1} . Due to the viscosity and surface tension, the drop cannot reach the grounded metallic plate at low voltages. As the voltage is increased, the suspending droplet at the tip starts to be charged with voltage. When the electrostatic and capillary pressure reach equilibrium at any point on the surface of the droplet at the tip, the hydrostatic pressure equates to zero and the half angle at the apex of the cone is equal to $49,3^\circ$ [4]. Gradually increasing the applied voltage makes the electrical force greater than the surface tension

of the droplet. This creates a charged jet to the anode plate [4]. After solvent evaporation, chaotic structures of fibers remain behind.

Following this brief description of the design and process, now the main parameters of the experiment should be stated in two categories. Process variables can be divided into two parts: (i) solution parameters, and (ii) instrumental parameters. Viscosity, dielectric property, conductivity, surface tension are the properties of the fiber forming material; these are the solution parameters [5]. Applied voltage, tip-to-target distance, temperature during spinning, spinning atmosphere can be counted within instrumental parameters. The instrumental parameters have a direct effect on fiber morphology and defect structures [6]. Below, both solution and instrumental parameters are described briefly.

Voltage: Voltage, which is needed for the distortion of the spinning drop and a continuous drawing of fiber, is necessarily related to the solution surface tension and the radius of the drop [4]. Above a minimum value of voltage, a mixture of droplets and fibers come out from the nozzle. Below a minimum value, the electrical force is not sufficient to provoke the jet. As the concentration of the solution increases, a greater force is required to form a jet. The applied voltage is an important determining factor on fiber diameter, jet length and solution feed rate. The solution feed rate influences the diameter and the jet length. A linear relation is observed between the applied voltage and the solution feed rate. The fiber diameter decreases with increasing voltage first and then increases as a function of spinning distance. This effect is caused by the increasing feed rate of the polymer solution through the target with increasing voltage [1,6].

Viscosity: Viscosity is a critical property. Surface tension is the determining factor in case of a low viscosity solution. 1-200 poise is needed for the initiation of a jet without breaking into droplets [6]. Solution viscosity influences fiber diameter, jet length, and determines the droplet shape. Jet length and fiber diameter increase with solution viscosity. As viscosity increases, the spinning drop changes its shape from a hemispherical into a conic one. The diameter of electrospun fibers is proportional to the 0.5 power of viscosity [1].

The jet diameter correlates with the distance between the two electrodes and it decreases with increasing the distance of the apex from the collector plate. Both monomeric and polymeric jets display the same behavior in vertical electrical fields. This behavior is obtained when the aerodynamic tangential drag becomes equal to the sum of the forces due to the electric attraction and gravity.

Spinning atmosphere: This phenomena was investigated by Baumgarten in the PAN / DMF system [1]. At 30% and 40% relative atmospheric humidity, spinning can not be observed because of the precipitation of droplet at the tip. The conductivity of the medium determines the magnitude of the electrical field. In case of Helium, the gas breaks down electrically at 2500V, so no fiber spinning is observed.

Surface tension: The minimization of surface tension is the basic rule for minimizing the energy. Surface tension will be the dominant factor at low viscosity for continuous spinning. For a high viscosity solution, the initiation and continuation of the jet will be prohibited because of the difficulty of controlling the flow rate [6].

Each polymer/solvent system has its own limit of concentration. At high surface tension, bead formation takes place. Bead formation results in the minimization of the surface area; the jet turns into drops. To give an example, the PEO/water system produces fibers with beads. Adding alcohol to aqueous solution without changing the weight percentage of the solution helps to avoid the formation of beads because alcohol increases the solution viscosity and decreases surface tension [7]. Similarly, using chloroform as a lower surface tension solvent prevents the formation of beads on PEO fibers [8]. Both of these effects favor the formation of fibers without beads. Thus, the surface tension of the solvent and the polymer is one of the key factors in the formation of fibers without beads. Lower surface tension is a desirable condition for forming fibers without beads. Volatility of solvent also plays an important role for preventing fibers from beads, because solvents mostly evaporate during their path to the conductive plate. It is useful to mix a solvent with another solvent, which is miscible and volatile.

Charges: Charged particles are sensitive to the electrical field. The charge density of the jet influences the amount of force in a given electrical field. More charged particles disintegrate and dislocate easily than neutral particles. As the net charge density increases, the size of the beads becomes smaller and beads become more spindle-like as a result of electrical force. Thus, the higher the net charge density carried by the jet, the more likely that a smooth fiber will be formed. Adding salt to the solution decreases the bead density.

Net charge density can be computed by the following equation (1.1);

$$\text{Net charge density} = (\text{jet current}) \times (\text{collecting time}) \times (\text{concentration}) \times (\text{Solution density/Mass of dry polymer}) \quad (1.1)$$

Neutralization of charges reduces the influence of electrical force on the jet, so that the jet loses its charge and beads appear on fiber [7].

Beads: Beads are the usual side products in electrospinning process. These can be considered as a defect that is formed during the process and stem from both solution parameters and the applied voltage. Regularly spaced droplets of similar or alternative sizes may form along the fiber. The diameters of the droplets are about 1-5 μm [9]. The instability of the polymer liquid jet under the electrical field creates such kind of undesirable morphology. Uncontrolled flow rate of solution, viscosity, net charge density carried by jet, concentration and the surface tension play important roles in the formation of bead-on-string structures on electrospun fibers. Beads, observed commonly, disturb the uniformity along the fiber and decrease the surface area to volume ratio of electrospun fibers. Size of the beads and the distance between them are also important variables. Balancing surface tension by changing the type of solvent, concentration or viscosity prevents the formation of beads.

Fluid transportation takes place with charge transport from tip to the conductive plate. Increasing the current between the electrodes transports more polymer solution flow to the anode. The current versus voltage graph may give us a clue about the formation of beads. A change in the slope of the plot indicates a change of electrospun fiber morphology. An aqueous solution of 4-10 % with 400,000-g/mol PEO system initiates electrospinning jet at 5,5kV. No beads are formed at this voltage. Beads begin to appear on fibers at 7 kV. Bead formation becomes common at 9 kV. Monitoring the spinning current can control bead defect density. Balancing feed rate to the tip and flow rate from the tip is needed for preventing the formation of beads [6].

The rest of this section, electrospinning literature will be reviewed in a historical order. The followings are main claims of some important papers.

Disintegration of liquid surface in strong electrical fields studies date back to Zeleny [10]. He claimed that the instability of electrified liquid surfaces occurs when the internal pressure is the same as that of the outside the drop. This assumption was corrected by Taylor who has shown that the 'instability of a drop would not occur unless a pressure difference existed' [11].

Fiber spinning resulting from the instability of polymeric liquids in electrical fields was first patented in 1938 [12]. Theoretical and experimental activities in this area first came from Taylor. A conducting liquid exists in equilibrium only when the semivertical angle is $49,3^\circ$ under the electrical field [4]. This angle is the balance of

surface tension and electrical forces. Taylor also calculated the critical electrical potential needed to form a cone of liquid. Behaviors of conducting and non-conducting liquids were identified. Conducting liquids produce a fine jet whereas non-conducting fluids throw off a drop [4,11].

Two years later, Baumgarten electrospun acrylic resin in DMF [1]. He showed the electrical field maps and the important role of conductivity in the spinning mechanism. Electrical field lines have also been mapped with systems containing more than one High Voltage Generator (HV) [8,13]. Baumgarten also made the first attempts to calculate the spinning velocity and the effects of parameters on fiber diameter and jet length. The velocity of spinning was found to be very close to the velocity of the sound in air and the fiber diameter increased approximately as the 0,5 power of solution viscosity. Coming to the eighties, Larrondo and Manley electrospun PE and PP from the pure melt. They observed that the thinner fibers can be drawn from the higher melt temperature. They also pointed out that macromolecule orientation due to the electrical force is similar to the situation in conventional spinning technique [2]. Birefringence due to the orientation of molecules was also noted in electrospinning of solutions [14-17].

Reneker and his coworkers contributed invaluable insights to this research area. Reneker and Srinivasan obtained highly oriented nanofibers from liquid crystal polymer, poly (*p*-phenylene terephthalamide) [14]. Reneker and Doshi set and characterized the electrospinning process [5]. Fang electrospun calf thymus Na-DNA, and compared the oriented wet spun DNA fiber [18]. Kim produced, and characterized nonwoven fabrics of polybenzimidazole [16]. Fong and Chun showed the characterization of the formation of electrospun beaded nanofiber [7]. Elastomeric nanofiber of styrene-butadiene-styrene triblock copolymer from tetrahydrofuran and DMF solution was electrospun by Fong [17]. A biocompatible protein thin film, silk-like polymer, was processed with electrospinning by Buchko. He also proposed the shish kebab model for the filament morphology for electrospun fibers [19]. Chun reported the usage of conductive electrospun nanofibers in electromechanical device [15]. Carbon nanofiber from polyacrylonitrile was produced as an alternative way to obtaining conductive nanofiber [20]. Conductivity values for ultrathin conductive fibers were first reported by Norris and his co-workers [21]. PEO, which is known as an easily soluble and crystallizable polymer in aqueous solutions, has been used for setting the optimum conditions and characterization of fibers [5-9]. Ordered surface layer resulted

from electrospinning process and monoclinic crystal phase of PEO (7/2 helix) was characterized by scanning probe microscopy [9]. Kim and Lee studied thermal properties of electrospun polyesters before and after the process. The thermal properties before and after the electrospinning process were found to be unequal. Crystallinity increased, and glass transition temperature decreased after electrospinning [22].

The permeability of porous thin film structure was studied with the comparison of polyacrylonitrile and polybenzimidazole electrospun membrane with commercial membrane laminate. It was found that pore size on random nature of the electrospun fiber deposition can exclude macroparticles [23]. Vansco has electrospun of nylon-4,6 fibers in formic acid solutions and prepared transparent composites with an epoxy matrix [24]. Deitzel et al. specially investigated the effects of process variables on the morphology of electrospun nanofiber. They conducted a systematic study on the effects of spinning voltage and concentration. Bimodal distribution of fiber size was seen at high concentration. They also noted a very good comparison between droplet generation in electrospray, and fluid jet generation in electrospinning [6]. Ring electrode connected to the second HV and placed near the drop has minimized the characteristic electrospinning instability. After the focusing of the electrical field line into the system, a single continuous aqueous solution of PEO jet may spin as a single electrospun filament [13]. The mathematical model of bending instability of charged jets were developed and described by Reneker and Yarin [25]. Bognitzki and his co-workers have obtained nanofiber from polylactide in dichloromethane. They dissolved approximately 1,5 wt% tetraethylbenzylammonium chloride within this polymer solvent system. The addition of salt to the polylactide solution caused significant decrease in fiber diameter [26]. They also produced nanometer fibers with diameter in the range of 10-100 nm. The significance of their work is being able to adjust the size of the pores between nanofibers [27].

As the above quick literature review suggests, electrospinning is a relatively recent technique of fiber spinning. The technique works with over 30 different polymer solvent systems. In the current project, the electrospinning of polyurethane derivative/DMF and polyacrylonitrile derivative/DMF, polymer solvent systems were studied. The rationale behind in preferring polyurethane derivatives was to electrospin ultrathin elastic fibers. No research was found in the available literature. Annual production of elastic fibers by conventional techniques is around tens of thousands of tons around the world. Therefore, elastic fiber production has importance from both

technological and scientific point of view. Secondly, polyacrylonitrile based polymers, which contain acrylic acid groups, were studied. Ionically associating groups, which control the orientation of fibers, make the polymer a reversible gel. Hence it is a new approach in fiber forming polymers. Hopefully, this project sets the ground for fibers, with original properties.

2. A BRIEF DESCRIPTION OF ELASTIC FIBERS

J.C. Shivers was the first to prepare elastic fibers from linear polymers consisting of alternating segments connected through urea or amide linkages. In the 1940s, the IG-Farben Company developed Perlon U from polyurethane, a nonelastic fiber like rayon. Elastic fiber obtained from (PUR), "Lycra", was developed by Du Pont in 1959.

The polyurethane elastic fiber, in fact, is a copolymer made of hard and soft segments. The soft segments provide rubber-like elasticity whereas the hard segments increase polymer strength. These segmented polymers may be represented by the by the formula shown in Figure 2.1.



Figure 2.1. Schematic structure of a polyurethane derivatives

where I represents diisocyanate, and A represents diamine. The sequence I-I-I corresponds to soft segments and IA IA IA corresponds to hard segments. Hard segments contain both a cyclic structure and hydrogen bonds coming from urethane. Hydrogen bonding between chains and cyclic groups on the backbone make the segment relatively stiff [28].

In the polymerization process, a high molecular weight diol polytetramethyleneoxide (PTMO) reacts with isocyanate to prepare end-functionalized prepolymer. Prepolymer is converted into high molecular weight polyurethane by a chain propagating group that contains an active hydrogen compound (In this project, the chain propagating group is (DYTEK) 3-methyl-1,5-diaminohexane). The urea and urethane bonds coming from diamine and diol, respectively, produce hard segments in this reaction.

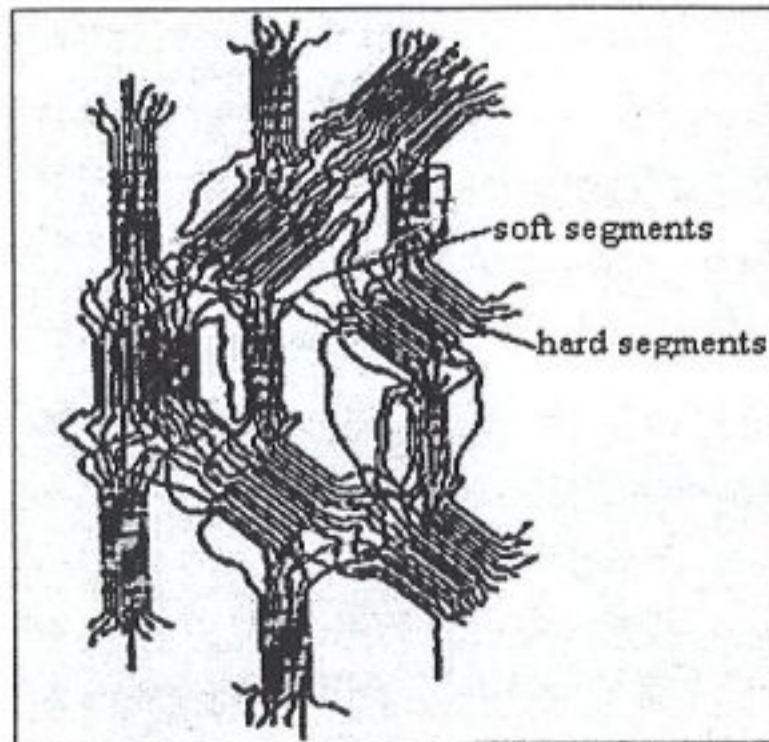


Figure 2.2. Schematic structure of a polyurethane

Polyurethane (PUR) was first synthesized in 1937 [29]. In Figure 2.2, the schematic structure of a polyurethane elastomer in a low drawn state is presented. These highly elastic yarns have a breaking elongation of over 200%, preferably over 400%, and recover immediately and almost completely to the original state if tension is removed. PUR based fibers are obtained by three techniques: wet, dry and reaction spinning. Wet spinning is the most complex process among them. Spinning of PU & urea by electrospinning is the major part of this project. The dry spinning process is considerably simpler than the wet spinning process. Today more than 80% of the spandex¹ [30] produced by dry spinning technique because no after-treatment is required.

There are two methods of wet spinning, one uses a solution of the final polymer and the other uses a prepolymer. The former method will be explained in the wet spinning section 4.2. In the latter, on the other hand, the solution of prepolymer is extruded into the diamine solution where chain propagation takes place. Therefore, this spinning method is often called reaction spinning.

Electrospinning allows the production of nanoscale elastic fibers. Styrene-butadiene-styrene triblock copolymer in tetrahydrofuran and DMF solution was

¹ It is an elastomeric fiber that can be stretched up to five times its original length without being damaged. It is lightweight and flexible. It resists deterioration from perspiration, detergent and body oils. It is characterized by its strength and durability. Main uses are athletic wear and foundation garments [31].

electrospun successfully. Elastic and birefringent nanoscale fibers were produced. A thin sheet of nonwoven fibers was elongated three times of its original length [17].

Simons first electrostatically spun a polyurethane filament from a solution of methyl ethyl ketone in 1966. The successful range of viscosity was between 100 to 3000 centipose. He inserted electrodes within a pattern on a grounded belt. Electrodes were maintained at a potential that repelled the coming fibers. Controlled pattern structures resulted in the aggregation of fiber bundles. As a result, different pattern structured thin mats were obtained [32].

2.1. Conventional Spinning Techniques of Elastic Fibers

Dry spinning: "In dry spinning, a polymer solution is extruded from a spinneret through a zone in which the solvent is rapidly evaporated, leaving filaments that are wound up at speeds up to about 1000 m/min. Before extrusion, the solution is heated to a temperature just above the boiling point of the solvent. The evaporation zone consists of a vertical enclosed cell 3-10 m high, into which heated gas is blown. Because the viscosity of the polymer solution is a function of temperature, solution temperature at the extrusion point is a very important factor in this method. In solvent removal, an inert gas such as nitrogen may be used for oxidation sensitive fibers." [30]

Reaction Spinning: "It involves a chemical reaction to convert a derivative of a polymer into the original polymer. The term reaction is normally reserved for cases in which the viscous liquid extruded into the bath is a prepolymer of relatively low molecular weight, possibly but not necessarily in solution, and the bath contains a reagent that rapidly reacts with the prepolymer to form a high molecular weight." [30]

The most important example of reaction spinning is the production of certain segmented polyurethane elastomeric fibers. The prepolymer is the source of the soft segment of the final polymer. A very rapid reaction between amine and isocyanate groups happens in the bath, which contains a diamine. The product of this reaction is a polymer with urea linkages. The internal structure of the polymer remains incompletely cured and further steps are required to complete polymerization [28].

3. EXPERIMENTS

3.1. Materials

3.1.1. Source of the Polymers

Polyurethane & urea copolymer has been synthesized by Professors İskender and Emel Yilgor of Koç University, and polyacrylonitrile & acrylic acid copolymers have been synthesized in the Laboratory of Professor Khokhlov, Laboratory of Physical Chemistry of Polymers, Moscow University. Both polymers, used in the electrospinning experiments, have been processed as received. Dimethylformamide (DMF) has been used as a solvent in both cases.

Polyurethane and polyacrylonitrile based polymer solutions came in DMF solution at concentrations of 21,2 wt% and 23,0 wt%. Their viscosity molecular weights were 70,000 g/mol and 110,000 g/mol respectively. Their chemical structures are shown in Figure 3.1.

3.1.2. Source of the Solvents

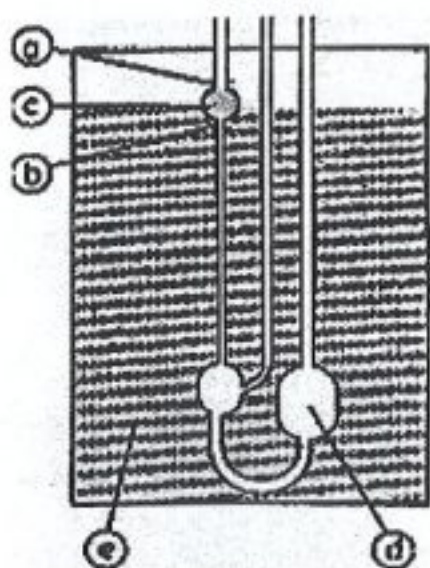
DMF (Diedel-de Haen) and DMAC (Akkim) have been used as solvents without any purification. Tap water, containing 1,7 wt% acetone, was used as a coagulation solvent.

3.1.3. Solution Preparation

Six different polyurethane & urea solutions have been prepared from 21,2 wt% concentrated solutions. Dilution has been made with DMF Riedel-de Haen. Solution concentrations were 17,7; 15,0; 12,8; 10,1; 5,2; 3,8; 2,5 wt% for polyurethane & urea.

In the polyacrylonitrile based polymer, five different solutions have been prepared from 23wt% solutions, with concentrations of 14,9; 11,6; 9,1; 6,4 and 3,3 wt%.

The samples have been gently stirred at least 3 hours before electrospinning to obtain a homogenous solution. Care was taken to isolate the solution from humidity, because both of the polymers used in the experiment coagulate under the effect of



Relative viscosity, $\eta_{rel} = \eta/\eta_0 \approx t/t_0$

Inherent viscosity, $\ln \eta_r / C$

Specific viscosity, $\eta_{sp} = (\eta_r - 1)$

Reduced viscosity, η_{sp} / C .

Figure 3.2. Ubbelohde solution viscosimeter

where η_r is the relative viscosity, η is the velocity of solution, η_0 is the viscosity of the solvent, t is the flow time of the solution, t_0 is the flow time of the solvent, C is the concentration of the stock solution, and η_{sp} is the specific viscosity

The inherent viscosity and reduced viscosity are plotted as a function of concentration, and the intercept is considered as the intrinsic viscosity of the solution. In Figure 3.2., (a) and (b) are calibration marks, (c) volume for determination, (d) solution storage, (e) constant temperature bath [29]. The molecular weights (MWt) of synthesized PU & urea and PAN & Ac copolymers were characterized by viscometer in Figure 3.3.

The viscosity average molecular weights M_η of two polymers were determined according to the following Mark-Houwink equation (3.1):

$$[\eta] = K M_w^a \quad (3.1)$$

The Mark-Houwink constants K and a are extensively tabulated for a wide variety of polymer-solvent systems and temperatures.

For PU & urea: $\eta = 72 \text{ dl/g}$, $K = 101 \times 10^{-4}$ $a = 0,59$, 70.000 g/mole

For PAN & Ac: $\eta = 115 \text{ dl/g}$, $K = 1,77 \times 10^{-4}$ $a = 0,78$, 110.000 g/mole

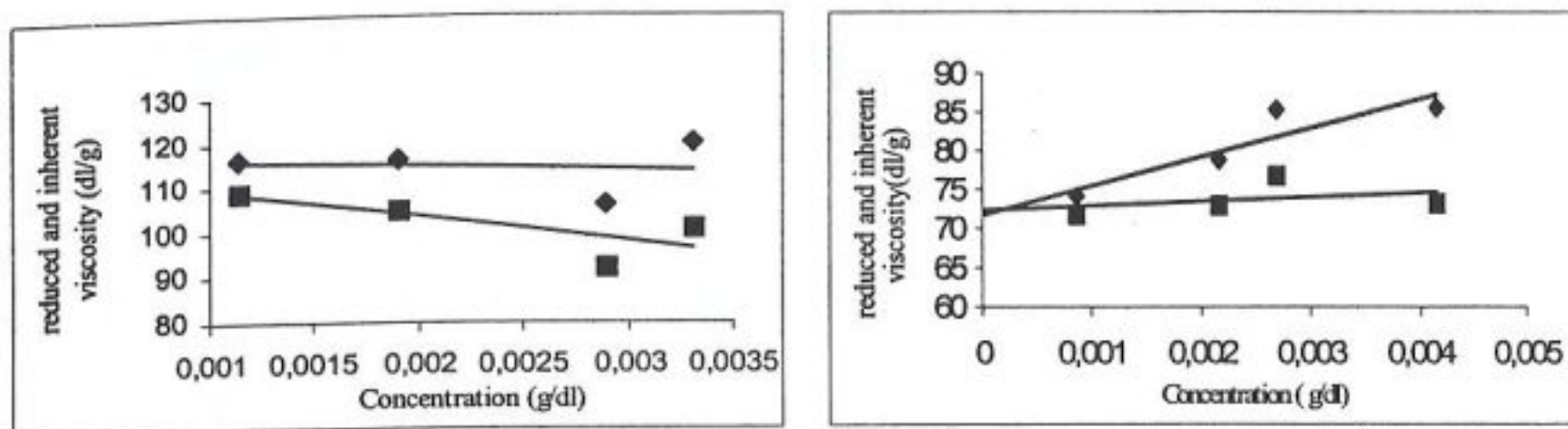


Figure 3.3. Determination of average viscosity MWt of PAN & Ac and PU & urea

3.3. Solution Characterization

Solution viscosity, electrical conductivity, and surface tension properties were determined. Viscosity and electrical conductivity were measured at 25 °C, and surface tension were measured made at 40 °C.

Table 3.1. Variation of solution characteristics of PU & urea in DMF

Concentration (wt %)	Viscosity (cP)	Surface Tension (dyn / cm)	Conductivity ($\mu\text{S} / \text{cm}$)
12,8	1630,0	31,70	7,6
10,1	496,0	31,75	6,4
5,2	32,5	31,40	6,3
3,8	15,3	31,37	4,0
Pure Solvent (DMF)	-	32,40	3,3

Solution properties of DMF solutions of PU & urea were measured, and are shown in Table 3.1. Surface tension of the solutions remained nearly constant because it depends on the type of polymer and solution. After a critical concentration, concentration does not change the surface tension more. Conductivity of the solution changes with concentration but no significant change was observed. Adding polymer to the solution increases the conductivity of solution.

Solution properties of DMF solutions of PAN & Ac copolymer were measured and recorded in Table 3.2. Adding more Ac to the polyacrylonitrile based polymers lowered the viscosity of the solution beyond 5 wt%.

Table 3.2. Viscosity of PAN copolymer solution for different Ac content, Pa s.

Copolymer concentration (wt %)	Ac content(mol %)			
	5.300	7.350	11.700	16.200
5	0.048	0.032	0.038	0.037
10	0.480	0.224	0.390	0.335
20				

3.3.1. Measurement of Solution Viscosity

Bulk viscosity of the solution was measured by using Brookfield, Model DV-II+. 1st, 2nd and 3rd spindles were used for having an exact measurement. Temperature was kept constant at 25°C. For 12,8 wt% solution, the 3rd spindle was used with rotational speeds of 12, 60 and 100 rpm. The measurements were performed with different spindles. Three measurements were recorded to determine an average ratio.

3.3.2 Measurement of Electrical Conductivity of Solution

Electrical conductivities of solutions were measured using a hand held conductometer, Hanna instruments, Model HI 8633. Measurements were repeated two times and average values were determined. The probe was cleaned with solvent between each measurement to avoid inaccurate reading resulting from the strong tendency of the polymer to form a thin film on dry surfaces.

3.3.3 Measurement of Surface Tension

The surface tensions of the solutions were measured using a Petrotest Digital-Tensiometer K10ST. Platinum ring method was used to measure the surface tension of the solutions. The ring was immersed into solution, and then slowly drawn out of the solution. The force required to take the ring out against the tension was measured.

Experiments were repeated two times at 40°C and average values determined. The platinum ring was cleaned after each measurement to avoid experimental error.

3.3.4. Rheological Properties of PAN & Ac

Rheological properties of PAN copolymer solutions in DMF with different content of acrylic acid in PAN chains were studied. Rheometer Rheostress RS150-L (HAAKE GmbH) was used for viscosity measurements. A special device, which allows to monitor the change of the rheological properties of polymer solutions at different copolymer concentrations, was used for determining the concentration of gelation [33]. In this device the droplet of the polymer solution is placed between the two surfaces as shown in Figure 3.4. When the surfaces are moved apart, a thin filament is formed from this droplet of solution. The lifetime was measured as a function of concentration.

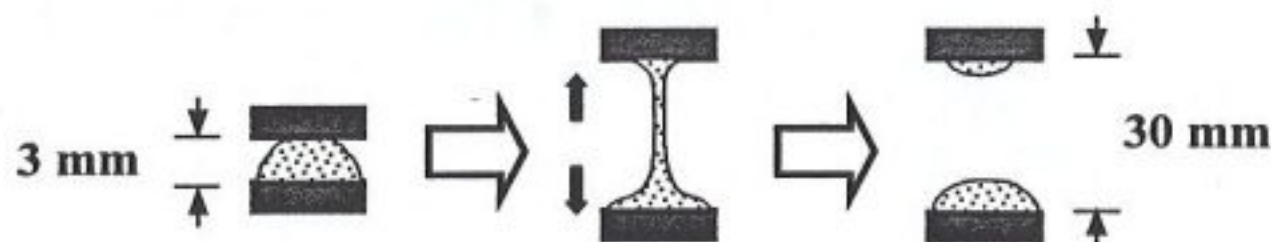


Figure 3.4. Rheological characterization of PAN based solutions

Ionically associating PAN & Ac, copolymers of acrylonitrile with acrylic acid was dissolved in organic solvents, such as N,N-dimethylformamide. This copolymer forms associative gels. The reason for this is the formation of ion pairs between counter ions and negative charges on polymer chains in organic medium. The fiber from copolymer of PAN & Ac formed after spinning of such gel should have ionic inclusions. Therefore the incorporation of polar compounds into such fiber (to obtain functional fibers) is possible.

The lifetime, from the moment of a filament formation to the moment of its rupture, was measured by means of special optical scheme. A typical dependence of the inverse lifetime of this filament on the copolymer concentration for PAN with 23 wt. % of Ac is shown in Figure 3.5.

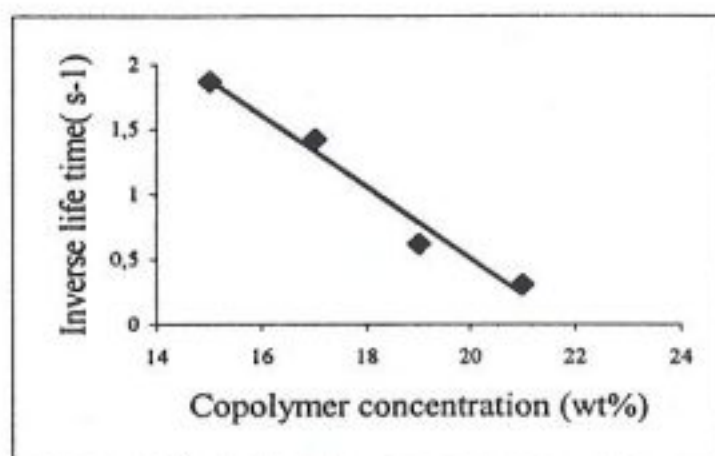


Figure 3.5. The inverse lifetime for PAN & Ac with 23% of Ac vs. concentration

The lifetime for this sample becomes infinite at the 22 wt% concentration of the copolymer. At this concentration the copolymer solution forms a physical gel. The viscosity of PAN copolymer solutions in DMF with different Ac content were measured. The results are shown in the Table 3.2. There is an exponential increase of the copolymer viscosity with the increase of their concentration in DMF. Physical gels were observed for the copolymer concentrations higher than 22-wt. % for all the Ac contents in PAN chains.

3.4. Electrospinning Apparatus and Process Characterization

A high voltage generator, with an output voltage of 50 kV maximum at 500 μ A, was used for direct current (D.C.) power supply. For safety reasons, specially selected HV produced microscale current along with high voltage. A pasteurre pipette was filled with the fiber forming polymer solution, and the high voltage generator probe was inserted into the solution. A conductive sheet was located opposite and perpendicular to the nozzle of the pasteurre pipette. The pipette was tilted a few degrees from horizontal so that surface tension maintained a small droplet of the solution at the tip without dripping. The image of the pipette is shown in Figure 3.6.

The electrospinning apparatus consists of an adjustable stand insulated with rubber sheet. Metal parts were kept at a minimum during the construction of the apparatus. Metal parts were coated with Teflon seal to prevent charge accumulation and static discharge. In addition, the apparatus was kept dry in order not to conduct electricity. This apparatus is represented in Figure 3.7.

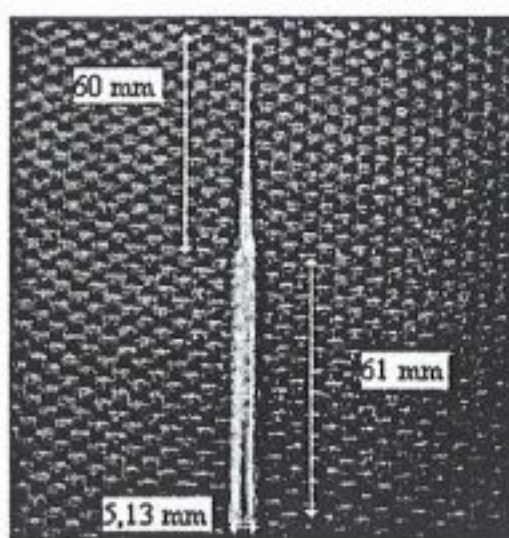


Figure 3.6. Geometrical shape of pasteur pipette

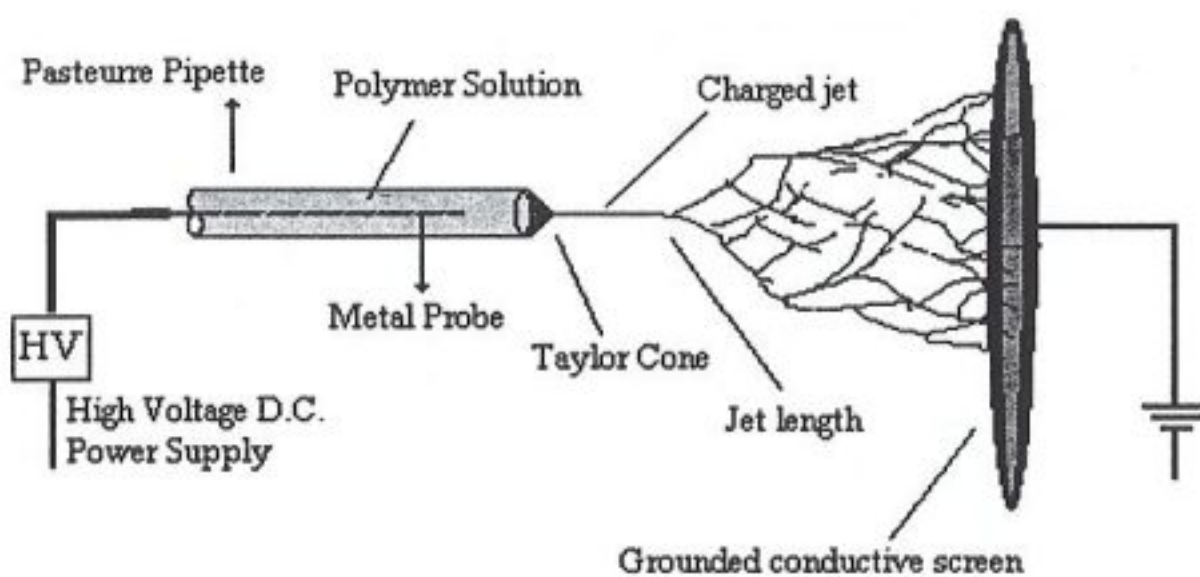


Figure 3.7. Electrospinning apparatus

3.4.1. Measurement of Current and Voltage

CPS High voltage power supply (Model 2594) produces up to 50 kV output voltage with a maximum current at 500 μ A. The applied voltage to the system was measured with an independent 5V power supply. Simple connection with BNC receptacles on the front panel was used for both voltage and current measurements. A Pasco scientific galvanometer was used for taking current data.

3.4.2. Measurement of Flow Rate

An aluminum sheet was used for grounding. It was easily used and disposable. Mass difference of the aluminum sheet before and after electrospinning gave the amount of fiber deposited during spinning after solvent evaporation. Time of deposition was

also recorded. Mass difference divided by the measured time gave the approximate mass flow rate.

3.4.3. Measurement of Jet Diameter

The jet consists of an initial straight segment, which then breaks into several subjects (See Figure 3.7.). The diameter of the jet becomes thinner, as a result of solvent evaporation and continuous stretching due to the electrical field. Jet diameter was calculated by using a 632,8 nm laser light beam which was positioned perpendicularly to the jet. As the laser beam bombarded the jet, diffraction patterns formed on a screen as shown in Figure 3.8. All measurements were done in complete darkness to see the diffraction properly. By increasing the electrical potential, keeping all the other parameters constant, the measurements were repeated. The distance between the first order diffraction maxima was measured.

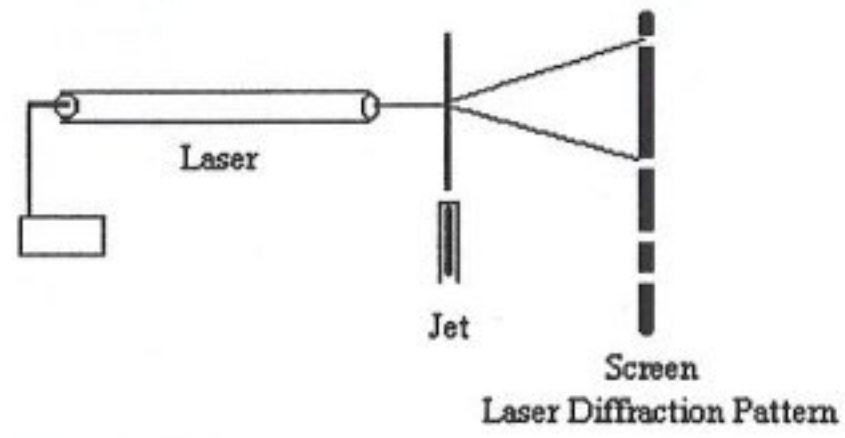


Figure 3.8. Measurement of jet diameter by laser diffraction pattern

The diameter of the fiber is obtained from the following expression, equation 3.2,

$$\text{Jet Diameter} = (2 m \lambda X) / l_m \quad (3.2)$$

where m is the order of diffraction, λ the wavelength of the laser light, X the distance between the jet and the screen on which the pattern was observed, and l_m the distance between the maxima [34].

3.5. Wet Spinning

Wet spinning is a conventional fiber production technique better known than electrospinning. It is a more complex method than the other known techniques such as melt spinning, dry spinning, etc. In wet spinning, choosing coagulant according to the solvent is the most significant parameter in determining fiber morphology, cross-section geometry and diameter. The main process parameters are polymer solution concentration, rate of extrusion, rate of drawing, temperature and composition of the nonsolvent bath. The wet spinning apparatus used in the present work is shown in Figure 3.9.

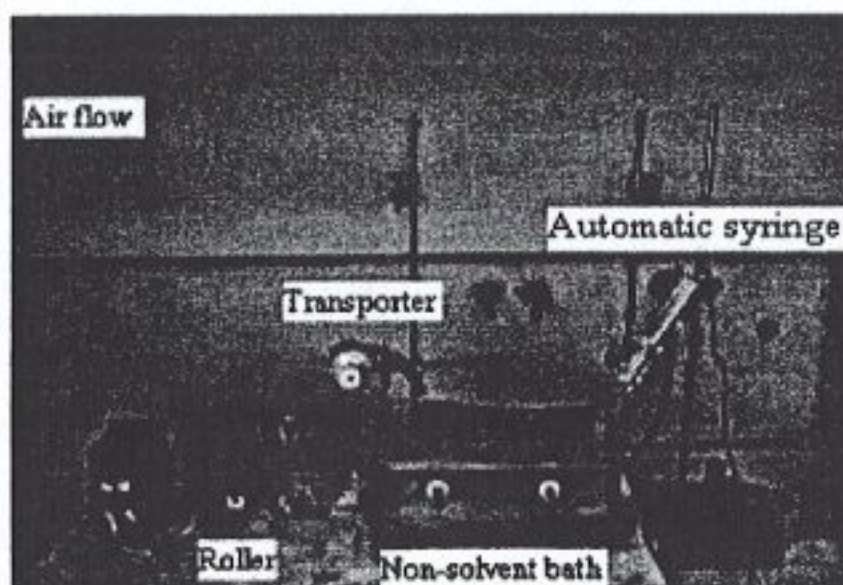


Figure 3.9. Wet spinning apparatus

An automatic syringe, Hamilton 801 syringe, is the main part of the apparatus. It produces pulse free continuous flow within a range between $0,1\mu\text{l} / \text{min}$ to $100\mu\text{l} / \text{min}$ of polymer solution into the non-solvent bath through the needle of the syringe. The solvent of the polymer solution is miscible with the nonsolvent in the bath, 3200 cm^3 . The polymer coagulates in the nonsolvent bath. The single filament that goes through the bath is transferred onto a roller on teflon bearings by hand. A $0,25\text{ W}$ motor, shown in Figure 3.9 controls the angular speed of the roller. Both the motor and the controlling machine (micromaster 6SE92) are products of Siemens. The rotating pin of the motor was covered with 3 cm diameter cylindrical teflon. Teflon was preferred due to its inertness to the probable organic chemicals in the nonsolvent bath.

A third bearing (transporter in Figure 3.9.) was added to transfer the filament to the rolling by motor to help the relieve some of the stress on the filament.

Continuous airflow at a temperature of approximately 50°C and a speed of 500 l/min is supplied to remove the solvent and the nonsolvent on the filament. At the end, dry yarn is rolled on the spindle of the motor. The nonsolvent was water and polymer solution was PU & urea in DMF. The polymer solution was observed to coagulate slowly in the nonsolvent bath. To increase coagulation rate, a small amount of acetone (1,7 wt%) was used in the nonsolvent bath. Solvent free fiber was rolled onto the teflon coating.

The experiments were conducted at room temperature. A 5-ml, 45 mm graduated glass syringe was used for wet spinning. The needle of the syringe was 115 mm long. The nozzle of the needle, which is known as spinneret, is shown in Figure 3.10.

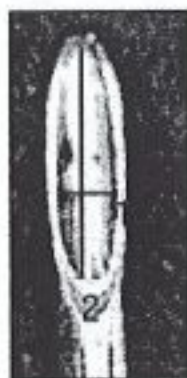


Figure 3.10. Nozzle of the needle used in wet spinning

The end of the needle that defines the geometry of the spinneret was in the form of an ellipse, shown in Figure 3.10 with the minor axis(1) $\approx 500 \mu\text{m}$, and the major axis(2) $\approx 2000 \mu\text{m}$.

For the photographic study, an Intel web camera was employed. 3,33 x 2,50 inch images were obtained by 20 frames/second with connection to the computer.

3.6. Measurement Techniques

3.6.1. Atomic Force Microscopy

Atomic force microscopy was used for the characterization of fiber surfaces. The basic working principle of AFM is to measure the force between material surface and the AFM tip. The measurements were carried out with a Nanoscope III (Digital instruments, Inc., Santa Barbara, CA, USA) in both tapping and contact mode. Si and Si_3N_4 tip were used for tapping mode and contact mode respectively. The spring constant of the cantilever was in the range of 20-100 N/m for Si tip, 0,3 N/m for Si_3N_4

tip. Experiments were carried out with the E-type scanner in air at room temperature. The scanner has a maximum scanning area of $17 \times 17 \mu\text{m}^2$.

AFM measurements were performed in two modes. Contact mode has been used to plot the force curve of material and Tapping mode has been used to obtain phase differences on material surface. The explanation of two modes are following:

Contact mode: The probe tip simply slides on the sample surface. Height difference and frictional force are measured by the help of piezo crystal. The resulting image is a topographical map of the sample surface. This technique has been applied successfully to many samples. It is the only technique by which one can obtain "atomic resolution" images. In addition, tip is able to scan at high speeds, unlike in tapping mode. However, it has some serious drawbacks. Lateral or, in other words, shear forces of tip occurred during the scanning of the sample may distort the image quality. Also, sliding process damages the sample surface and the probe tip.

Tapping mode: Tapping mode technique solves these problems and offers a new characterization method that outputs height, amplitude and phase signal. It provides high resolution by oscillating the tip on the sample surface to avoid the lateral forces stemming from the contact mode [36].

For wet spun fibers, filament specimen with a length of 1 cm were cut from individual filaments and fixed on sample holder without any surface pretreatment. The tip was placed on the fiber without touching it. Tapping mode of AFM was used instead of contact mode. The direction of fibers in the AFM images was vertical or parallel direction to the scan direction. Scan size is more than five times smaller than the fiber diameter even if scan area is adjusted to maximum.

Electrospun fibers were characterized with AFM using the tapping mode. Section analysis has been used for measuring the exact diameter of nanofibers and surface roughness from Nanoscope software.

3.6.2. Electron Microscopy

Two different makes of scanning electron microscopes were used for characterizing electrospun fibers. They were an FEG (Gemini/LEO) SEM, (LEO, Oberkochen, Germany) and XL30 SFEG SEM, (FEI, Eindhoven, the Netherlands).

4. RESULTS AND DISCUSSION

4.1. Electrospinning Process

Electrospinning is a unique technique to obtain ultrathin fibers by the help of electrical field. The main advantage of this technique is being able to obtain nanoscale fibers with high surface area to volume ratio. Furthermore, fibers obtained by this technique form a nonwoven fabric with a porous structure. In order to obtain a fiber, the polymer used in the process should have the fiber forming characteristics. In the series of experiments that were conducted within this project, six different polymers were tried to obtain nanofibers by electrospinning. However, only polyurethane & urea and polyacrylonitrile & acrylic acid copolymers were found to be successful in electrospinning. Polyacryamide & nonylmethacrylate copolymer, polyvinylalcohol & adipoyl chloride copolymer, hydroxypropyl cellulose and 3-hydroxyalkanoates did not form fibers in electrospinning in the present project. It is important to note that cellulose and polyester derivatives were among the unsuccessful polymers, although these are known to be fiber forming by conventional techniques (For instance, cellulose is the oldest fiber known to humans). There are some other restrictions that affect fiber formation in electrospinning. Solution properties should be within required boundaries for the fiber forming polymers.

Electrospinning set-up is a simple circuit, as shown in Figure 3.7. A high voltage generator produces voltages up to 50 kV with microscale direct current for safety. HV probe is inserted into the fiber forming polymeric solution, which is in a small glass pipette. After an air gap, a grounded conductive sheet is positioned opposite and perpendicular to the nozzle of the pipette. A uniform electrical field is created between the nozzle and the grounded sheet when the voltage is applied to the system. As the applied voltage increases gradually, the drop at the nozzle of the pipette turns from spherical into conical shape. When the electrical force overcomes the cohesive surface tension at a threshold voltage, a charged liquid jet is ejected from the drop to the grounded sheet. In other words, the circuit is closed with a current that is formed by

mass transfer from the nozzle to the target. After solvent evaporation, a nonwoven material is left on the grounded sheet. (See Figure 4.1)

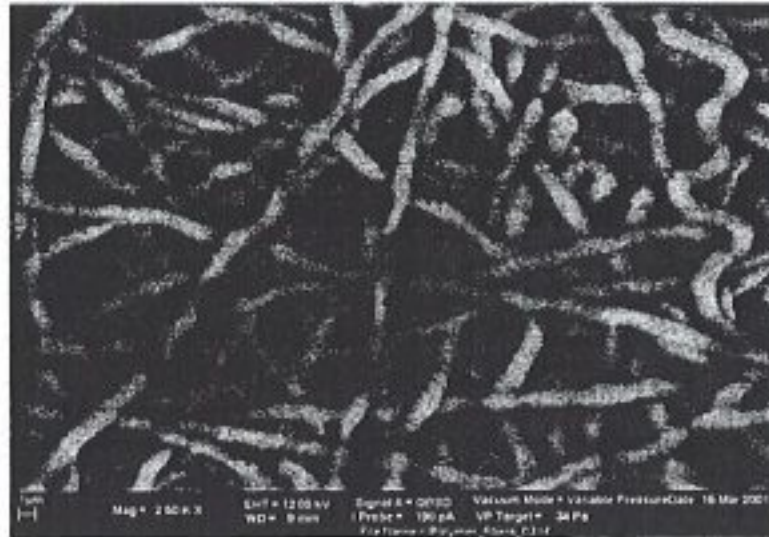


Figure 4.1. Electron micrograph web image of PU & urea

The first major attempt of the research is to determine the spinning concentration range of the polymer solutions and to see the effect of process parameters on fiber morphology. Process parameters are (i) solution and (ii) instrumental parameters. Solution parameters are chosen as viscosity, conductivity and surface tension. Instrumental parameters are chosen as the applied voltage and spinning distance. Spinning distance is the distance between the nozzle of the pipette and the grounded sheet. Process parameters affect the liquid jet properties. Thus, jet properties were examined as a function of solution characteristics and instrumental variables.

4.1.1. Jet Properties

Jet properties are the general and important parameters of electrospinning. These are jet current, jet length, jet diameter, and jet character.

Jet Current: Jet current is the transport of the electrons, which is a measure of the mass flow from nozzle to the target. Jet current depends on many parameters like conductivity of solution, electric field strength. Conductivity of the solution is the main parameter. Like in electrical circuits, a conductive wire can pass more electrons compared to a resistant one. The electrical field created between the nozzle and the ground, related to the applied voltage and the spinning distance, is another significant factor. Jet current increases with an increase in electrical field strength, which is a result of increasing applied voltage or decreasing spinning distance. According to Ohm's rule, the current depends on both the voltage applied and the resistivity. Voltage has a linear

relationship with current. Resistivity is the slope of the I versus V curve. In electrospinning, jet current increases as the third power of the spinning voltage, as shown in Figure 4.2. In order to see the exact effect of voltage on jet current, the spinning distance was held constant in our experiments. With higher voltage, a higher number of electrons migrate to the grounded sheet. Figure 4.2 shows the change of current as a function of voltage for 3,8 wt%, 10,1 wt%, 12,8 wt% PU & urea solutions, respectively. Non-ohmic behaviour was observed in electrospinning circuit, the resistance decreases with an increase in voltage.

Mass of the conductive sheet was recorded before and after electrospinning. A significant change was observed with increasing the voltage. This provides us a rough knowledge of the mass migrated from the tip to the grounded sheet. Results of the 3,8-wt% PU & urea solution flow rate, and the current versus voltage plot are presented in Figure 4.3, where voltage is 9,4 kV and the spinning distance is 8 cm. Both mass flow rate and current demonstrate nearly power law dependence on the applied voltage.

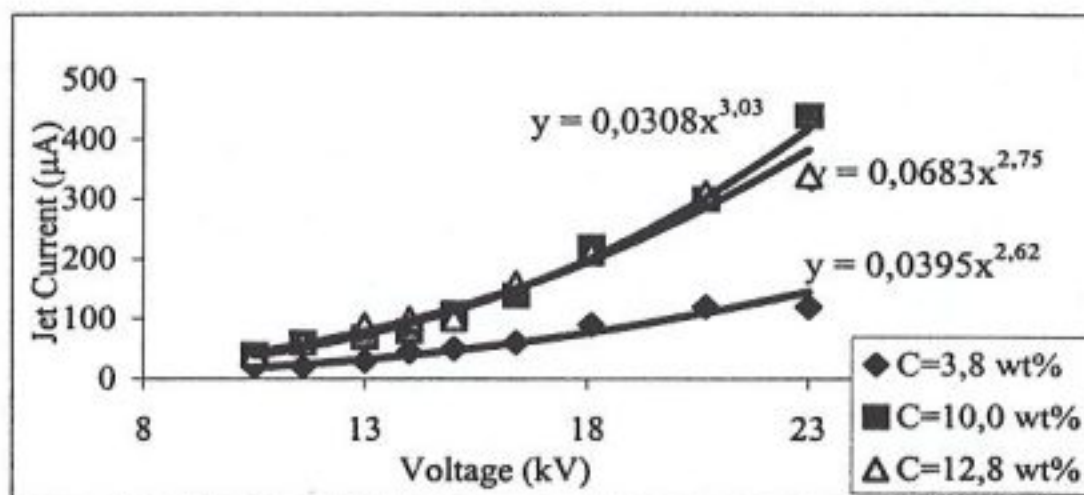


Figure 4.2. The relationship between jet current and the spinning voltage.

It is important to say that the amount of polymer solution reaching the anode was usually less than the ejected amount of solution from the drop. Losses may originate due to various sources: The charged fibers ejected from the drop may reach the metal part of the set-up instead of the grounded sheet. Current loss takes place because of the improper insulation of the set-up tools. Thus, the number of electrons reaching the anode is less than those provided by the power supply. Therefore, initial four data in the first graph of Figure 4.3 are not taken into account. These points can be explained as experimental errors because of mentioned reasons.

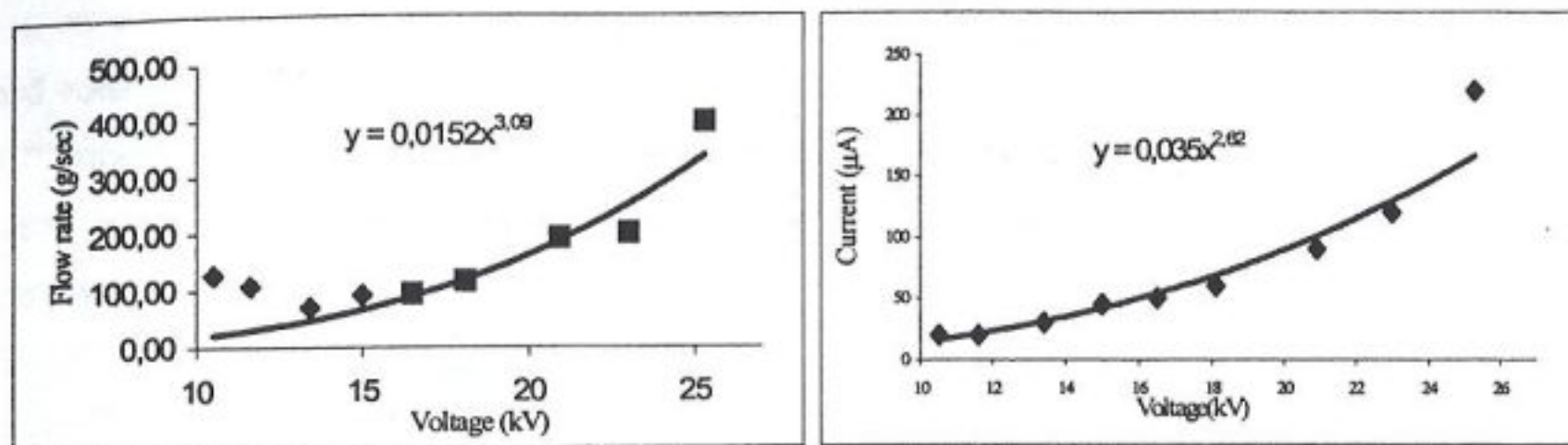


Figure 4.3. Comparison of the current value with flow rate

Electrical field strength is defined as the ratio of applied voltage to spinning distance, an increase in voltage and a decrease in spinning distance increase the electrical strength. Decreasing the electrical field results in decreasing the number of electrons migrating from tip to the ground. In order to see the effect of distance on jet current, the applied voltage and concentration were held constant. Nearly one and a half-negative power law relationship were found between current and spinning distance. In Figure 4.4, the effect of spinning distance on jet current is presented, ((a) 5,2 wt% PU & urea solution when the applied voltage was 13 kV, (b) 6,4 wt% of PAN & Ac when the voltage was 12,5 kV).

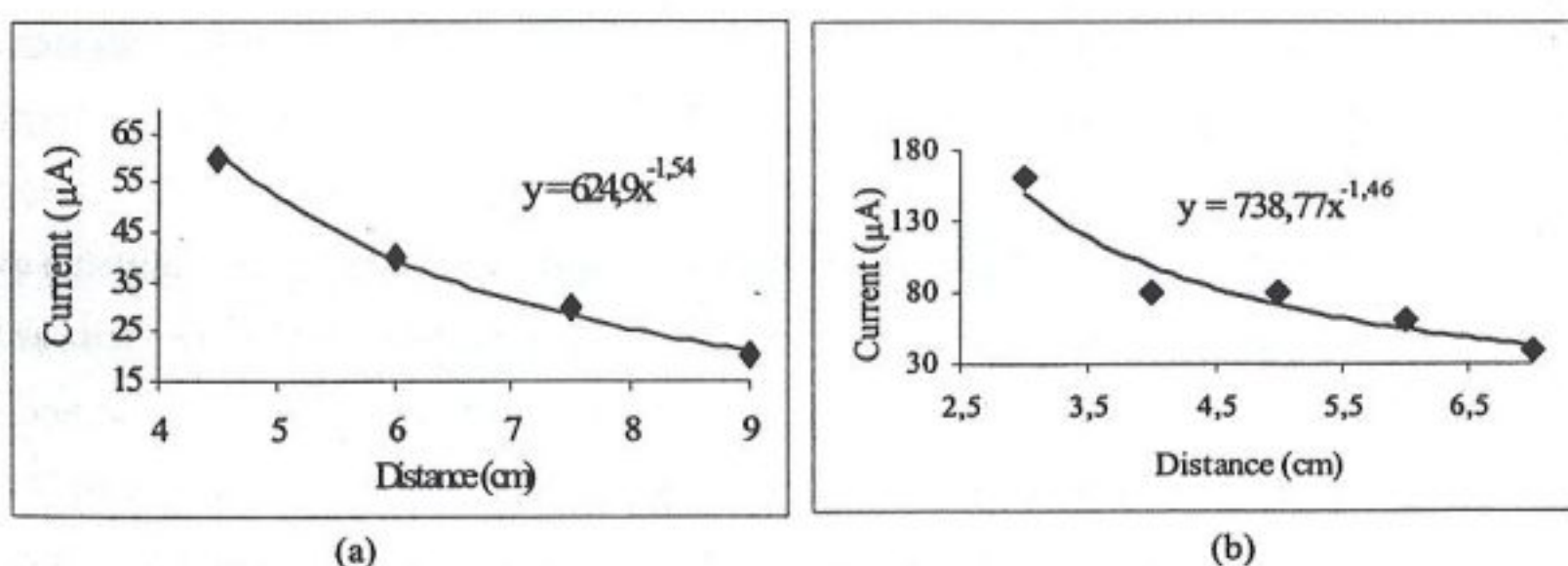


Figure 4.4. Effect of spinning distance on jet current

To see the effects of conductivity, a small amount of triethyl benzyl ammonium chloride was added to the solution. The effect of salt concentration on the jet current

was investigated in terms of concentration where the applied voltage and distance were held constant. It was found that conductivity increases with salt concentration, as shown in Figure 4.5. Our main purpose for adding salt was to change the solution properties and to have the effect of morphological changes of nanofibers. No significant change was observed.

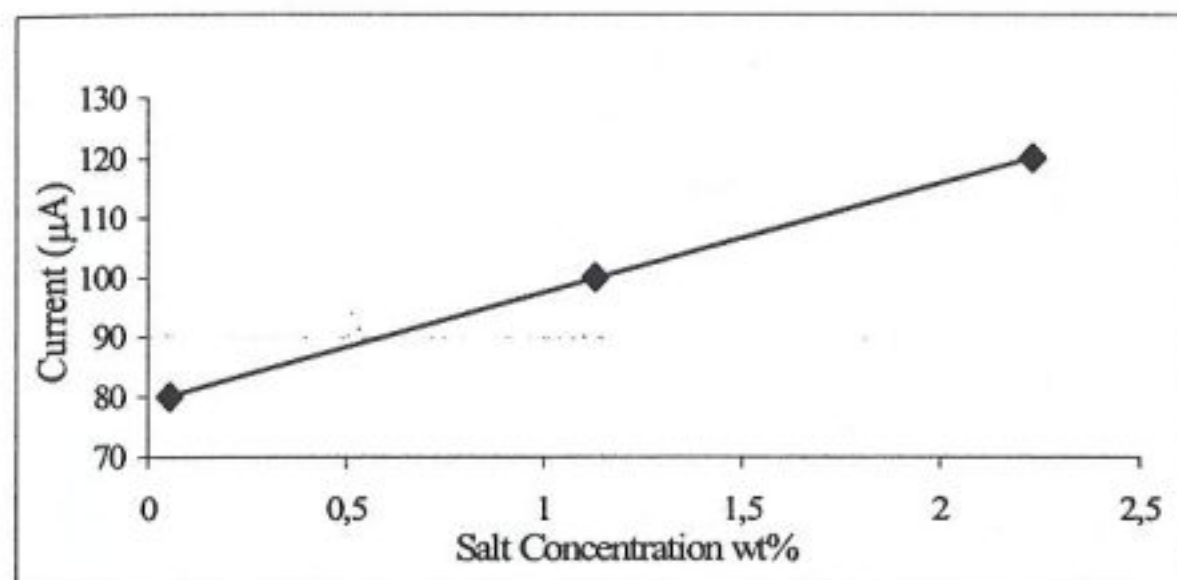


Figure 4.5. Effect of salt concentration on jet current

Jet Diameter: Migration of electrons with the polymer solution affects the fluid jet character. The jet becomes thinner as it travels in air due to both solvent evaporation and continuous electrical force stretching [5]. As a result, the charge density on the jet increases so the jet breaks up into many subjects because of charge repulsion. This feature of the jet is known as splaying. In our experiments, the diameter of the jet was measured by laser diffraction. The distance between two nodes was taken into account to calculate the jet diameter. The concentration of solution was 3,8 wt% PU & urea, and the distance between the capillary and the screen was set to 8 cm. As the electrical potential was increased, the diameter of the jet also increased. The measurements were recorded at a given position nearly 5mm away from the nozzle of the pipette. When the applied voltage was increased from 8,4 kV up to 15 kV, the jet diameter increased from 4,56 μm to 6,02 μm , (Figure 4.6). The details of calculations are specified in the section 3.4.3.

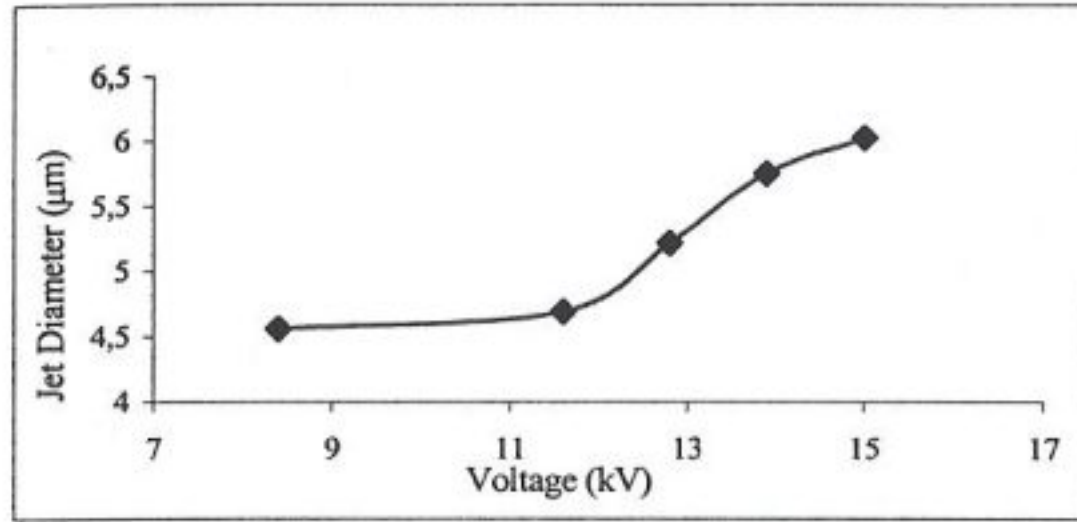


Figure 4.6. Diameter of jet as a function of voltage

Jet Length: The distance between the drop and the critical point where the jet breaks is known as the jet length. It varies with the applied voltage and the spinning distance.

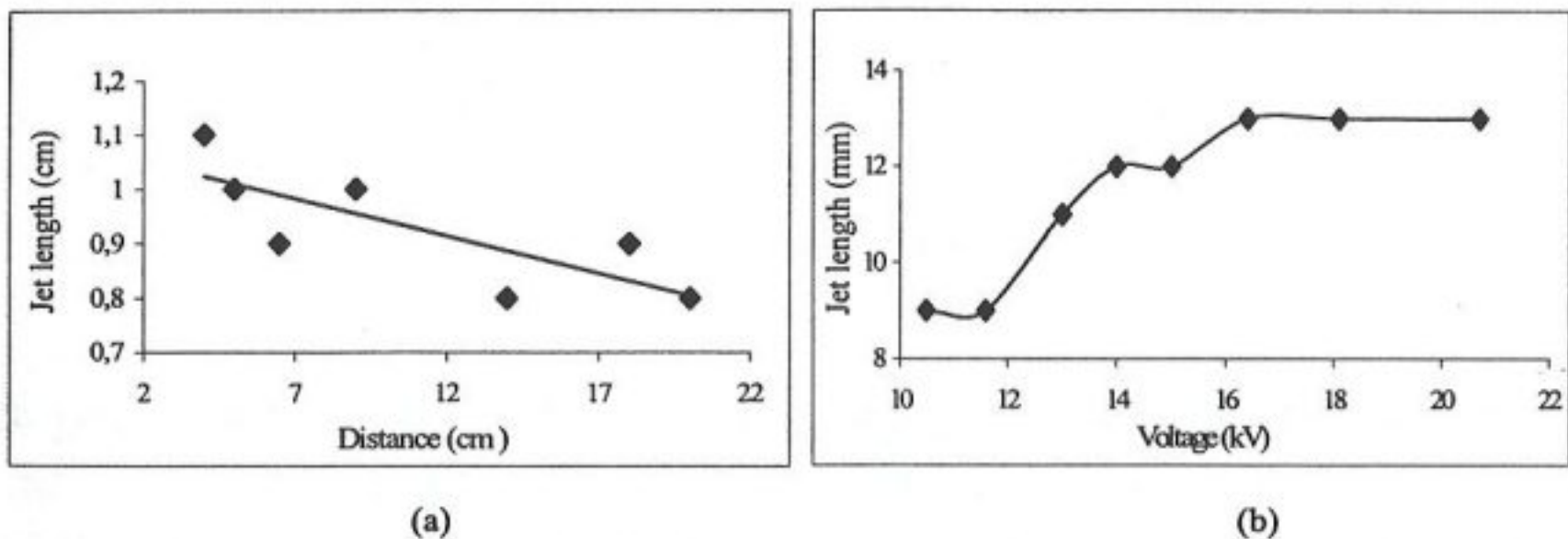


Figure 4.7. Jet length as a function of spinning distance and applied voltage

The results of the jet length for 12,8 wt% concentrated PU & urea is shown in Figure 4.7. The current increased with the third power of the applied voltage. Velocity of electrons moving to the ground increased as well as the current. The electrical force resulting from the electrical field accelerates the polymer solution, according to Newton's second law. The jet length stabilises at a threshold voltage above which it remains constant. For the same applied voltage, a decrease in distance increases the jet

length as a result of increasing electrical field strength. Jet length is inversely proportional to the spinning distance.

Jet Character: The character of the jet can be seen by naked eye if the background is black and a good source lights up the path of the jet. In the experiments, more than one jet was formed at high electrical field. Since electrical field strength is defined as the ratio of applied voltage to spinning distance, an increase in voltage and a decrease in spinning distance increase the number of jets. Viscosity also affects behaviour of the jet. An electrospaying phenomenon, droplet formation, occurs for low viscosity solutions whereas electrospinning, charged liquid jet, takes place for high viscosity solutions. The three conditions for the formation of multiple jets are (i) short distance (ii) high voltage (iii) low viscosity (Figure 4.8).

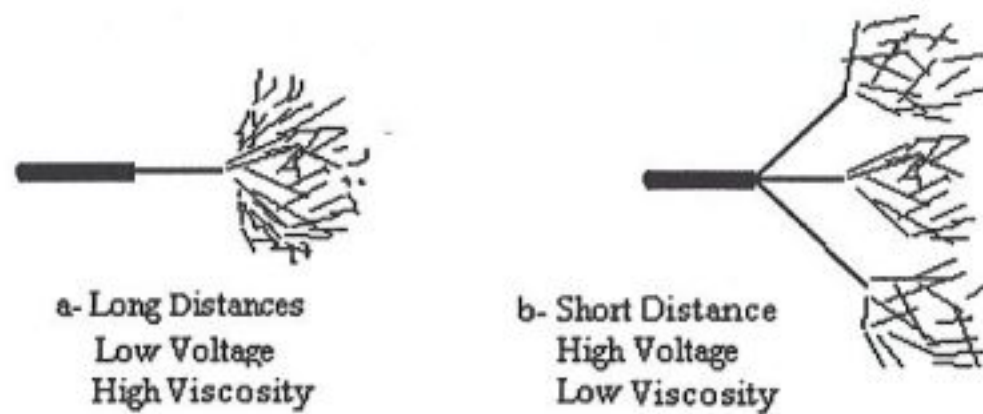


Figure 4.8. Model of multiple jet formation

(i) Effect of spinning distance on jet character: A jet ejected from the solution as a consequence of electric field always has an umbrella shape, Figure 4.8. The main jet splits into many subjects due to electrostatic charge repulsion. Transport of the polymer solution with the help of electrons usually creates more than one identical jet. The results are shown in Table 4.1.

Table 4.1. Number of jets with increasing distance, 9,72 wt% PAN & Ac

Distance (cm)	Number of Jets
3	5
4	3
5	3 or 4
6	1 or 2
7	1 or 2

Figure 4.9 shows the basic features of the electrospinning process. PAN & Ac solution with 9,72 wt% concentration was electrospun when the applied voltage was 12,5 kV. It is easy to see the well-separated areas with fibers on the target foil. The number of these filled areas coincides with the number of observed jets during electrospinning.

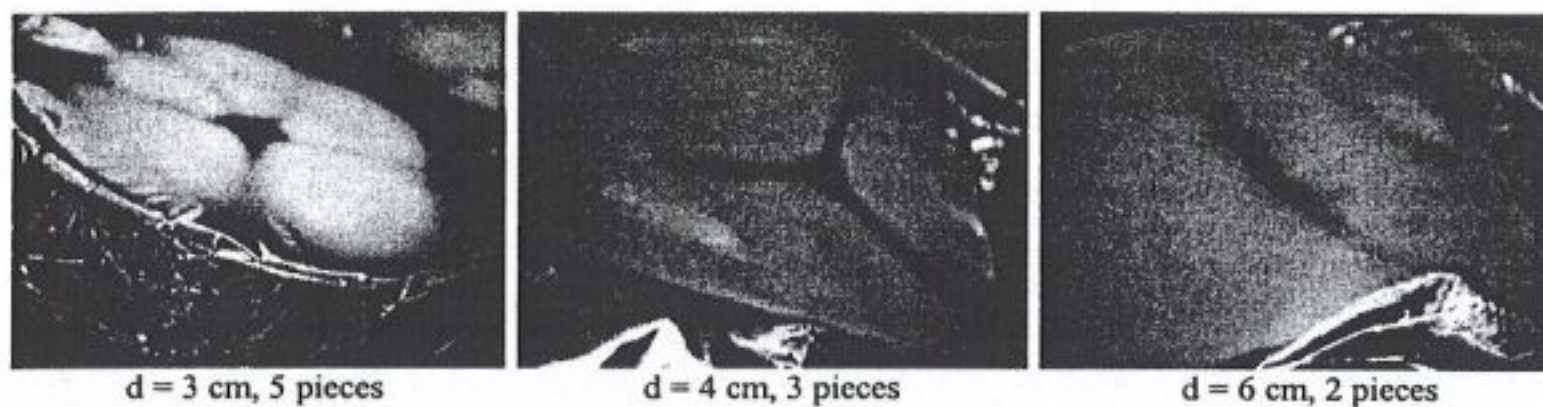


Figure 4.9. Formation of multiple region on Al foil

(ii) Effect of applied voltage on jet character: The number of liquid jets was found to increase when the applied voltage increases. Also, the angle between the jets becomes larger and the jet length gets longer. Mass transport increases gradually when the applied voltage increases. Increasing voltage, initially, accelerates the charged jet due to increasing electrical force. Further increase of the voltage favours the formation of several jets. The jets repel each other due to the flowing charge on their surface so they distribute themselves with a larger angle.

Table 4.2. Multiple jet formation as a function of voltage

Voltage (kV)	Number of jets
6,4	1 - 2
7,4	2
8,7	2 - 4
10,1	3 - 4
11,4	4
12,8	4 - 5
15,0	4
18,0	5 - 6
21,0	5 - 7
25,0	6 - 7

Multiple jet formation as a function of applied voltage can be seen in Table 4.2. (5,2 wt % PU & urea and spinning distance was 8 cm)

(iii) **Effect of viscosity on jet character:** The most concentrated solutions for both copolymers exhibited single jet, 12,8 wt % for PU & urea and 14,9 wt % for PAN & Ac. For low viscous solutions multiple jet formation took place.

4.1.2. Effect of Solution Characteristics on Fiber Diameter

4.1.2.1. Viscosity

Different concentrated solutions were prepared to study the effect of viscosity on fiber diameter. In polyurethane-based polymers, the solution was 21,2 wt% concentration at the beginning. Jet formation was not observed until 12,8 wt% which is the upper limit of viscosity interval. 3,8 wt % solution was the lower limit of viscosity interval of PU & urea. However, an electrospaying phenomenon takes place below the lower limit. Figure 4.10 shows a series of the height images of the nanofiber obtained from four different PU & urea concentration solutions, (a) 12,8; (b) 10,1; (c) 5,2; (d) 3,8 wt%. All images have 17 μm scan size in order to be able to compare the diameters. These images point that diameter increases with an increase in viscosity.

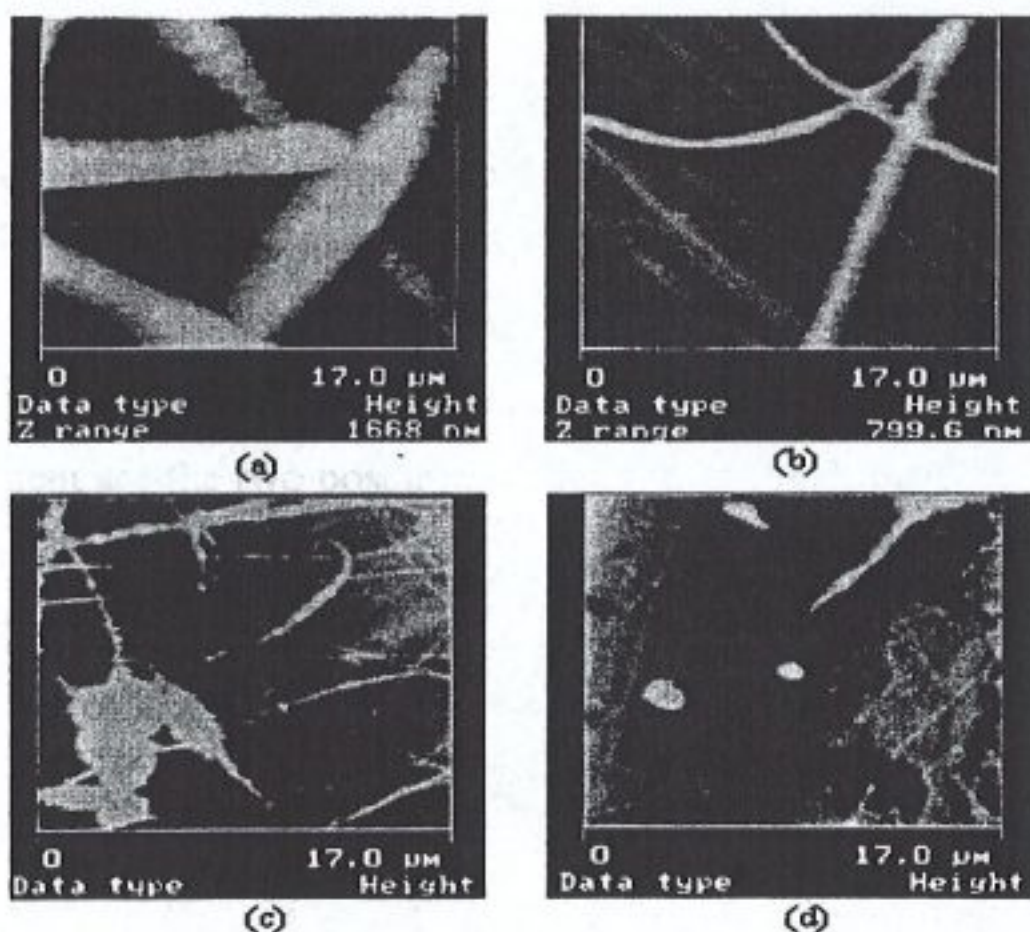


Figure 4.10. AFM images of different concentration PU & urea solutions in DMF

The fiber diameter changes from nearly 10 nm to 1-micron. The applied voltage and the spinning distance were kept constant at 9,4 kV and 9 cm respectively.

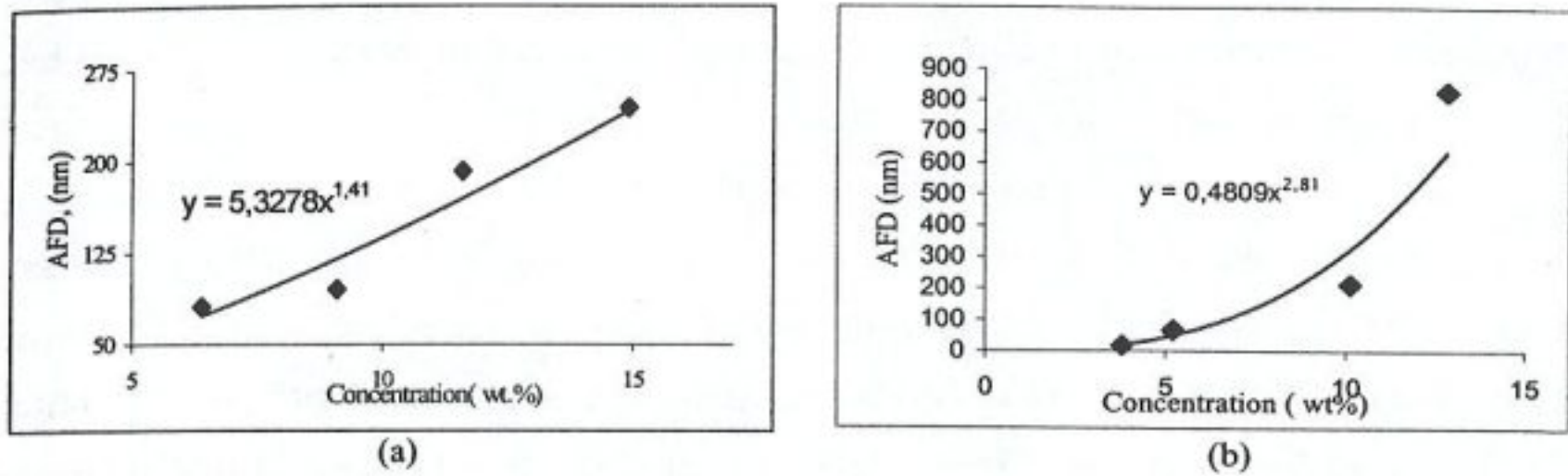


Figure 4.11. AFD as a function of concentration (a) PAN & Ac (b) PU & urea

AFD as a function of concentration is shown in Figure 4.11. A power law relationship was observed for two polymer/solvent systems. If solution properties were investigated, it could be seen that viscosity of polymer solution changes dramatically with concentration (Table 3.1). Hence, viscosity has a dominant effect on fiber diameter.

Similar results were obtained for PAN & Ac and appropriate concentration range was 14,9 – 6,3 wt %. The type of polymer/solvent system plays an important role in determining upper and lower boundaries of solution.

The jet breaks up into droplets at low viscosity solutions. This is known as electrospaying. Charged droplets take place instead of charged fibers as can be seen from AFM images of 2,5 wt% of PU & urea solution (Figure 4.12). Surface tension and molecular entanglement are the two possible factors for jet breaking.

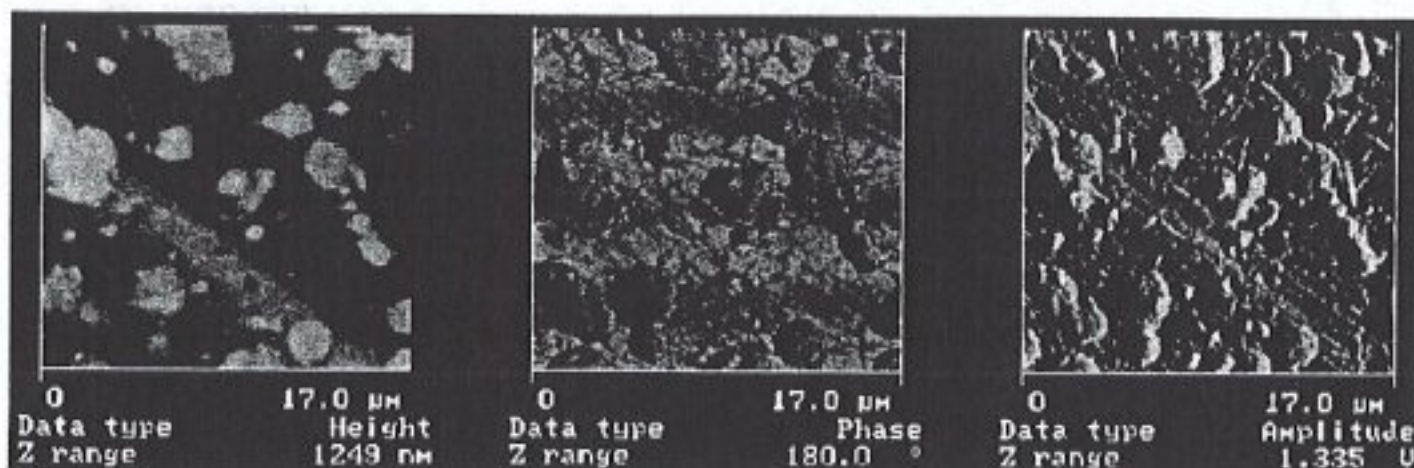


Figure 4.12. AFM images of electrospaying for 2,5wt% PU & urea solution

High molecular weight chains favor a continuous jet in the electrospinning process. There is a lower limit for observing this effect and it is called critical entanglement concentration. 2,5 wt% PU & urea and 3,3 wt% PAN & Ac are lower than the critical entanglement concentration so polymer chains can not even touching each other. Therefore a continuous jet was not obtained.

Amount of acrylic acid monomer in polyacrylonitrile chain varies the viscosity of the solution in Table 3.2. Effect of Ac content on nanofiber diameter was also investigated. Four different solutions with same weight concentrations were prepared which contains different acrylic acid content; as 5, 7, 8, 10 wt% (Figure 4.13). The process was conducted for two different levels of solution concentrations; 9,1 wt% and 11,6 wt%. Spinning distance and applied voltage were held constant for all solutions during experiment. AFD was found to decrease with increasing Ac content for both concentrations because of decreasing viscosity.

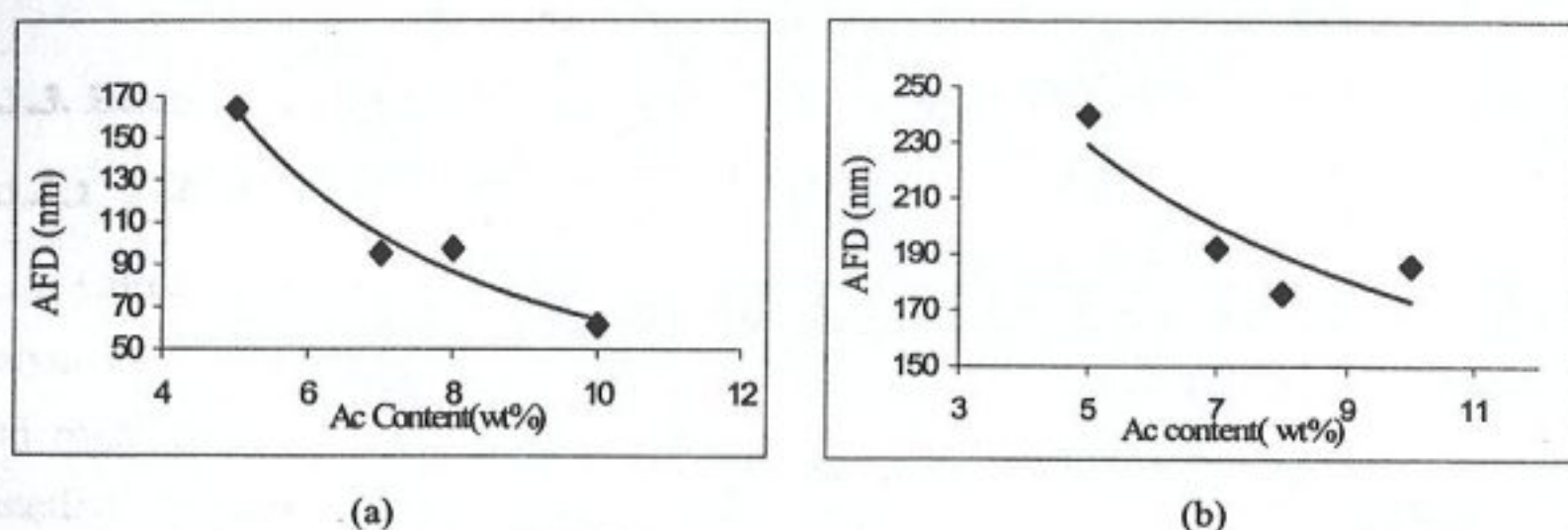


Figure 4.13. AFD as a function of Ac composition in PAN&Ac (a) 9,1 (b) 11,6 wt%

4.1.2.2. Conductivity and surface tension

Tertiary ammonium salt is a well-known organic material for increasing solution conductivity and surface tension [26]. In our experiments, The salt was synthesized with triethylamine and benzylchloride, the reaction can be seen in Figure 4.14. The addition of tertiary ammonium salt into 5,2 wt% and 10,1 wt% PU & urea solution was expected to cause a significant change in fiber morphology. Conductivity and surface tension were increased by adding salt. However, no significant change was observed in fiber diameter.

Silicon was added to decrease the surface tension of solution. Silicon, which has a very low surface tension, was added from 1 wt% to 3,7 wt% into original solution to

decrease the surface tension. Silicone was totally miscible with PU & urea and a single-phase solution was obtained up to 3,7 wt%. Furthermore, co-solvent DMAC (Dimethyl acetamide) was mixed with 10 wt% PU & urea without changing the solution concentration for the same reason [7,8,26]. Again, no significant change was observed in fiber diameter for all cases. Detailed investigation on conductivity and surface tension will be investigated along with its characterization.

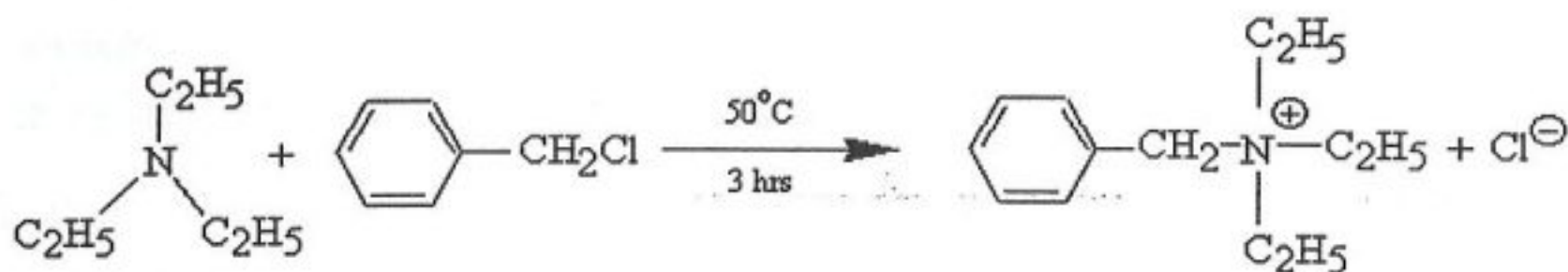


Figure 4.14. Synthesis of triethyl benzyl ammonium chloride salts

4.1.3. Effect of Instrumental Characteristics on Fiber Diameter

4.1.3.1. Voltage

Current increases with an increase in applied voltage. Therefore, the flow rate of polymer solution from tip to the screen increases. In addition, jet length becomes longer and mass flow from tip to target accelerates. Fiber diameter was investigated as a function of voltage. Effect of applied voltage on diameter was not as significant as that of concentration. Average fiber diameter was found to increase with increasing voltage (Figure 4.15). Concentration and spinning distance were held constant at 10,1 wt% and 8 cm, respectively.

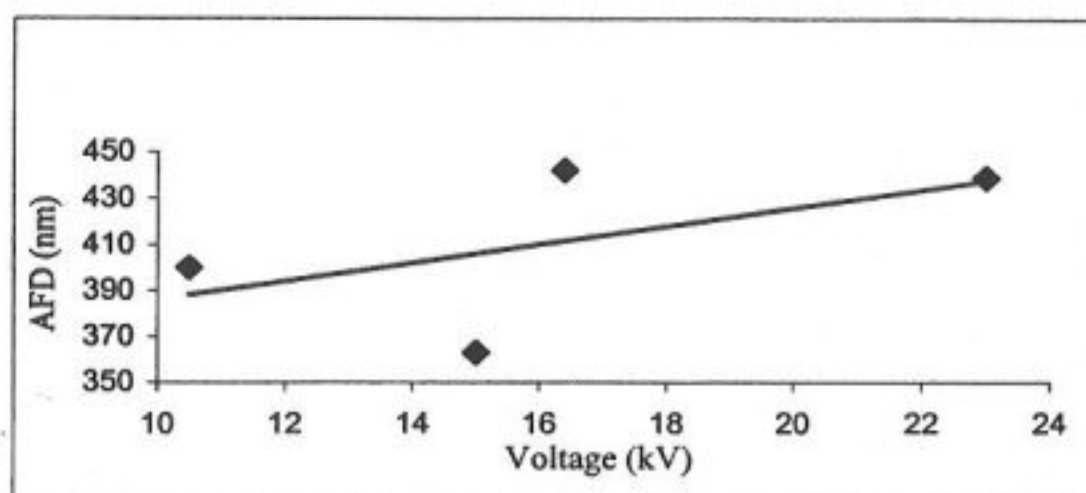


Figure 4.15. AFD as a function of applied voltage

4.1.3.2 Spinning distance

Electrical field lines start from the conductive sheet and ends at the surface of the drop. Changing the geometry of the target leads to change in the path of the field lines. The magnitude of the field lines remains same if spinning distance and applied voltage is kept constant. The jet breaks into many smaller subjects due to the solvent evaporation. The same mechanism repeats itself several times until subjects reach the anode. Increasing spinning distance increases the probability of occurrence of splaying. Therefore smaller subjects are formed as the distance is increased. At the end, thinner fibers are obtained when the spinning distance gets longer.

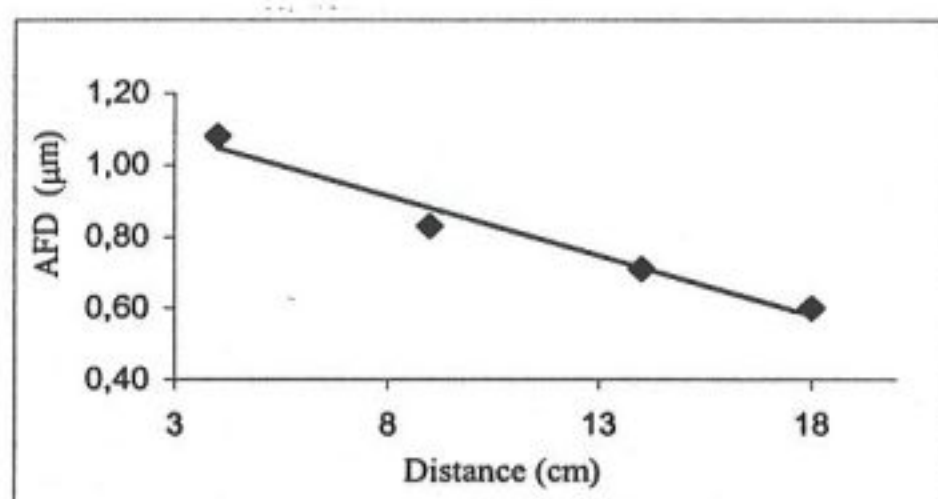


Figure 4.16. AFD as a function of spinning distance

Average fiber diameter is plotted as a function of distance shown in Figure 4.16. Fiber diameter was found to be inversely proportional with the spinning distance. PU & urea solution with 12,8 wt% concentration and the applied voltage was 9,4 kV were kept constant to see effect of on AFD. Fiber diameters were measured with electron microscope images.

4.1.4. Morphology of Nanofibers

Fibers were not uniform in diameter and morphology. There was a bimodal distribution in fibers obtained from 12,8 wt% PU & urea solution. There were two different fiber populations with respect to diameter. The diameter of primary population of fibers was approximately 1 μm whereas the second population's was approximately one third of the primary one, that is 0,3 μm (Figure 4.17).

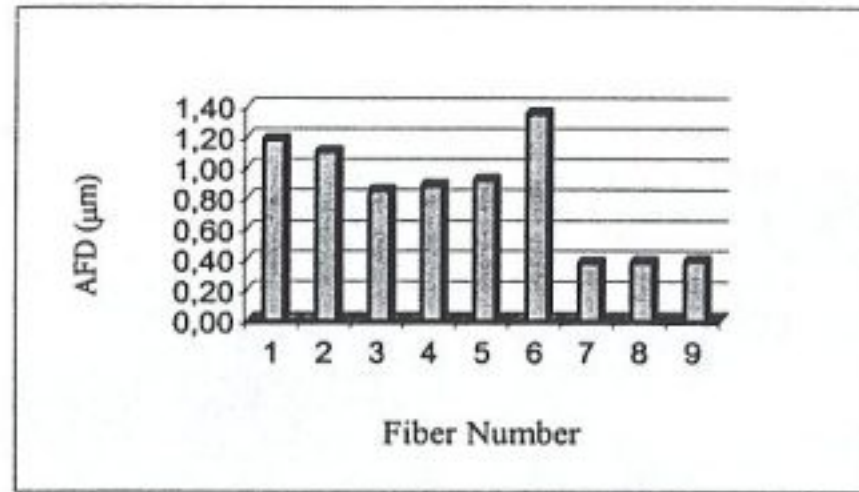


Figure 4.17. Fiber diameters of 12,8 wt% concentrated PU & urea solution

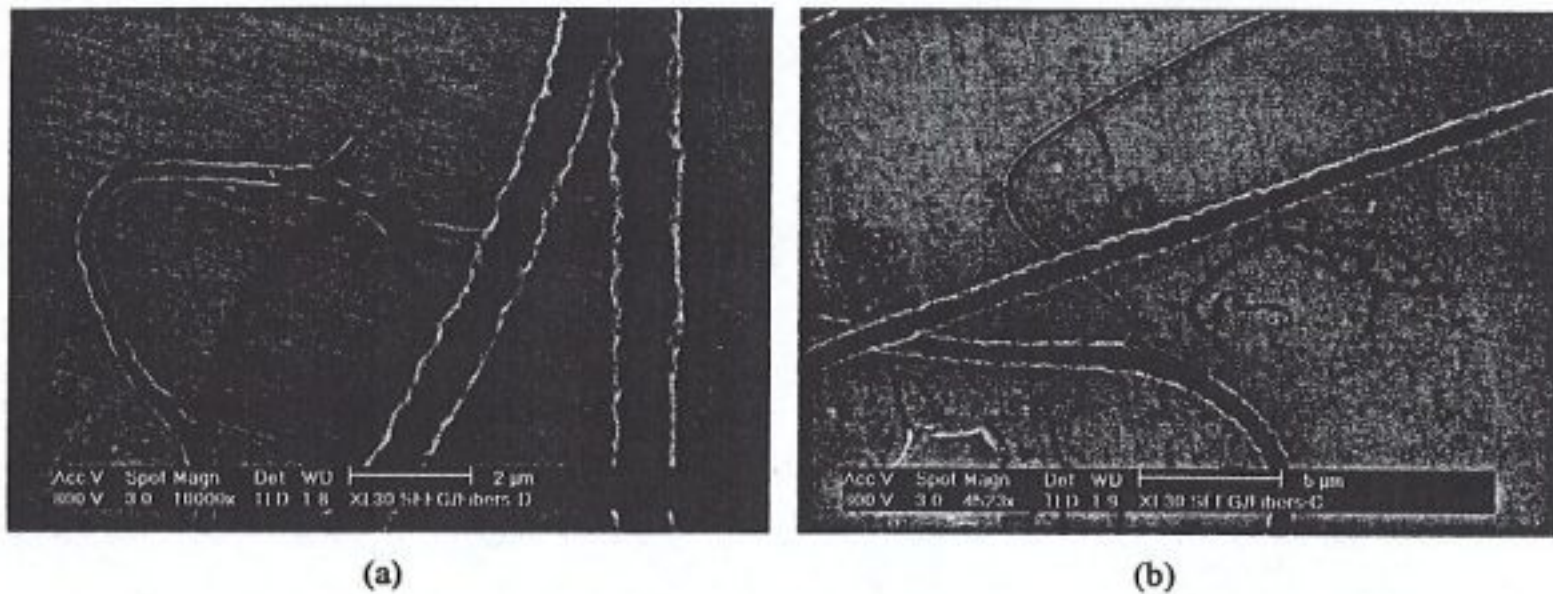


Figure 4.18. Electron micrographs of size distribution in AFD

The jet character can explain the bimodal distribution of fiber diameters. A splaying phenomenon occurs due to the charge repulsion. The primary jet breaks up into many arms, forming many subjects. The subjects were not uniform in diameter, which led to a nonuniform distribution of fiber diameters on the aluminum foil (Figure 4.18).

Viscosity of polymer solution was decreased by increasing the medium temperature up to $\sim 70^\circ\text{C}$. The electron microscope image of the final product is shown in the following Figure 4.19 (a). Process parameters were as follows: the spinning distance was 4,5 cm; the applied voltage was 21 kV and the system was open-air atmosphere. Fiber diameters were uniform at around $1\ \mu\text{m}$. Polymer chains gained mobility with heat energy. Therefore, the number of jets was higher and the angles between the jets were larger. Instead of heating, viscosity was lowered by dilution. In this case, a jet was not observed until to the 12,8 wt% PU & urea solution. Fiber

diameters were not uniform and showed a size distribution from 380 nm to 1,2 μm , Figure 4.19 (b).

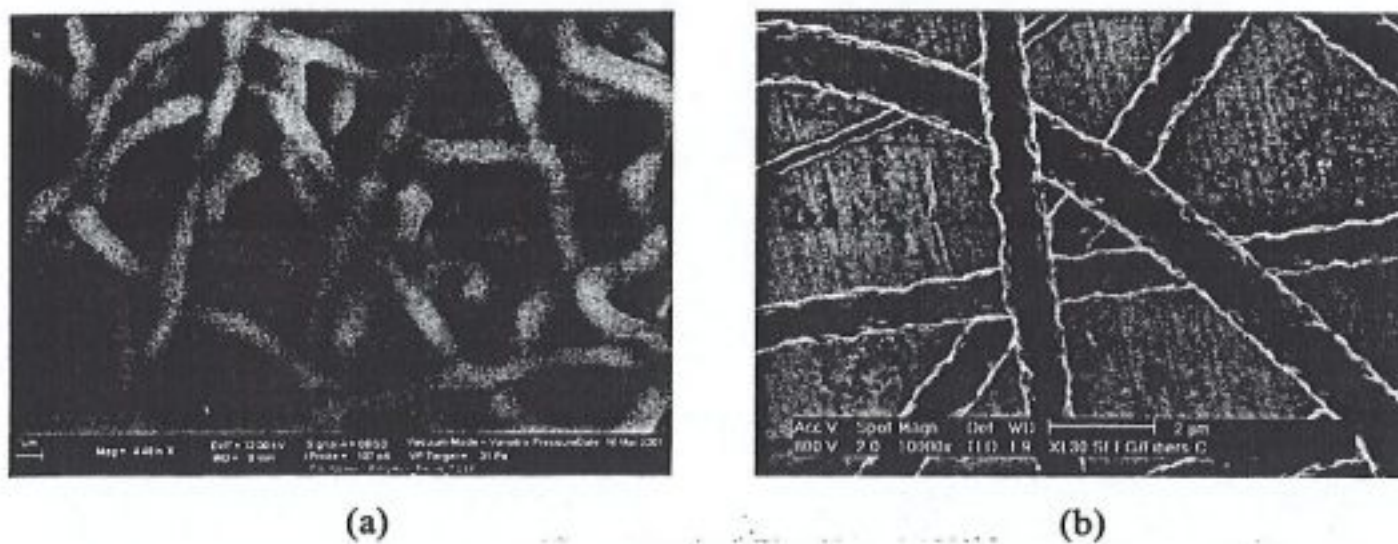


Figure 4.19. Electron micrographs of fiber morphology with (a) without (b) heating

Fibers obtained from high viscous polymer solutions exhibited curly, wavy and straight structures. In Figure 4.20 (a), the fiber indicated with white arrow (x) has identical knots with regular distance. The same fiber is shown in Figure 4.20 (b), which has five times larger scan area than the first one. Figure 4.20 (b) shows that the fiber structures are not uniform. In addition to the curly (x) structures, wavy (y) and straight (z) structures indicated white arrows are observed on the same sample. The fibers on the image were obtained from 12,8 wt% PU & urea solution.

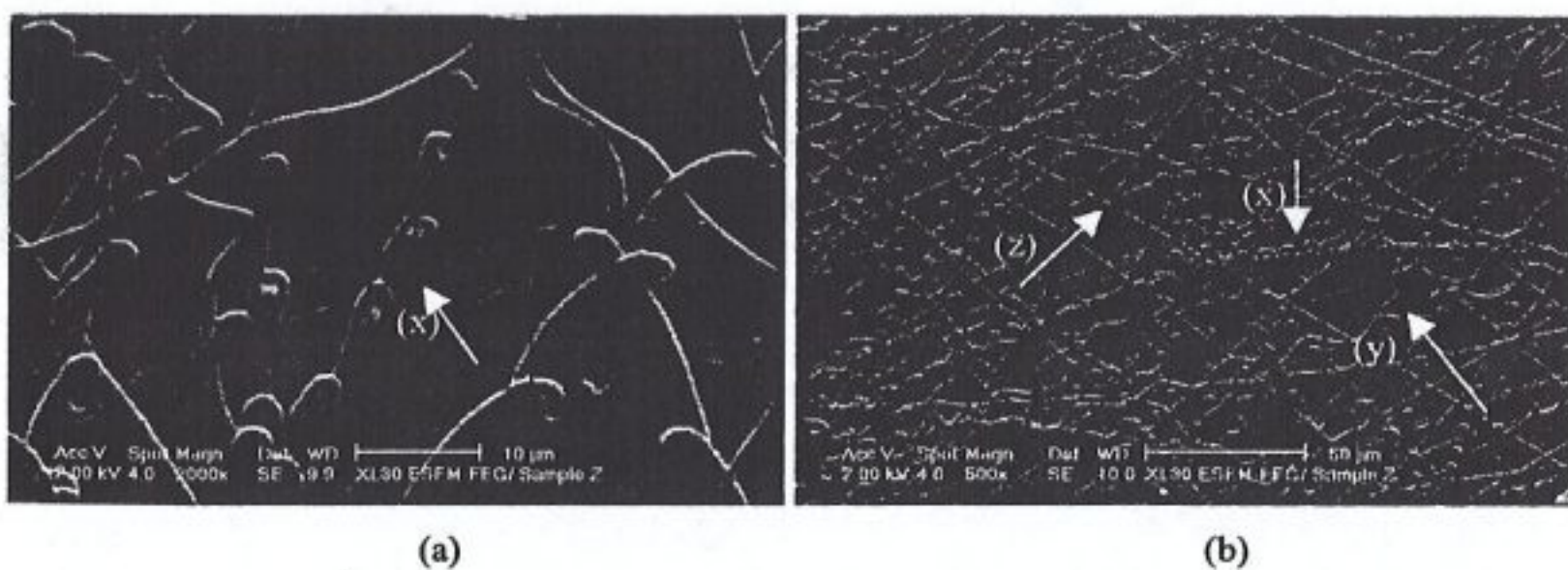


Figure 4.20. Electron micrographs of nanofiber morphology

4.1.4.1. Beads

Bead structures were found in 3,8 wt% and 5,2wt% PU & urea solution samples as seen in Figure 4.21. It is known as 'beads on string' morphology in the literature [7]. The average diameter of the spindle shaped beads are 700 nm . The number of beads decreases with increasing the spinning distance. In Figure 4.21, AFM images of 5,2 wt% PU & urea are shown (Applied voltage was 9,4 kV and the spinning distances were (a) $d = 4$ cm, (b) $d = 18$ cm.) Beads were not observed in the nanofibers obtained from the highest concentrated solution as shown in Figure 4.22. The fibers on the micrograph were obtained from 12,8 wt% PU and urea solution. Thus, lower viscosity solutions favor formation of beads on fibers and also favors formation of thinner fibers. However, bead formation was not observed in PAN & Ac nanofiber even for the lowest viscosity solution. Several images were captured from solutions at four different concentrations, but nearly all of the nanofibers were straight and bead free (Figure 4.23).

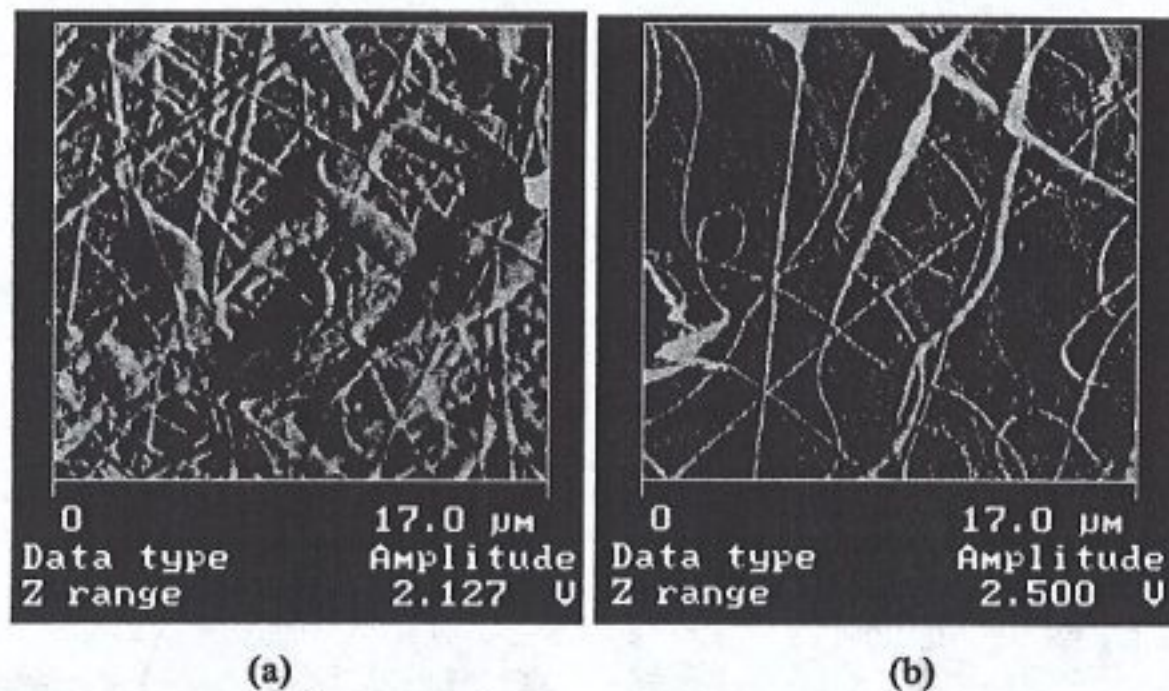


Figure 4.21. AFM images of bead formation of 5,2 wt% PU & urea solution

In Figure 4.23, representative AFM images of PAN & Ac nanofibers are presented for concentrations of (a) 14,9; (b) 13,8; (c) 11,6; (d) 6,4 wt%. Process parameters in obtaining the fibers were as follows:

- (a) Spinning distance 5 cm, Applied voltage 12,5 kV
- (b) Spinning distance 3 cm, Applied voltage 12,5 kV
- (c) Spinning distance 3 cm, Applied voltage 13,8 kV
- (d) Spinning distance 5 cm, Applied voltage 12,5 kV

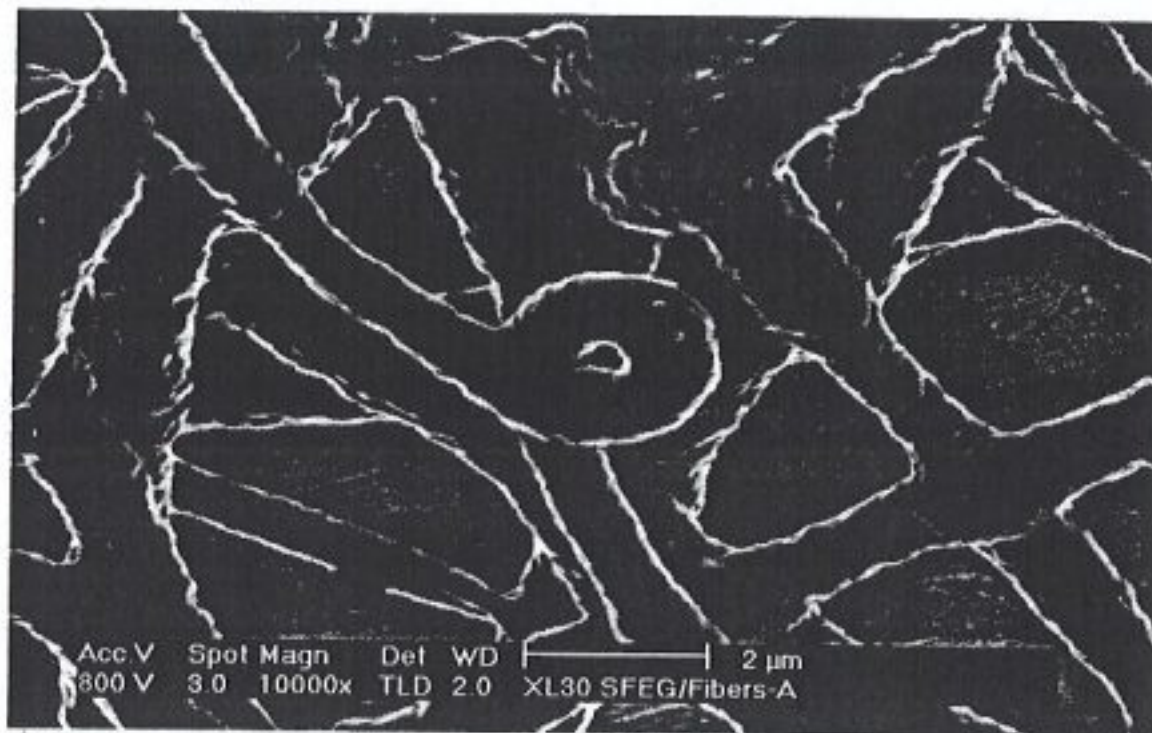


Figure 4.22. Electron micrograph of bead free nanofibers from high viscous solution

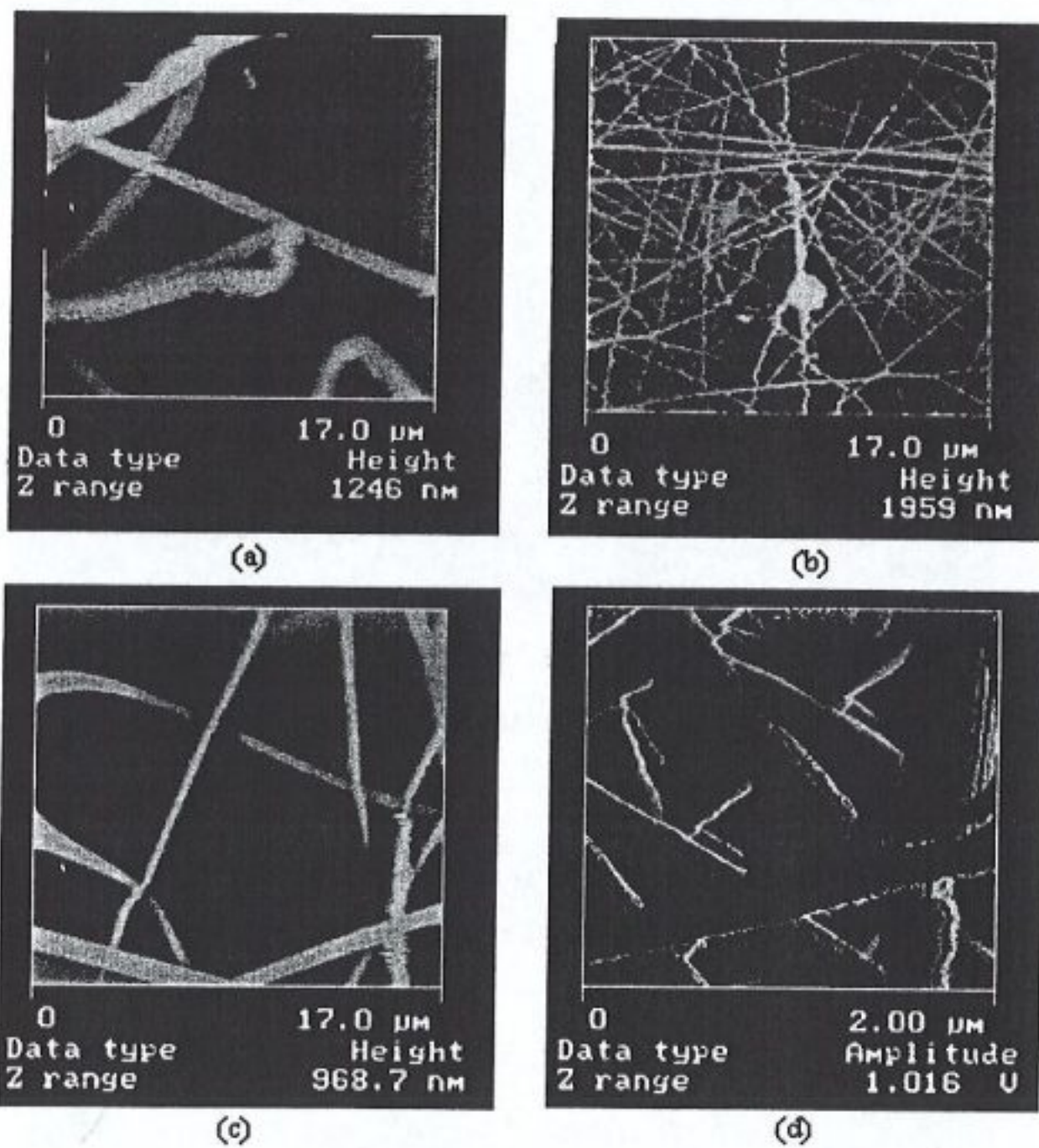


Figure 4.23. AFM images of electrospun fibers from PAN & Ac solutions

4.2. Wet Spinning Process and Morphology of Wet-spun Fibers

4.2.1. Wet Spinning Process

Commercial textile fibers are produced by either melt or solution spinning. Melt spinning is more rapid and efficient than solution spinning. However, many polymers degrade thermally below their melting temperatures, so those fibers must be formed from solutions. The polymer solutions extruded from the spinneret take the form of fibers. These can be solidified by a bath of coagulant liquid to remove the solvent coming up from the solution. This technique is called wet spinning. Blowing air can evaporate the solvent, which is called dry spinning. Wet spinning is the most complex solution spinning technique among the other conventional techniques. The process is mainly based on coagulation. The rate of coagulation has a determining effect upon the final structure. The important process variables are concentration, temperature of the spinning solution, temperature of the coagulant bath and the stretch force applied during drawing. The spin bath does not usually remove all of the solvent in the filament. Thus, blowing air to the region between the coagulant bath and the yarn is likely to produce dry fibers. Wet spinning process is different and complicated when we compare its after-treatment with dry spinning. Only because of this after-treatment and heat setting, the filaments obtain their optimum property [29]. The apparatus of wet spinning was shown in section 3.5.

Fibers made by wet spinning have higher void content than those from the other processes. This offers greater accessibility to dyestuff. The surface of the wet-spun fiber is rougher than that of the dry and melt spun fiber [30].

After the preparation of a homogeneous solution, the most important factor in successful wet spinning is good filtration to remove gels and insoluble parts, and to degas the solution. In our experiments, polyurethane & urea was dissolved in dimethyl formamide at 18 wt%. Two mechanical parameters were varied: rate of extrusion and the rate of drawing. The former determines the amount of polymer solution released into the non-solvent bath whereas the latter determines the drawing speed of the filament.

Extrusion was set to its maximum value and held at 666 $\mu\text{l}/\text{min}$ by the pumping mechanism. As shown in Figure 4.24, as the revolution per minute of the roller was increased, the fiber diameter decreased. This results from the Poisson effect. The revolution of the roller varied from 16 rpm (3,01 m/min) to 62 rpm (11,68 m/min).

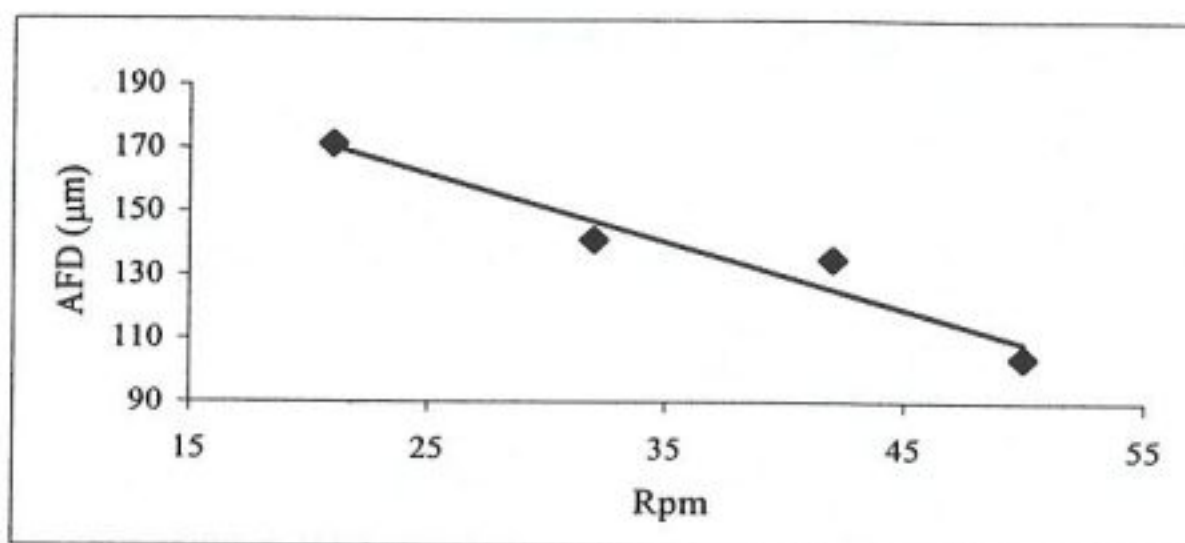


Figure 4.24. AFD as a function of rpm in wet-spun PU & urea

The effect of the rate of extrusion on fiber diameter was also investigated. The revolution of the roller was kept constant, at 39 rpm – 7,35 m/min, in this experiment. Extrusion varied from 233 $\mu\text{l}/\text{min}$ to 666 $\mu\text{l}/\text{min}$. The lowest value of extrusion was 233 $\mu\text{l}/\text{min}$. Fiber rupture took place below this value. Fibers became thinner as the roller took up the filament due to the mechanical drawing. AFD was found to increase with an increase in the rate of extrusion at constant drawing, Figure 4.25.

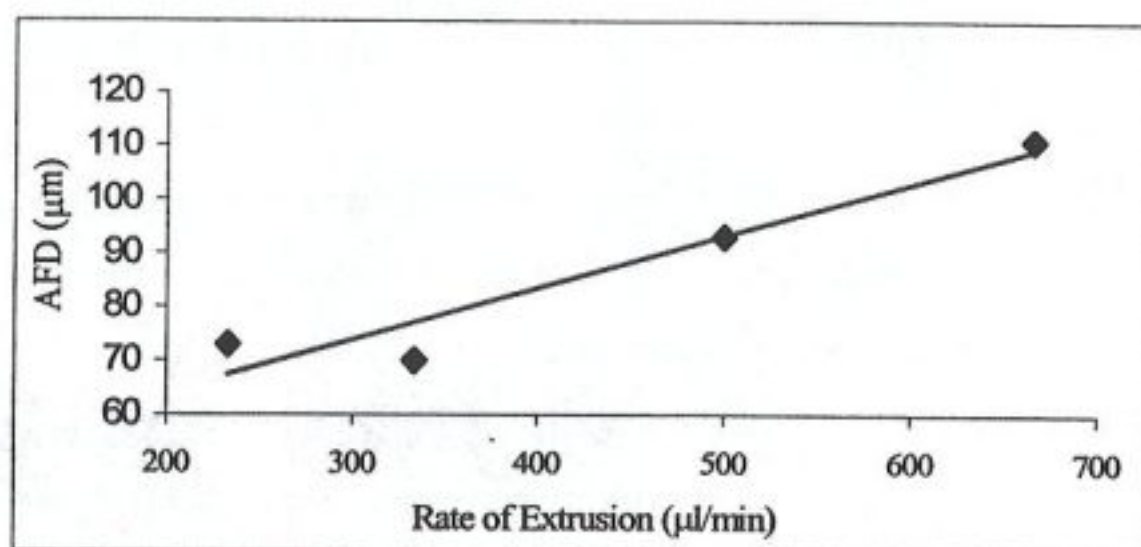


Figure 4.25. AFD as a function of extrusion rate in wet-spun PU & urea

4.2.2. Surface Morphology of Wet-spun Fibers

Fiber was formed when a polymer solution met the coagulant. The fiber surface gains all of its properties mainly in the coagulation bath. The solvent, DMF, was easily miscible with coagulant, water. Solvent-coagulant affinity plays an important role in morphological structure formation.

The surface morphology of wet-spun fibers has been investigated with tapping mode AFM that provides nanometer scale information. The cantilever was oscillated onto the sample surface to minimize tip-sample interaction. Tapping mode scan includes height, phase and amplitude images. Amplitude data are used for demonstration because of having the highest resolution among others. Amplitude imaging uses the cantilever deflection coming from the mirror whereas phase imaging uses the same deflection data not from the mirror, but directly from the piezo crystal.

AFM images have shown that the surfaces of wet-spun PU & urea fibers were heterogeneous in nature. The surface consists of three different morphological patterns; flat, fibrillar, disordered. A large number of scans, more than 60, were captured to claim the heterogeneity of filament surface. None of the formations became a dominant feature of the surface. The morphology exhibited on wet-spun fiber surface did not depend on the processing parameters. Fibril size and shape were totally irregular and no direct relation was found with the two process variables. Wet spun fibers are well known rough fibers, so they are indispensable textile tools displaying an easy dyeability. This is valid for our fibers since surface structure of PU & urea was found very rough especially in disordered regions.

Figure 4.26 shows three AFM images of different places on the same fiber sample. Three different morphologies; flat, fibrillar, and disordered structures were observed on different areas of the fiber surface. The fiber was extruded at a rate of 500 $\mu\text{l}/\text{min}$ into the solvent bath, and rolled up with 39 rpm.

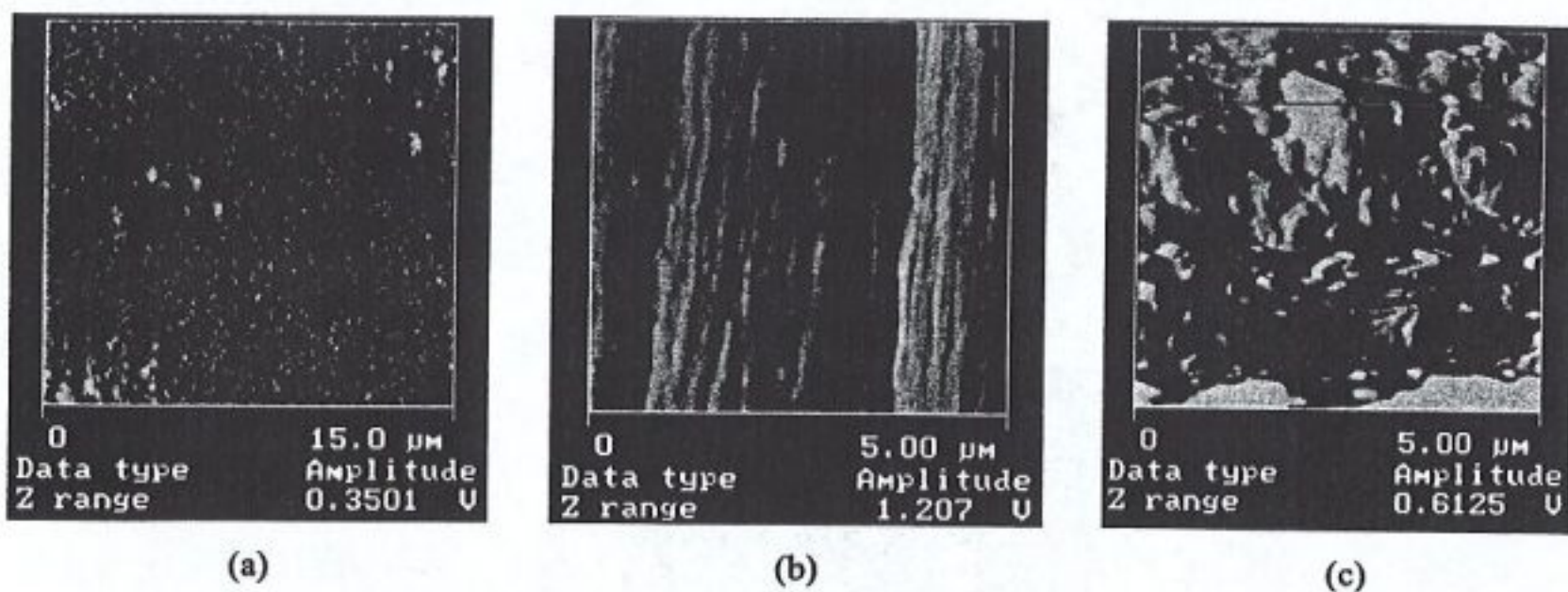


Figure 4.26. AFM images of flat (a), fibrillar (b), disordered (c), structure on wet-spun PU & urea fiber surface at 500 $\mu\text{l}/\text{min}$ extrusion, 39 rpm take-up roll.

The heterogeneity in surface morphology was not a matter of common knowledge until the following research. Scihiraldi and his co-workers observed more than one structure on heterogenic surface of poly (ethylene terephalate) PET film [35].

This heterogeneous morphology is true for all process conditions. Three images in Figure 4.27 were captured from different places of the same sample surface. Two neighboring regions of different morphology are seen in (a) and (b) whereas only one morphology is seen from (c). They are sharply separated by straight line without any transition area.

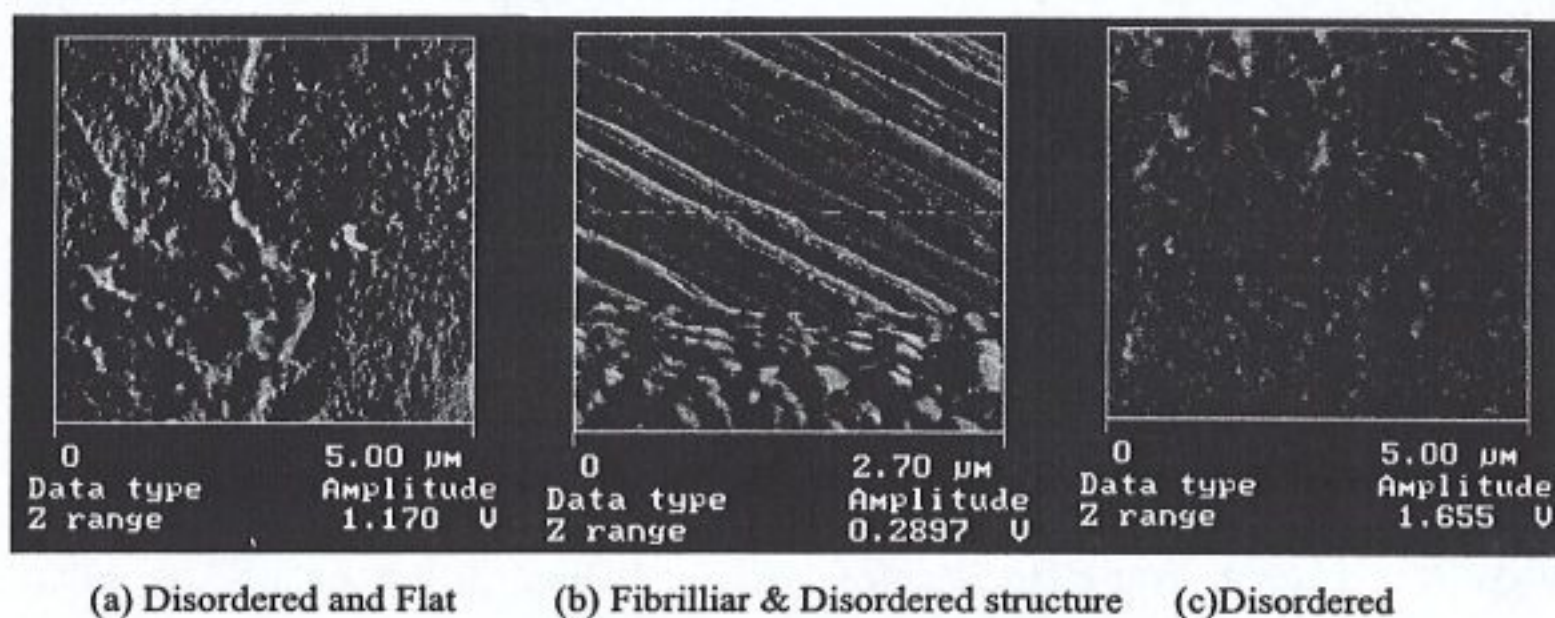


Figure 4.27. AFM images of wet-spun PU & urea fiber surface at 666 $\mu\text{l}/\text{min}$ extrusion, 16-rpm take-up roll.

In Figure 4.28, all three morphologies were found on the same image. The image imparts all three morphological structures within a $5\mu\text{m} \times 5\mu\text{m}$ scan area, and summarizes overall investigations on wet-spun fiber morphology.

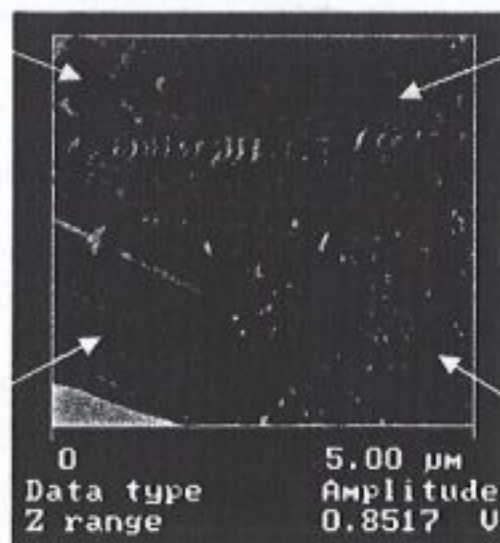


Figure 4.28. AFM image of wet-spun PU & urea fiber surface at 666 $\mu\text{l}/\text{min}$ extrusion, 62-rpm take-up roll.

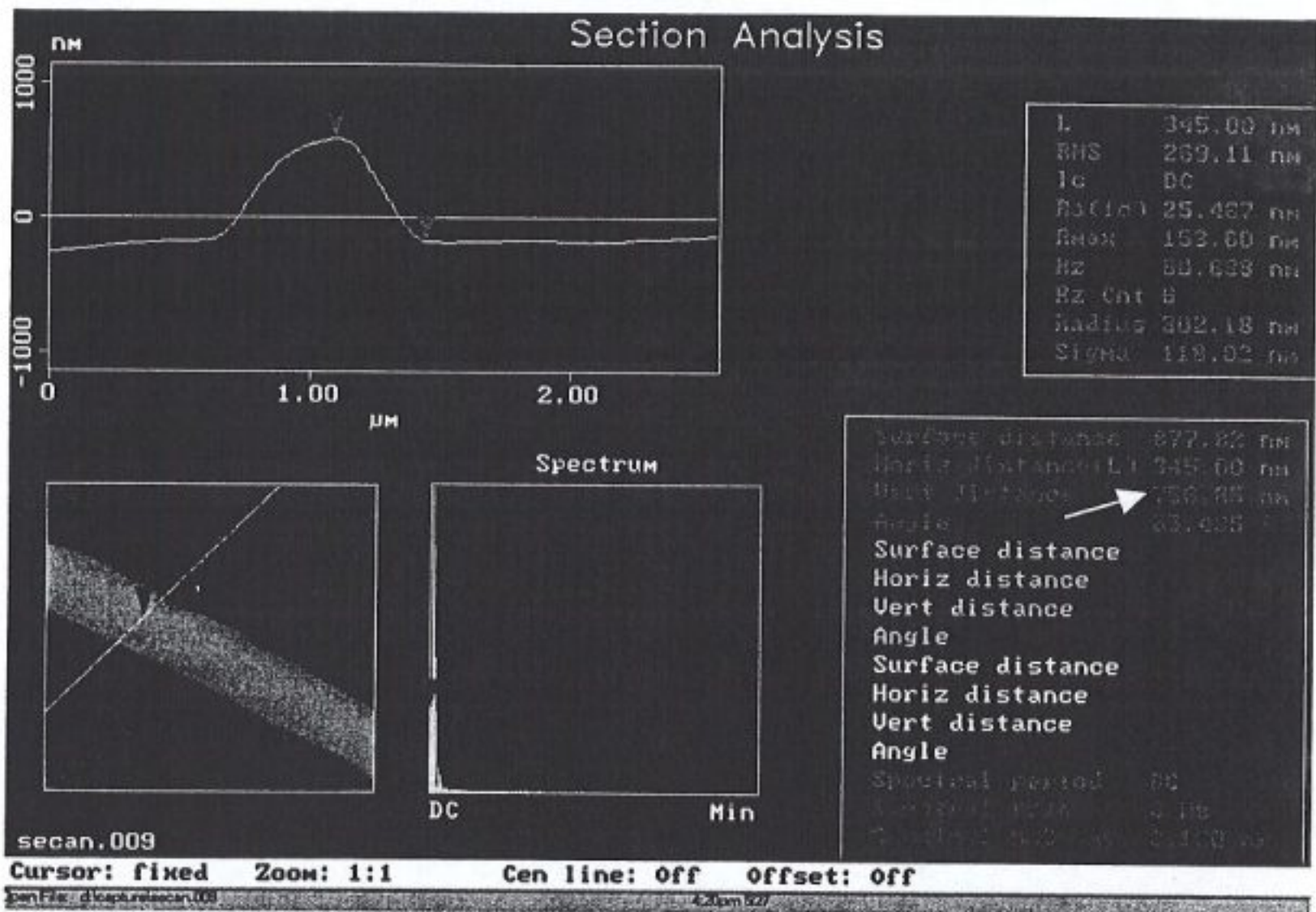
4.3. Comparison of Nano and Micro Fibers

The PU & urea fibers were produced by two methods: electrospinning and wet spinning. The fibers obtained from the two techniques were compared with respect to fiber diameters, surface elasticity, and roughness values. AFM is a high-resolution tool for studying morphology, mechanical properties, and viscoelastic properties of materials' surfaces. Electrospun fiber diameters and roughness values were measured by using tapping mode AFM. Optical microscopy was used for measuring the wet-spun fiber diameters. Surface elasticity measurements were conducted by contact mode AFM.

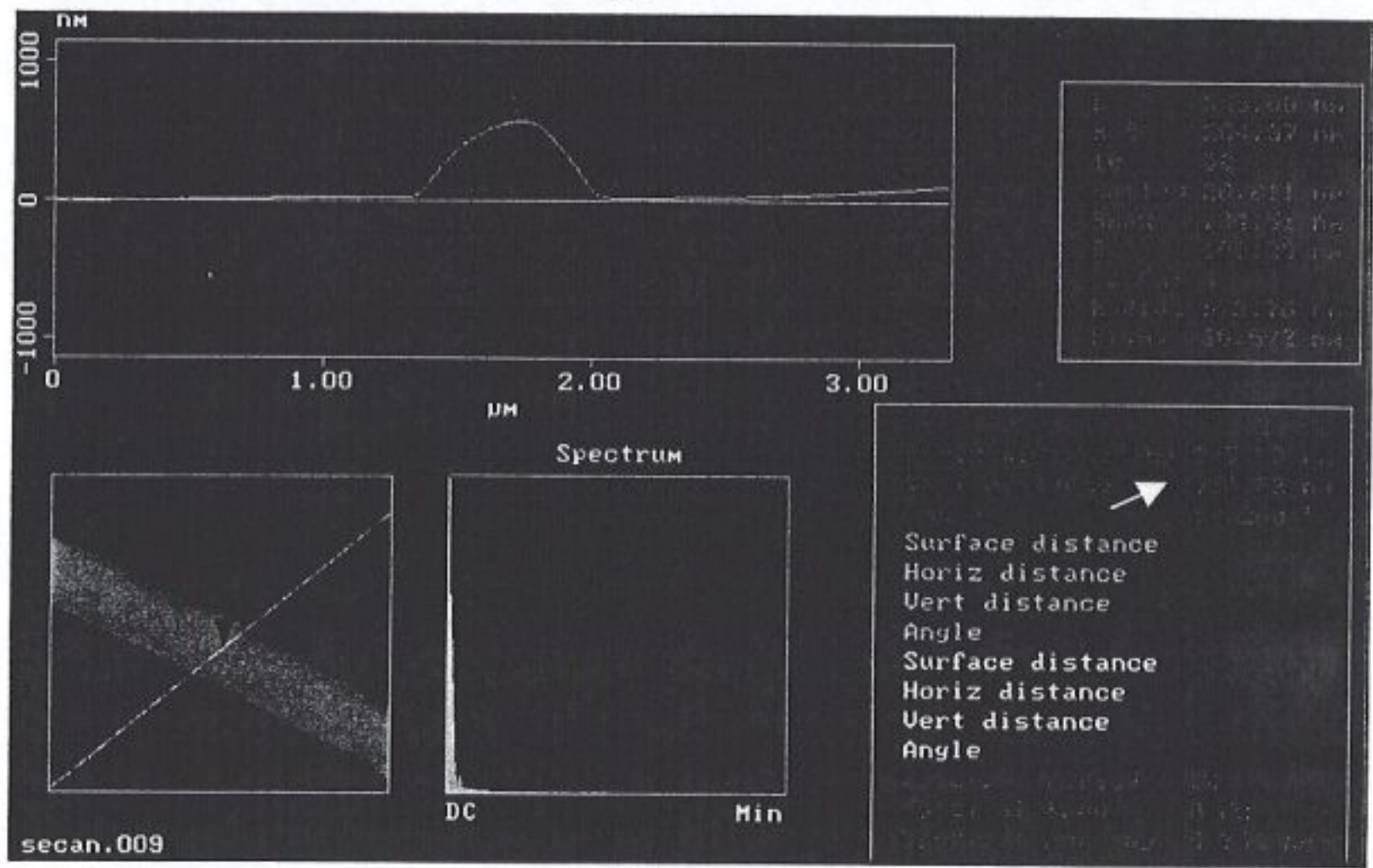
4.3.1. Diameter Comparison

An accurate measurement of the electrospun fiber diameter requires a rather precise procedure. The fibers appear larger than their actual diameter because of AFM tip geometry [14]. There are two primary features of the tip that affect the images. The first is the radius of the curvature and the second is the angle's tip sidewall. The sharper tip is better in imaging data, because it is capable to sense smaller objects. The cantilever has a broad tip that is not as effective as the sharper one in detecting surface topography. Dirty or dull tips do not affect the measurements of vertical dimensions of the sample. Hence, the vertical distance is precise in fiber diameter when compared with the horizontal distance. A strategy is needed to measure the exact value of fiber diameter. This is because of the fact that the zero point, where the tip starts to collect data, is not exactly known. For a precise measurement, a fiber cross was selected, and analyzed with the section analysis. The lower fiber was taken as reference, and the vertical distance above this reference was considered as the exact diameter of the nanofiber. At least three section analysis values were recorded and averaged. This value is called the Average Fiber Diameter (AFD).

A fiber diameter was measured by using two different references. One is on the aluminium ground, the other is at a fibers cross. The vertical distance in the former was found to be 756 nm. The latter gave the result of 556 nm (Figure 4.29). The comparison of the figures of section analyses shows that the measurement taken at cross has way more accuracy than the measurement taken on the aluminum ground.



(a)



(b)

Figure 4.29. Section analyses comparison of fiber diameter (a) on Al foil (b) on fiber cross

Optical microscope images of Al foil, electrospun and wet-spun fibers from the same polymer are shown in Figure 4.30. They were captured in equal scan areas. The diameter of the wet-spun monofilament in (c) is 152 μm that was measured by optical microscope whereas the diameters of electrospun fibers were less than 1 micron.

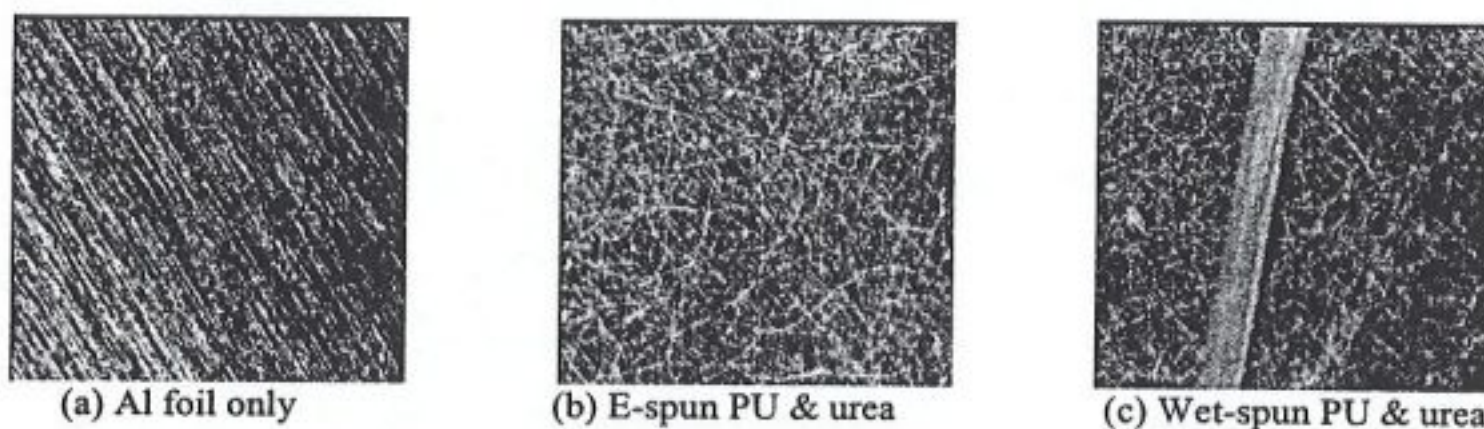


Figure 4.30. Optical microscope images of PU & urea fibers

4.3.2. Surface Elasticity

Nanoscale mechanical characterization was obtained through a force versus deflection curve. The slope of force curve gives information about material elasticity and stiffness [36,37]. Obtaining material properties by using the force curve is a unique feature of AFM. Structural analysis was done to the fibers, and compared to well known materials.

The operating principle for AFM in plotting force curve is to measure the attractive and repulsive forces between tip and the material surface. A typical force curve of contact mode in AFM is shown in Figure 4.31:

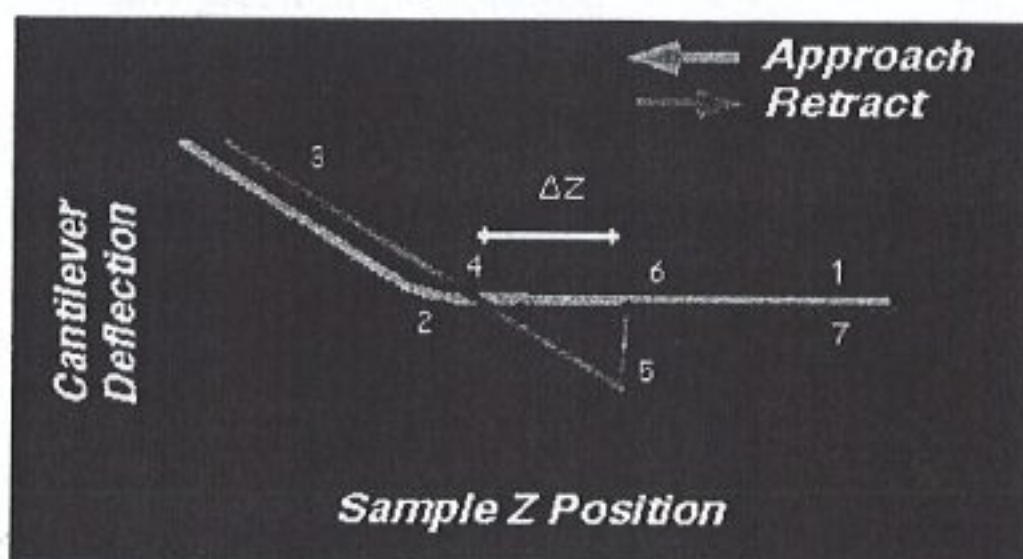


Figure 4.31. Anatomy of force curve

Force curve consists of seven tip movements. These are the followings. 1-Piezo extends, tip descends. 2- Tip is pulled down by attractive forces near surface. 3- As tip presses into the surface cantilever bends upword. 4- Piezo retracts, cantilever relaxes downward until tip forces are in equilibrium with surface forces. 5- Piezo continues retraction Cantilever bends downwards as surface attraction holds on the tip. 6- As piezo continues retracting, tip finally breaks free of surface attraction. Cantilever rebounds sharply upwards. 7- As piezo continues retracting, tip continues its ascent. No further contact is established with the surface during this cycle [37,38].

Contact mode was used instead of tapping to avoid tip breakage since Si₃N₄ is softer than the Si tip. Because of pliant property and lower spring constant of silicon nitride probe, they are sensitive to attractive and repulsive forces.

In Figure 4.31, the tip was in contact with the sample between the second and third stage. As the tip is pressed further and further into the material, the probe cantilever flexes. The amount of cantilever flexion for a given amount of downwards tip movement gives an indication of the material elasticity. Different test materials were used to compare the AFM sensitivity. AFM sensitivity represents the cantilever deflection signal versus voltage applied to the piezo [36]. The contact force is defined by the following equation:

$$F = k (\Delta Z) \quad (4.1)$$

where ΔZ is the distance from the control point to the bottom point in retrace curve. It is possible to calculate the contact force from the force curve. The constant force is calculated for glass slide and parafilm as following:

For Glass slide

$$\Delta Z = 0,4 \text{ div} \times 6,43 \text{ V} / \text{div} \times 42,15 \text{ nm} / \text{V} = 108 \text{ nm}$$

$$\begin{aligned} \text{The contact force, } F &= 0,3 \text{ N/m} \times 108 \text{ nm} \\ &= 32,5 \text{ nN} \end{aligned}$$

For Parafilm

$$\Delta Z = 2,5 \text{ div} \times 6,43 \text{ V} / \text{div} \times 62 \text{ nm} / \text{V} = 996,6 \text{ nm}$$

$$\begin{aligned} \text{The contact force, } F &= 0,3 \text{ N/m} \times 996,6 \text{ nm} \\ &= 299 \text{ nN} \end{aligned}$$

Force curves provide useful information about adhesion and hardness characteristics of sample. Large adhesion force is observed in Figure 4.32(b) for parafilm contrarily glass slide has small adhesion force as shown in (a). As it can be understood from the above-mentioned dynamic (Figure 4.31), the constant force of parafilm is higher than the force of glass slide.

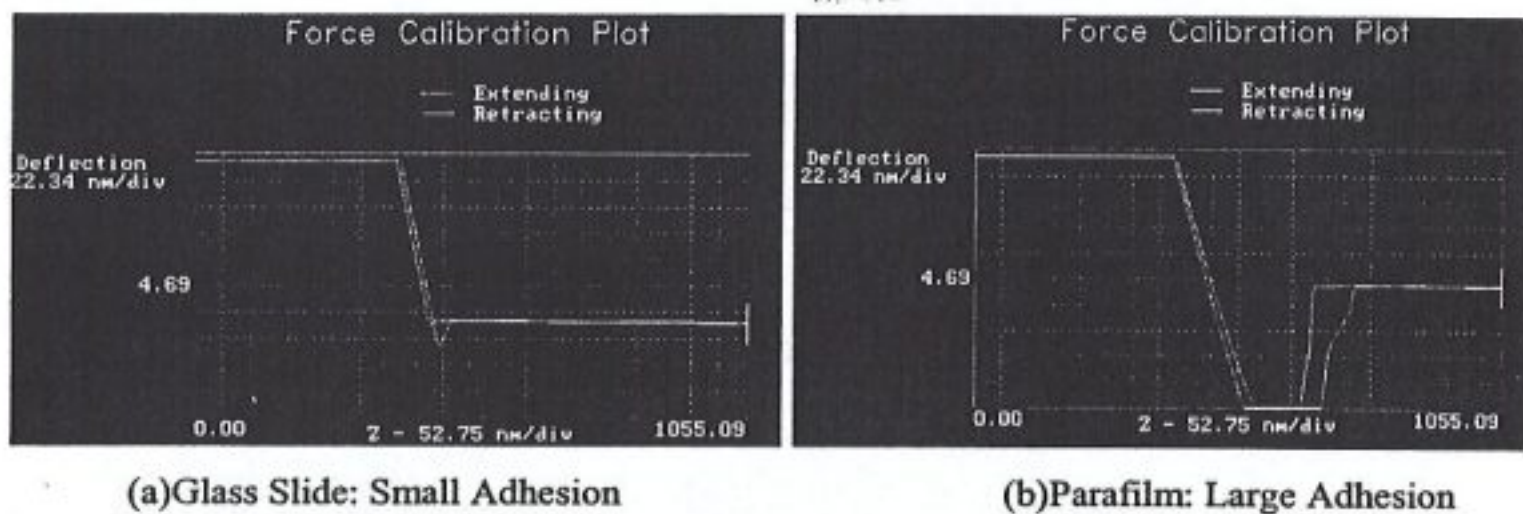


Figure 4.32. Force curve of glass slide and parafilm

Force calibration curves were plotted at scan size of 274 nm^2 and 500 nm^2 . Equal scan areas were taken to obtain comparative values. The same cantilever was used for all tests, and all tests were completed in one day with 2 Hz scan rate so that sensitivities could be compared [37]. The slope of the curve was determined from the average of the trace and retrace values. AFM sensitivity is equal to the slope of the force curve while the cantilever is in contact with sample surface.

In electrospinning case, one sample was selected from 12,8 wt % PU & urea. Then a random nanofiber was chosen among many of the fibers, and three different measurements were taken. Zoom on a fiber was a must after capturing web image in large scan area. In order to make an exact comparison, scan area should be equal to the wet spun's, 500 nm^2 . However, 500 nm^2 could not be adjusted so 431 nm^2 and 587 nm^2 were set and their average was used for comparison.

For wet-spun fibers, AFM sensitivity was measured on the fiber surface. Their diameters were nearly $100 \text{ }\mu\text{m}$ and maximum scan size of the E-type piezo crystal of

AFM was 17 μm . That is, the diameter was bigger than the scan area. To match the cantilever tip onto the fiber needs attention because of the curvature of the cylindrical shape of the wet spun fibers. Perpendicular and parallel directional scanning was conducted during the characterization. For example, 35 $\mu\text{l}/\text{min}$ wet-spun fiber was scanned perpendicular and parallel to the fiber direction. Sensitivities of trace and retrace values of parallel scan were 56 nm/V and 71 nm/V, respectively. However, 45,7 nm/V and 45,8 nm/V were the values from perpendicular scanning of the same sample. At this point, it is important to say that the frictional signals of the scanning in a different direction produce different magnitude signals for oriented crystalline molecules. Scanning perpendicular to the oriented chain detects about 4 times greater friction signal than that was measured by scanning along the chains [39]. Hence, scanning direction affects the sensitivities of wet spun fibers.

The mechanical properties of electrospun fibers are expected to have better or comparable results than conventional fibers have [16]. Here is a description of a set of AFM sensitivity results chosen among many others (Figure 4.33).

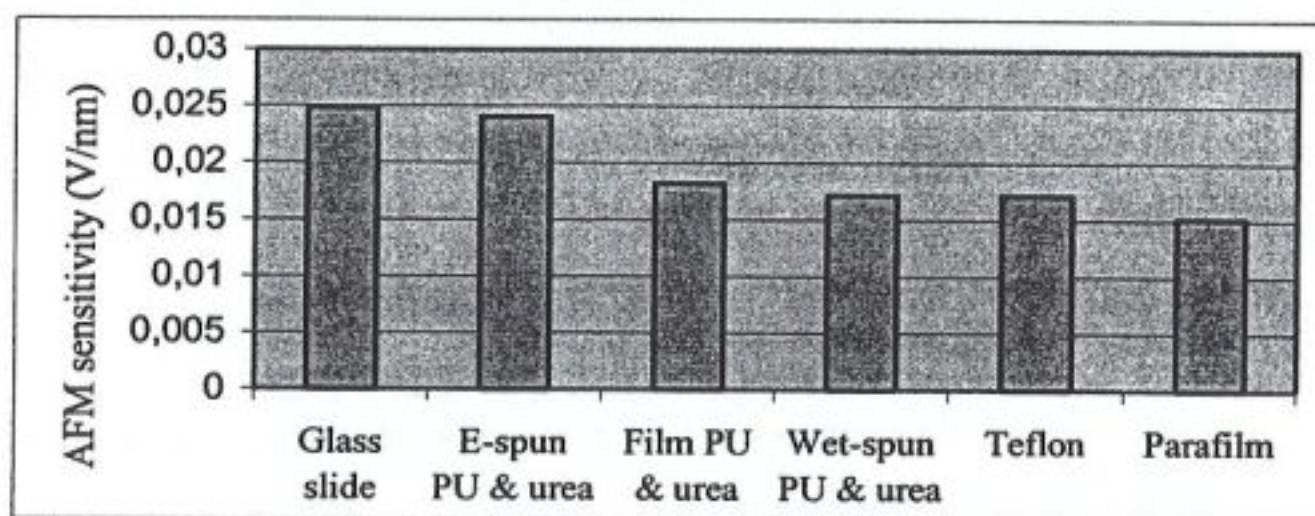


Figure 4.33. AFM sensitivity of different materials

Nanoscale surface properties were compared for different materials, which are Glass slide, Teflon film and Parafilm. They were compared with electrospun, wet-spun and film samples obtained from the same PU & urea solution. Hard materials demonstrated high AFM sensitivity, soft ones displayed low AFM sensitivity [37]. Glass slide was found to have the highest sensitivity whereas parafilm had the lowest sensitivity. The sensitivities of electrospun, wet spun fiber and cast film were in between that of glass slide and parafilm. As a result of a serial of experiments, it was found that sensitivity of wet-spun fibers strongly depends on their own spinning

parameters. Remaining five materials displayed same order in all experiments. Hardness difference between the electrospun fibers and the film allows us to consider orientations in the electrospun fiber. Electrical force applied to the polymer solution orients the molecules through the electrical force direction.

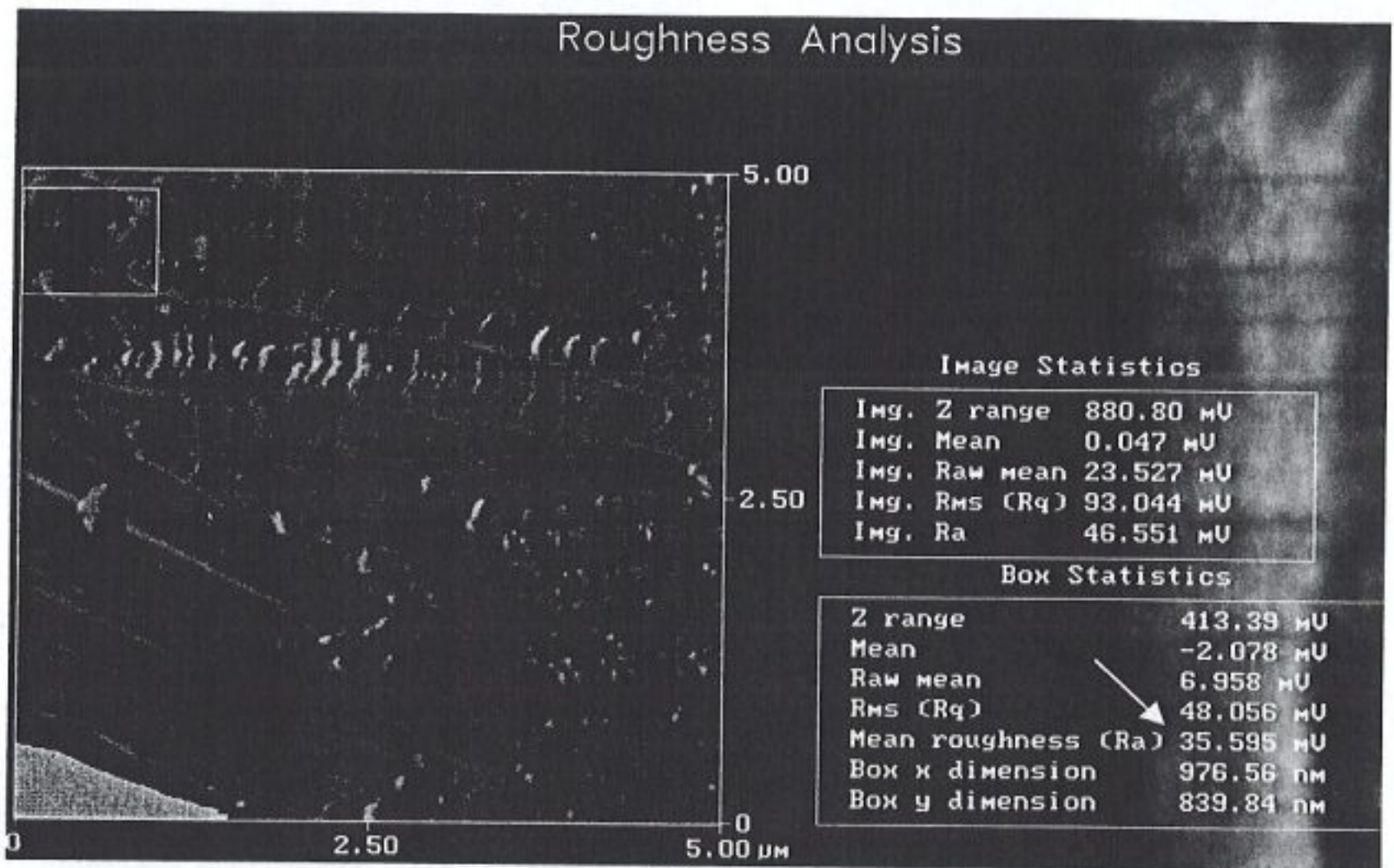
4.3.3. Roughness Analysis

The roughness stands for the arithmetic average value of the total amount of ups minus the total amount of downs from the center plane of sample surface. Here is the equation of mean roughness, R_a :

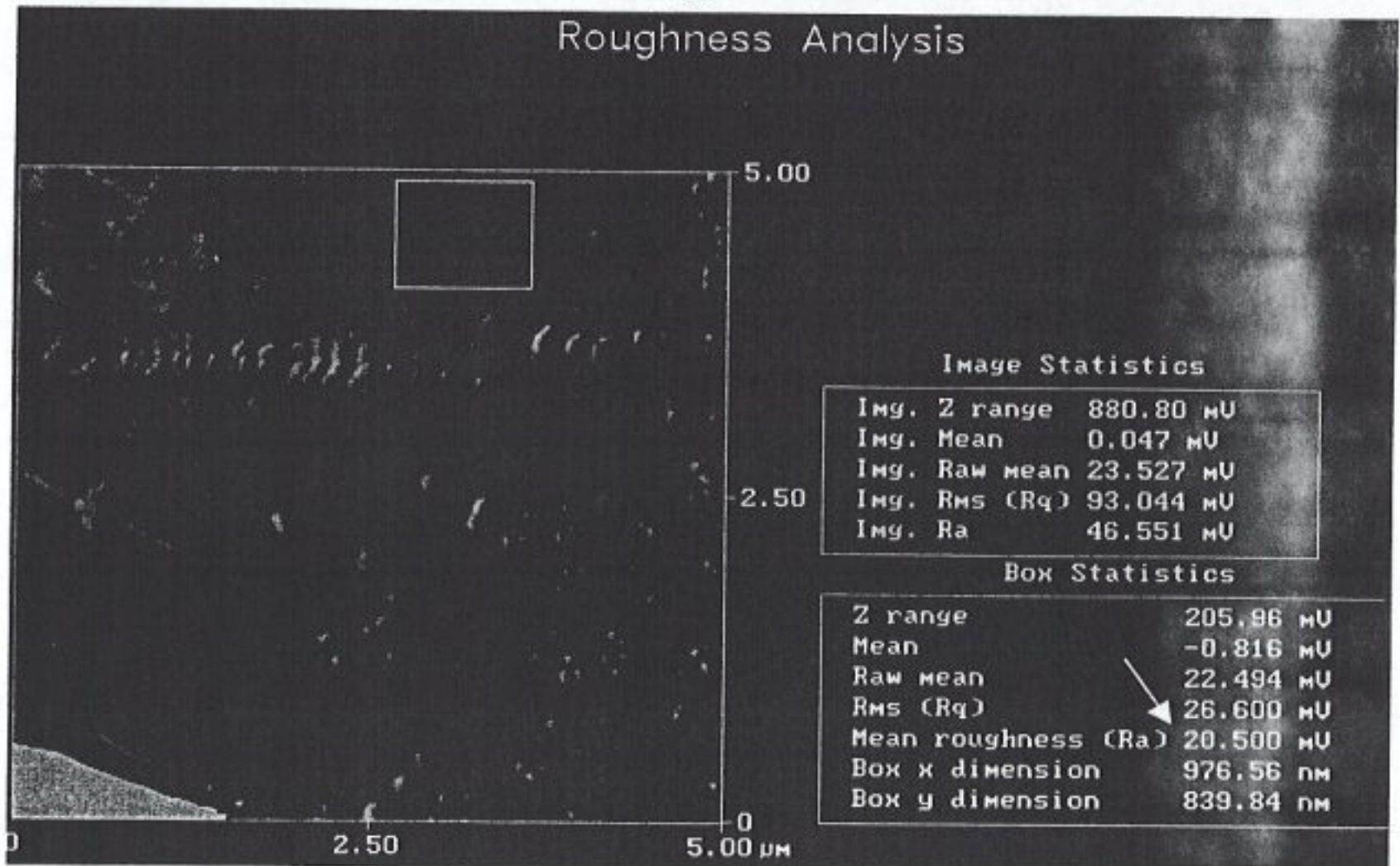
$$R_a = \sum |Z_i - Z_{cp}| / N \quad (4.2)$$

Z_{cp} is the Z value of the center plane, and Z_i , is the current value, and N is the number of points within a given area [36].

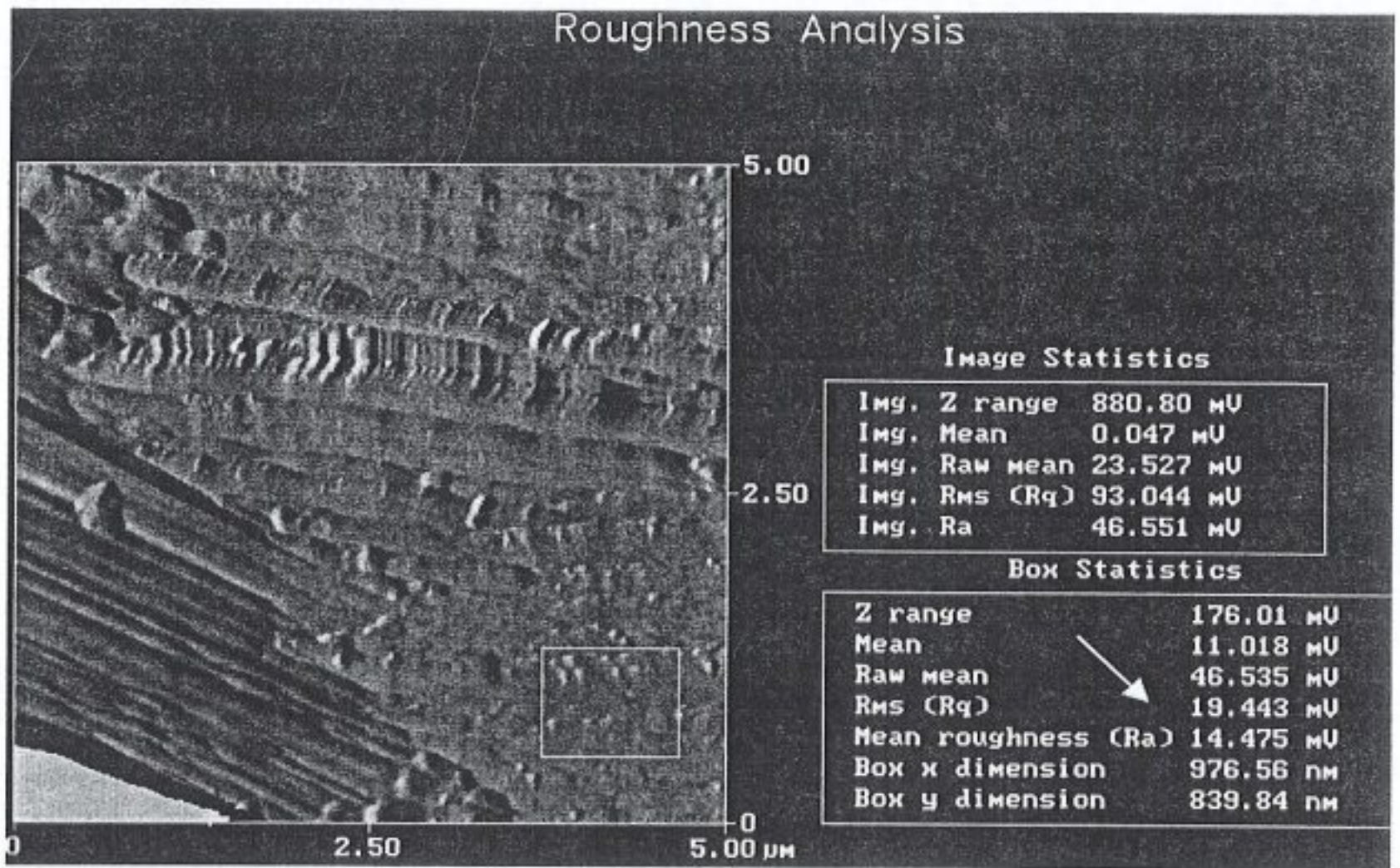
Both electrospun and wet-spun fiber surfaces were analyzed for comparison. Three different surface morphologies were observed on wet-spun fiber. Specific images containing all three topographical patterns were provided, in Figure 4.34. Each roughness value of the regions on wet-spun fibers was compared with that of an equal sized region of the electrospun fibers surface (Figure 4. 34 (d)). The value of roughness in the box may vary with the box area. Roughness may vary according to the area on which analysis done. Thus, selecting area gains importance in order to arrive at real roughness values. There are four-roughness analyses in Figure 4.34. The first three images display roughness measurements of wet-spun surface. The last one is a roughness analysis of electrospun fiber surface. All AFM images were amplitude image of tapping mode. The disordered region of the fiber was 35,6 mV, and the roughest among wet-spun morphologies. The fibrillar region has the roughness value, 20,5 mV. The third, a flat structure, has the lowest roughness value among the others, which is 14,5 mV. Thus, electrospun nanofiber was found to be rougher than the disordered morphology, 88,8 mV. The roughness value of electrospun PU & urea was found to be the highest. Electron repulsion within the charged fiber and electron attraction with the ground may be the cause of such rough surface (Table 4.3). This result is completely in accordance with the results in the literature [14].



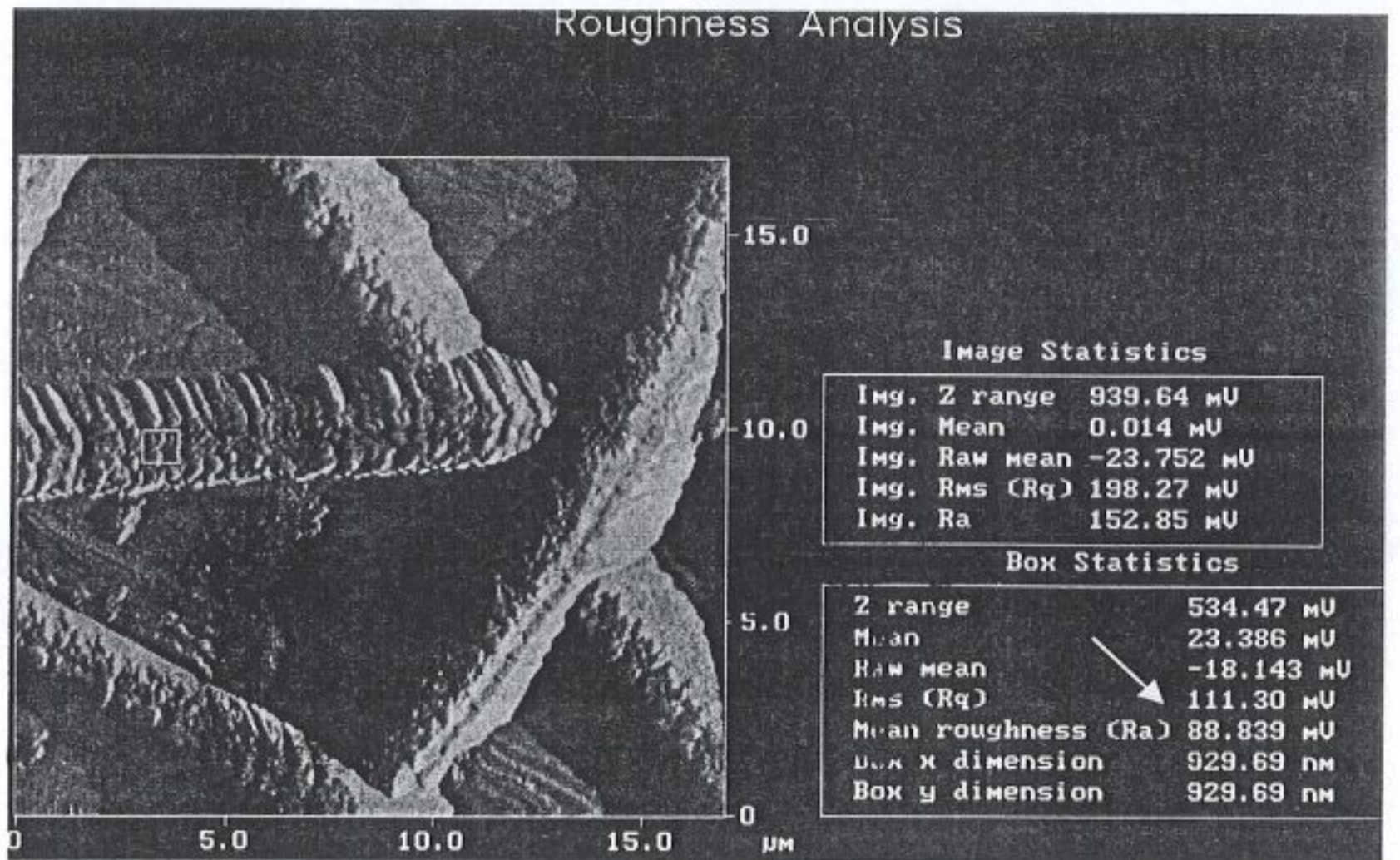
(a)



(b)



(c)



(d)

Figure 4.34. Roughness comparison of wet-spun and electrospun fibers

Table 4.3. Roughness comparison of fiber types and morphologies

Fiber Type and Morphology	976,5 x 839,8 nm ²	929,8 x 929,8 nm ²
Wet-spun Disordered	35,6 mV	-
Wet-spun Fibrillar	20,5 mV	-
Wet-spun Flat	14,5 mV	-
Electrospun	-	88,8 mV

5. CONCLUSION

In this research, two fiber-forming processes were performed: electrospinning and wet spinning. Several process parameters were identified and characterized for both. Fibers obtained from the novel electrospinning technique were compared with the fibers produced with the conventional wet spinning technique with respect to fiber diameters, surface elasticity and roughness values. AFM and SEM were used for characterization.

In the context of the present thesis, a standard electrospinning technique has been used. In electrospinning, an electrical field was applied to the polymer solution; after an air gap, a grounded conductive sheet was positioned. A uniform electrical field developed between the drop and the ground. When the electrical force became equal to the surface tension of the liquid drop, a charged liquid jet was ejected from the drop to the grounded sheet. After solvent evaporation, a nonwoven mat composed of ultrathin fibers was collected on the grounded sheet. Solution and instrumental parameters effect the properties of the resulting fiber. By varying those parameters, stable and continuous jets of polyurethane and polyacrylonitrile solutions were formed. The jet properties were current, length, and character. Jet current and jet length were found to increase with the electrical field strength. Jet current was affected directly with the conductivity of the solution. The jet diameter and flow rates were found to increase with increasing the voltage.

The spinnability interval of concentration was determined for polyurethane and polyacrylonitrile based polymers; 12,8 – 3,8 wt % and 14,9 – 6,4 wt % respectively. Below the lower limit, the jet broke up into droplets whereas above the limit, the solution resisted to form a continuous jet because of viscosity. The nanofiber diameters increased with an increase in the concentration of the polymer solution. The electrical field strength also had a direct linear relationship with the fiber diameter. Viscosity, i.e. concentration, was found to be the dominant factor among all the solution and instrumental parameters. Fibers electrospun from the high concentration polyurethane based solution had curly, wavy, and straight structures. The morphology of fibers was characterized by high resolution SEM. However, beads on string

morphology were observed on fibers obtained from low viscous solutions of the same polymer.

In wet spinning, 18 wt % polyurethane in DMF was extruded through the nozzle of the needle into the coagulation bath containing tap water. 1,7 wt % acetone was mixed with water to remove easily the solvent of polymer solution. The single filament was transferred from bath to the roller by the help of a teflon bearing. Two process variables, the rate of drawing and the rate of extrusion were investigated. The diameter of wet-spun fibers was found to be inversely proportional with the rate of drawing. The rate of extrusion increased the fiber diameters with a linear relationship.

AFM has been used to study the surface characterization of electrospun and wet-spun fibers. Elastic wet-spun fibers' surfaces were totally heterogeneous. Three different morphologies; flat, disordered, and fibrillar have covered the entire filament surface. Irregularities in surface were attributed to the presence of both oligomeric chains in polymer and phase difference of hard and soft segments. The morphology did not exhibit any dependency on the rate of drawing and the rate of extrusion.

The main difference between electrospun and wet spun fibers is in their diameters. Nanoscale diameter fibers were obtained as a nonwoven mat in electrospinning whereas, in wet spinning, a macroscale single filament was wound up. Additionally, in roughness comparison, electrospun fibers were found to be significantly rougher than the wet spun fibers. In addition to the morphological analysis that has been presented, a characterization of the nanoscale mechanical properties of electrospun and wet spun fibers was also performed by using AFM. The surface elasticity of fibers was compared with three different reference materials. Forces versus deflection curves were plotted and AFM sensitivities of the materials were calculated from their slopes. Glass slide was found to be the hardest material and parafilm was the softest among others including electrospun, wet spun and film casted polyurethane based polymer solution. The force applied to materials varied from 32,5 nN to 299 nN, glass slide and parafilm respectively. AFM sensitivity of wet spun fibers has changed as a function of process variables. Hence, electrospun and wet spun fibers could not be compared to each other. However, polyurethane-based polymer film, obtained by film casting, was found to be softer than the electrospun fibers in all experiments. It can be concluded that orientation in the electrospun fibers increases the hardness.

Electrospinning is an easy, fast, simple, non-mechanical process. The main advantage of the electrospinning process is to obtain ultrathin fibers. The smaller diameters provide a large surface area to volume ratio. The filament obtained by electrospinning (if possible) would be nearly 10^4 times longer than the one obtained by wet spinning from an equal amount of polymer. Furthermore, the surface area of the electrospun fiber would be 10^4 times larger than the surface area of the wet-spun filament. (wet-spun and electrospun fiber diameter was taken as $100\ \mu\text{m}$ and $10\ \text{nm}$, respectively). Additionally, operation time of electrospinning is shorter with respect to that of wet-spinning. Only a small amount of sample can produce very thin films therefore it can be termed as a microprocessing technique. Thus, electrospun fibers are very good candidates for various commercial applications with the above-mentioned properties. High surface area property makes them indispensable for the composite and catalysis industry. Porous structure makes it an excellent candidate for nanofiltration and textile industry. It is possible to create a breathable fabric that can trap and deactivate lethal nerve gases. Mixing a catalyst capable of breaking down nerve gases provides a unique property for preventing the effects of chemical weapons. Also, by blending carbon nanotubes and conductive polymers into the mix, it is possible to make fabrics that conduct electricity [40].

In future work, the system used for electrospinning is going to be improved in our future projects. Firstly, a jacket or a chamber will be designed to change the spinning atmosphere, relative humidity, and temperature. Furthermore, a circular probe connected to a second high voltage generator, will be provided to control the paths and magnitudes of electrical field lines. Thus corona discharge will be avoided by the new system. Secondly, I will try to characterize the mechanical properties of electrospun fibers. Optical tweezer with x, y, z position detector is going to be used to measure the elasticity of polyurethane fibers. Finally, light sensitive polymers are going to be electrospun on optical fibers in order to see the change in refractive index. If we will be successful in these future projects, we can create a great impact in nano characterization of fibers and fiber optic sensors.

REFERENCES

1. Baumgarten P. "Electrostatic Spinning of Acrylic Microfibers." *Journal of Colloid and Interface Science* **36**, 1, 71-79 (1971).
2. Larrando L., John M. "Electrostatic Fiber Spinning from Polymer Melts I." *Journal of Polymer Science* **19**, 909-920 (1981).
3. Doshi J., Srinivasan G., Reneker D. "A Novel Electrospinning Process." *Polymer News* **20**, 206-213 (1995).
4. Taylor G. "Electrically Driven Jets." *Proc. Roy. Soc. Lond. A* **313**, 453-475 (1969).
5. Doshi J., Reneker D.H. "Electrospinning Process and Applications of Electrospun Fibers." *Journal of Electrostatics* **35**, 151-160 (1995).
6. Deitzel J.M., Kleinmeyer J., Harris D., Beck Tan N.C. "The Effect of Processing Variables on the Morphology of Electrospun Nanofibers and Textiles." *Polymer* **42**, 261-272 (2001).
7. Fong H., Chun I., Reneker D.H. "Beaded Nanofibers Formed during Electrospinning." *Polymer* **40**, 4585-4592 (1999).
8. Jaeger R., Bergshoef M., Vansco J., Battle C.M., Schönherr H. "Electrospinning of Ultra-thin Polymer Fibers." *Macromol. Symp.* **127**, 141-150 (1998).
9. Jaeger R., Schönherr H., Vansco G.J. "Chain Packing in Electro-Spun Poly(ethyleneoxide) Visualized by Atomic Force Microscopy." *Macromolecules* **29**, 7634-7636 (1996).
10. Zeleny J. "Instability of Electrified Liquid Surfaces." *Physical Review* **10**, 1, 1-7 (1917).
11. Taylor G. "Disintegration of Water Drops in an Electrical Field." *Proc. Roy. Soc. Lond. A* **280**, 383-97 (1964).
12. Formhals A., USPat. 1938, 2, 116, 942.
13. Deitzel J.M., Kleinmeyer J.D., Hirvonen J.K., Beck Tan N.C. "Controlled Deposition of Electrospun Poly(ethylene oxide) Fibers." *Polymer* **42**, 8163-8170 (2001).
14. Srinivasan G., Reneker D.H. "Structure and Morphology of Small Diameter Electrospun Aramid Fibers." *Polymer International* **36**, 195-201 (1995).

15. Reneker D.H., Chun I. "Nanometer Diameter Fibres of Polymer, Produced by Electrospinning." *Nanotechnology* **7**, 216-223 (1996).
16. Kim J.S., Reneker D.H. "Polybenzimidazole Nanofiber Produced by Electrospinning." *Polymer Engineering and Science* **39**, 5, 849-854 (1999).
17. Fong H., Reneker D.H. "Elastomeric Nanofibers of Styrene-Butadiene-Styrene Triblock Copolymer." *J. of Poly. Sci.: Part B: Poly. Phys* **37**, 3488-3493 (1999).
18. Fang X., Reneker D.H. "DNA Fibers by Electrospinning." *J. Macromol. Sci.-Phys.* **B36**(2), 169-173 (1997).
19. Buchko J.C., Loui C.C., Shen Y., Martin D.C. "Processing and Microstructural Characterization of Porous Biocompatible Protein Polymer Thin Films." *Polymer* **40**, 7397-7407 (1999).
20. Chun I., Reneker D.H., Fong H., Fang X., Deitzel J., Tan N.B., Kearns K. "Carbon Nanofibers from Polyacrylonitrile and Mesophase Pitch." *Journal of Advanced Materials* **31** 1, 36-41 (1999).
21. Norris I.D., Shaker M., Frank K., MacDiarmid A.G. "Electrostatic Fabrication of Ultrafine Conducting Fibers: Polyaniline/Polyethylene oxide Blends." *Synthetic Metals* **114**, 109-114 (2000).
22. Kim J.S., Lee D.S. "Thermal Properties of Electrospun Polyester." *Polymer Journal* **32**, 7, 616-618 (2000).
23. Gibson P., Gibson H.S., Pentheny C. "Electrospinning Technology: Direct Application of Tailorable Ultrathin Membranes." *Journal of Coated Fabrics* **28**, 63-72 (1998).
24. Vansco J., Bergshoef M. "Transparent Nanocomposites with Ultrathin, Electrospun Nylon-4,6 Fiber Reinforcement." *Adv. Mater.* **11**, 16, 1362-1365 (1999).
25. Reneker D.H., Yarin A.L., Fong H., Koombhongse S. "Bending Instability of Electrically Charged Liquid Jets of Polymer Solutions in Electrospinning." *Journal of Applied Physics* **87**, 9, 3018-3026 (2000).
26. Bognitzki M., Frese T., Wendorff J.H., Greiner A. "Submicrometer Shaped Polylactide Fibers by Electrospinning." *Abstract Paper American Chemical Soc.* **219**, 115 (2000).
27. Bognitzki M., Czado W., Frese T., Schaper A., Hellwig M., Steinhart M., Greiner A., Wendorff J.H. "Nanostructured Fibers via Electrospinning." *Advanced Materials*, in press.
28. Nakajima T. *Advanced fiber spinning technology*, Chambridge, England (1994).

29. Fourné F. *Synthetic Fibers*, Hanser, Germany (1999).
30. Krochwitz J.I. *Encyclopedia of Polymer Science & Engineering*, **6**, 812-817 (1990).
31. <http://www.ntgi.net/ICCF%26D/manmade.htm#spandex>
32. Simons H.L., USPat. 1966, 3,280,229.
33. Bazilevsky A.V., Entov V.M., Rozhkov A.N. *Proc. 3rd. European Rheology Conference 41* Edinburg (1990).
34. Doshi J. *The Electrospinning Process and Applications of Electrospun Fibers*, Ph.D. Thesis, Akron University (1994).
35. Schiraldi D., Ocelli M., Gould S. "Surface of Poly(ethylene terephthalate/isophthalate) Copolyesters Studied by Atomic Force Microscopy." *Journal of Applied Polymer Science* **80**, 750-762 (2001).
36. *Multimode Scanning Probe Microscope Instruction Manual*, V 4.22ce, Digital Instruments, U.S.A. (1997).
37. Rovere A., Shambaugh R.L., O'rear E.A. "Investigation of Gravity-Spun, Melt-Spun, and Melt-Blown Polypropylene Fibers Using Atomic Force Microscopy." *Journal of Applied Polymer Science* **77**, 1921-1937 (2000).
38. <http://www.di.com/AppNotes/ForceVol/FVMain.html>
39. Schönder H., Vansco G.J. "Molecular Resolution Imaging and Friction Anisotropy of Highly oriented Polyethylene and Poly(tetrafluoroethylene) by Scanning Force Microscopy with Chemically Modified Probes." *Macromolecules* **30**, 6391-6393 (1997).
40. Adam D. "A Fine Set of Threads." *Nature* **411**, 236 (2001).

REFERENCES

1. Baumgarten P. "Electrostatic Spinning of Acrylic Microfibers." *Journal of Colloid and Interface Science* **36**, 1, 71-79 (1971).
2. Larrando L., John M. "Electrostatic Fiber Spinning from Polymer Melts I." *Journal of Polymer Science* **19**, 909-920 (1981).
3. Doshi J., Srinivasan G., Reneker D. "A Novel Electrospinning Process." *Polymer News* **20**, 206-213 (1995).
4. Taylor G. "Electrically Driven Jets." *Proc. Roy. Soc. Lond. A* **313**, 453-475 (1969).
5. Doshi J., Reneker D.H. "Electrospinning Process and Applications of Electrospun Fibers." *Journal of Electrostatics* **35**, 151-160 (1995).
6. Deitzel J.M., Kleinmeyer J., Harris D., Beck Tan N.C. "The Effect of Processing Variables on the Morphology of Electrospun Nanofibers and Textiles." *Polymer* **42**, 261-272 (2001).
7. Fong H., Chun I., Reneker D.H. "Beaded Nanofibers Formed during Electrospinning." *Polymer* **40**, 4585-4592 (1999).
8. Jaeger R., Bergshoef M., Vansco J., Battle C.M., Schönherr H. "Electrospinning of Ultra-thin Polymer Fibers." *Macromol. Symp.* **127**, 141-150 (1998).
9. Jaeger R., Schönherr H., Vansco G.J. "Chain Packing in Electro-Spun Poly(ethyleneoxide) Visualized by Atomic Force Microscopy." *Macromolecules* **29**, 7634-7636 (1996).
10. Zeleny J. "Instability of Electrified Liquid Surfaces." *Physical Review* **10**, 1, 1-7 (1917).
11. Taylor G. "Disintegration of Water Drops in an Electrical Field." *Proc. Roy. Soc. Lond. A* **280**, 383-97 (1964).
12. Formhals A., USPat. 1938, 2, 116, 942.
13. Deitzel J.M., Kleinmeyer J.D., Hirvonen J.K., Beck Tan N.C. "Controlled Deposition of Electrospun Poly(ethylene oxide) Fibers." *Polymer* **42**, 8163-8170 (2001).
14. Srinivasan G., Reneker D.H. "Structure and Morphology of Small Diameter Electrospun Aramid Fibers." *Polymer International* **36**, 195-201 (1995).

15. Reneker D.H., Chun I. "Nanometer Diameter Fibres of Polymer, Produced by Electrospinning." *Nanotechnology* **7**, 216-223 (1996).
16. Kim J.S., Reneker D.H. "Polybenzimidazole Nanofiber Produced by Electrospinning." *Polymer Engineering and Science* **39**, 5, 849-854 (1999).
17. Fong H., Reneker D.H. "Elastomeric Nanofibers of Styrene-Butadiene-Styrene Triblock Copolymer." *J. of Poly. Sci.: Part B: Poly. Phys* **37**, 3488-3493 (1999).
18. Fang X., Reneker D.H. "DNA Fibers by Electrospinning." *J. Macromol. Sci.-Phys.* **B36**(2), 169-173 (1997).
19. Buchko J.C., Loui C.C., Shen Y., Martin D.C. "Processing and Microstructural Characterization of Porous Biocompatible Protein Polymer Thin Films." *Polymer* **40**, 7397-7407 (1999).
20. Chun I., Reneker D.H., Fong H., Fang X., Deitzel J., Tan N.B., Kearns K. "Carbon Nanofibers from Polyacrylonitrile and Mesophase Pitch." *Journal of Advanced Materials* **31** 1, 36-41 (1999).
21. Norris I.D., Shaker M., Frank K., MacDiarmid A.G. "Electrostatic Fabrication of Ultrafine Conducting Fibers: Polyaniline/Polyethylene oxide Blends." *Synthetic Metals* **114**, 109-114 (2000).
22. Kim J.S., Lee D.S. "Thermal Properties of Electrospun Polyester." *Polymer Journal* **32**, 7, 616-618 (2000).
23. Gibson P., Gibson H.S., Pentheny C. "Electrospinning Technology: Direct Application of Tailorable Ultrathin Membranes." *Journal of Coated Fabrics* **28**, 63-72 (1998).
24. Vansco J., Bergshoef M. "Transparent Nanocomposites with Ultrathin, Electrospun Nylon-4,6 Fiber Reinforcement." *Adv. Mater.* **11**, 16, 1362-1365 (1999).
25. Reneker D.H., Yarin A.L., Fong H., Koombhongse S. "Bending Instability of Electrically Charged Liquid Jets of Polymer Solutions in Electrospinning." *Journal of Applied Physics* **87**, 9, 3018-3026 (2000).
26. Bognitzki M., Frese T., Wendorff J.H., Greiner A. "Submicrometer Shaped Polylactide Fibers by Electrospinning." *Abstract Paper American Chemical Soc.* **219**, 115 (2000).
27. Bognitzki M., Czado W., Frese T., Schaper A., Hellwig M., Steinhart M., Greiner A., Wendorff J.H. "Nanostructured Fibers via Electrospinning." *Advanced Materials*, in press.
28. Nakajima T. *Advanced fiber spinning technology*, Chambridge, England (1994).

29. Fourné F. *Synthetic Fibers*, Hanser, Germany (1999).
30. Krochwitz J.I. *Encyclopedia of Polymer Science & Engineering*, **6**, 812-817 (1990).
31. <http://www.ntgi.net/ICCF%26D/manmade.htm#spandex>
32. Simons H.L., USPat. 1966, 3,280,229.
33. Bazilevsky A.V., Entov V.M., Rozhkov A.N. *Proc. 3rd. European Rheology Conference 41* Edinburg (1990).
34. Doshi J. *The Electrospinning Process and Applications of Electrospun Fibers*, Ph.D. Thesis, Akron University (1994).
35. Schiraldi D., Ocelli M., Gould S. "Surface of Poly(ethylene terephthalate/isophthalate) Copolyesters Studied by Atomic Force Microscopy." *Journal of Applied Polymer Science* **80**, 750-762 (2001).
36. *Multimode Scanning Probe Microscope Instruction Manual*, V 4.22ce, Digital Instruments, U.S.A. (1997).
37. Rovere A., Shambaugh R.L., O'rear E.A. "Investigation of Gravity-Spun, Melt-Spun, and Melt-Blown Polypropylene Fibers Using Atomic Force Microscopy." *Journal of Applied Polymer Science* **77**, 1921-1937 (2000).
38. <http://www.di.com/AppNotes/ForceVol/FVMain.html>
39. Schönder H., Vansco G.J. "Molecular Resolution Imaging and Friction Anisotropy of Highly oriented Polyethylene and Poly(tetrafluoroethylene) by Scanning Force Microscopy with Chemically Modified Probes." *Macromolecules* **30**, 6391-6393 (1997).
40. Adam D. "A Fine Set of Threads." *Nature* **411**, 236 (2001).